Aerodynamic modelling of vertical axis wind turbine struts

using the lifting line method CACTUS

Willie Lu

Technische Universiteit Delft

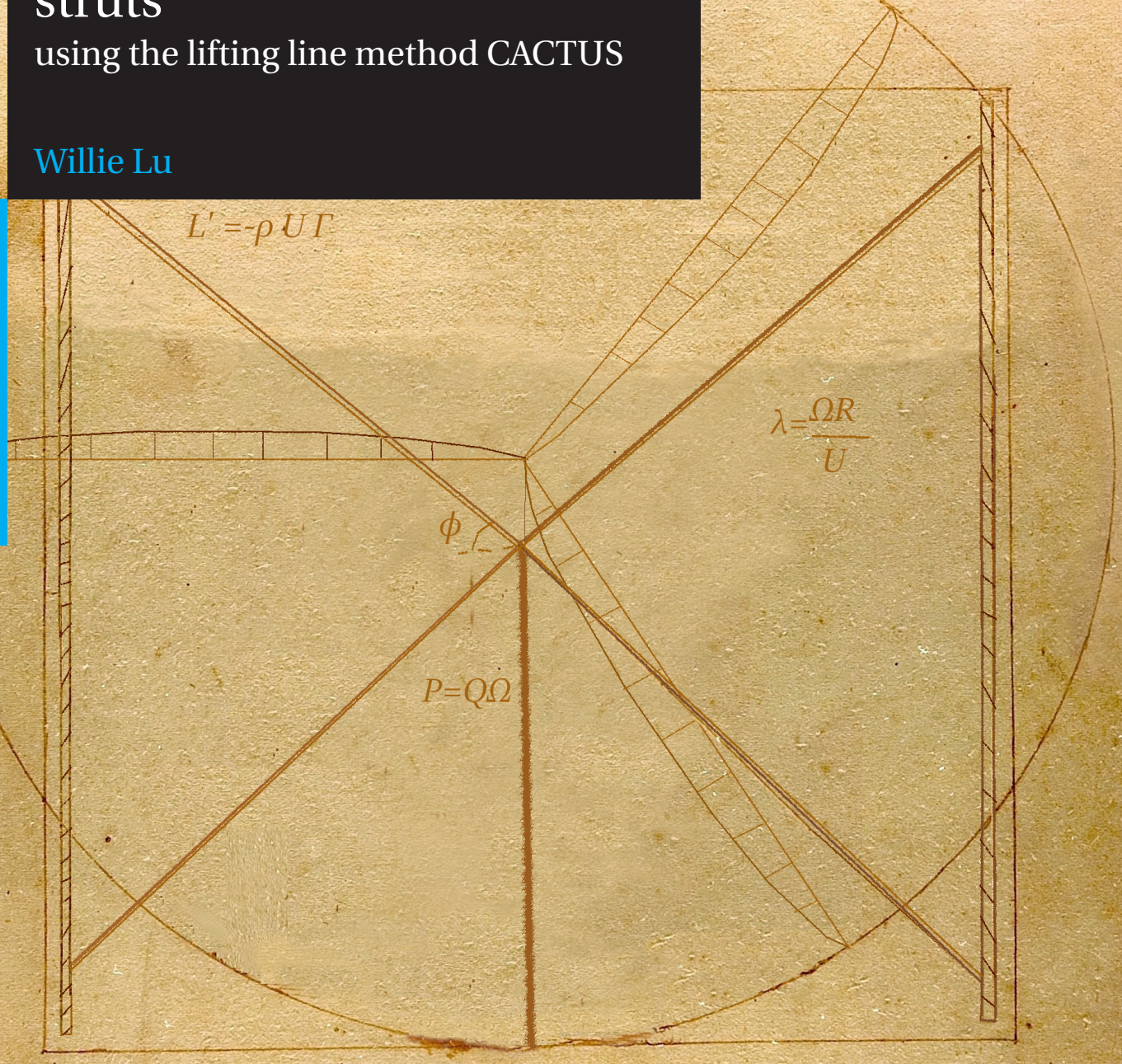

TU Delft Delft University of Technology

Challenge the future

AERODYNAMIC MODELLING OF VERTICAL AXIS WIND TURBINE STRUTS

USING THE LIFTING LINE METHOD CACTUS

by

Willie Lu

in partial fulfillment of the requirements for the degree of

Master of Science
in Aerospace Engineering
Flight Performance and Propulsion track

at the Delft University of Technology,
to be defended publicly on Monday January 20, 2020 at 13:00 PM.

Student number:	4467922	
Project duration:	February 5, 2018 – January 20, 2020	
Supervisors:	Prof. dr. ir. C. J. S. Ferreira,	TU Delft
	Ir. D. A. M. de Tavernier,	TU Delft
Thesis committee:	Prof. dr. ir. C. J. S. Ferreira,	TU Delft
	Dr. Ir. A. H. van Zuijlen,	TU Delft
	Ir. D. A. M. de Tavernier,	TU Delft
	Ir. T. Sinnige,	TU Delft

An electronic version of this thesis is available at http://repository.tudelft.nl/.

TU Delft Delft University of Technology

Abbreviations and Symbols

Abbreviations

ACM	=	Actuator Cylinder Model
AoA	=	Angle of attack
BEM	=	Blade Element Momentum theory
CACTUS	=	Code for Axial and Cross-flow TUrbine Simulation
CFD	=	Computational Fluid Dynamics
DBMS	=	Double-multiple streamtube model
HAWT	=	Horizontal axis wind turbine
LLM	=	Lifting line method
QMS	=	Quadruple Multiple Streamtube model
VAWT	=	Vertical axis wind turbine
VLM	=	Vortex Lattice Method

Symbols

AR_b	=	Main rotor blade aspect ratio [−], $\frac{H^2}{S_b}$
B	=	Number of blades [−]
B_s	=	Number of struts [−]
c	=	Chord [m]
C_D	=	Drag coefficient, $\frac{F_D}{0.5\rho S_e U^2}$ [−]
C_L	=	Lift coefficient of element, $\frac{F_L}{0.5\rho S_e U^2}$ [−]
C_M	=	Pitching moment coefficient, $\frac{M}{0.5\rho S_e c U^2}$ [−]
C_N	=	Normal force coefficient, $\frac{F_N}{0.5\rho S_e U^2}$ [−]
C_T	=	Tangential force coefficient, $\frac{F_T}{0.5\rho S_e U^2}$ [−]
C_P	=	Power coefficient, $\frac{P}{0.5\rho S U_\infty^3}$ [−]
C_Q	=	Torque coefficient, $\frac{Q}{0.5\rho S R U_\infty^2}$ [−]
C_X	=	Loading coefficient in freestream direction, $\frac{F_X}{0.5\rho S U_\infty^2}$ [−]
C_Y	=	Loading coefficient perpendicular to freestream direction and out of plane of rotation, $\frac{F_Y}{0.5\rho S U_\infty^2}$ [−]
C_Z	=	Loading coefficient perpendicular to freestream direction and in plane of rotation, $\frac{F_Z}{0.5\rho S U_\infty^2}$ [−]
dt	=	Time step [s]
D	=	Turbine diameter [m]
H	=	Blade span [m]
k	=	Reduced frequency, $\frac{\Omega \cdot c}{2 \cdot U}$ [−]
L_s	=	Strut length [m]
M	=	Mach number [−]
P	=	Generated power by turbine [W]
Q	=	Turbine torque [Nm]
R	=	Turbine radius, $\frac{1}{2}D$ [m]
Re	=	Reynolds number, $\frac{\rho U_\infty R}{\mu}$ [−]
S	=	Rotor frontal surface area, $H \cdot D$ [m^2]
S_b	=	Blade planform area [m^2]
S_e	=	Element planform area [m^2]
S_s	=	Strut planform area [m^2]
t	=	Time [s]

U = Local flow velocity m^2
U_∞ = Freestream velocity $[m/s]$
α = Angle of attack $[^\circ]$
$\dot{\alpha}$ = rate of change of angle of attack $[^\circ/s]$
ϵ = Spanwise mounting point strut to blade as fraction of blade span $[-]$
λ = Tip speed ratio, $\frac{\Omega R}{U_\infty}$ $[-]$
μ = Viscosity, $[Pa \cdot s]$
ψ = Strut pitch angle $[^\circ]$
ρ = Air density $[kg/m^3]$
δ = Blade pitching angle $[^\circ]$
ϕ = Strut inclination angle against the x-z plane $[^\circ]$
ξ = Gap between attachment point strut-blade and the strut as fraction of radius R $[-]$
σ_b = Rotor blade solidity, $\frac{Bc_b}{2R}$ $[-]$
σ_s = Rotor strut solidity, $\frac{B_s c_s}{2H\cos\phi}$ $[-]$
θ = Turbine azimuth angle $[^\circ]$
ω = Vorticity $[1/s]$
Γ = Circulation $[m^2/s]$
Ω = Turbine angular velocity $[rad/s]$

List of Figures

List of Tables

PREFACE

This thesis report is the culmination of 10 years of engineering studies, many international experiences and work experiences. While my background was more in aircraft design and gas turbines. Two years and a half years ago I took the challenge of starting a thesis on wind turbines as I always found them to be interesting and to make it even more challenging I started a research on an exotic version of a wind turbine. Out of curiosity in a total new area for me. It was big adventure with many challenges. Beside the theoretical components about unsteady rotor aerodynamics, the practical part of the thesis took some effort as well. The use of a simple 3D non-linear lifting method became a computational challenge requiring heavy computers or some inventive solutions to execute the computations. But in the end I learn to be on my edge of my competencies and it was worth it. Besides I also have learnt a lot about how to set up a research project, how to manage time and finally also how to deal with disappointments.

I would like to thank Carlos and Delphine for their supervision and support during my thesis. The thesis subject would have not been possible without your guidance. I might be very stubborn, but even then you kept faith in me to bring this thesis to a good end. I am grateful for that and really have learnt a lot from you. Especially the intricacies of vertical axis wind turbines.

Then I would also like to thank all my colleagues of ValueCare BV and in special Rob, Peter and Jan-Willem for the necessary skills they taught me to handle the computational parts of the thesis. Although I never thought that these skills could be used for my thesis, they eventually became paramount. You also gave me a good first introduction in the working life as 'burger'.

Of course there is the acknowledgements of friends and family. I would like to thank all my friends and many more for being the beacon of light during my darkest hours. I could not have done this without you. In particular AEGEE-Drienerlo for their ground and motivational support. Thijmen thank you for the many coffee/tea breaks we had at home and the university. Also of course for your critical (re)views on wind turbines. Your 'nuchtere' second opinions on flow related matters really helped me forward with my discoveries. As former housemate you made sure that I kept working on my studies. It was a real pleasure and honor to have you as housemate.

Jorinde, Marije and Ines. I could only say: more spring rolls, kimchi and sushi! Thank you all for the great time and food! Reinout and Klöppner, as one of the few who I knew from the start of my student time you gave me unconditional support in good and less good times. Thank you for everything! Dear housemates of Sjaak63 and in particular Rik Leenders, long have I lived with you under one roof and many things happened. I enjoyed our great times in the house and could always count on your support! I also learned a lot from you during my time in Sjaak63! It contributed to who I am today. Thank you all!

Of course I would also like to thank my family in special. For your unending support during my life. It gives me great joy to know that I can always count on you. Although I am not the typical Chinese you expected me to become, you are still accepting my values during my student period.

And finally Alexandra Kiss....there aren't words but I will try. Even though you are in Denmark, you always make sure I stayed on the thesis as well like you make me follow the traffic rules. You always make sure I feel hopeful in dire situation regarding the thesis and everything else as well. You always take care of me and unconditionally stand by my side until the end. Your love and care are greatly appreciated.

Willie Lu
Delft, December 2019

SUMMARY

To combat climate change and with increased demand of energy, the wind energy sector becomes more important over time. The wind energy producing systems consists predominantly of horizontal axis wind turbines (HAWT). Beside the HAWTs there are other types of wind turbines, one of them the vertical axis wind turbines (VAWT) which distincts from the HAWTs by having their axis of rotation perpendicular to the flow. This leads to the ability to catch wind from different directions without requiring yawing systems. These type of systems are very promising for offshore deployment due to their inherent structure. This can lead to cheaper wind energy systems and thus a more accessible source of alternative (green) energy.
This thesis is about the research on the modelling of H-shaped Darrieus vertical axis wind turbines with struts using CACTUS, a 3D numerical lifting line method developed by Sandia National Laboratories. Struts are often required to connect the blades to the tower. But the presence of these structures affects the wake and the performance of the turbine by blade-strut and blade-wake interactions. These effects are often described using empirical relations but are not fully understood yet. Thus one of the main goals is to improve the understanding of the aerodynamics of struts in the VAWT. In this research, the turbine including the struts are modelled and a parameter study is performed using CACTUS. This thesis consist of few objectives. The first one is to define and model the VAWT and its struts with varying design parameters in CACTUS. The second objective is to examine how the loadings of the struts can be modelled within CACTUS and thirdly to determine its effects on the rotor performance and wake. The research in this thesis paper is furthermore supported with a literature review on the theory of VAWTs aerodynamics, dynamic stall and similar studies performed by other researchers.
The original CACTUS program only models the rotor blade with the lifting line method and the struts are currently described with empirical relations. Thus the second objective is to model the loadings on the struts. CACTUS is extended to allow the application of its lifting line model on the struts as this gives a more physics based approach. After the extension the full rotor with blades and struts are simulated in CACTUS. In the study the inclination angle, the strut tip to blade attachment distance, the strut attachment point on the blade and tip speed ratio of the turbine were varied for the different cases. A strutless reference model is also simulated and used as for comparison with the cases.
The first check is to make sure that the blade-strut interference is present with the extended model as this was formerly modelled with a empirical relation of Hoerner. A gap was introduced between the strut tip and blade attachment point. It is found that by placing a strut tip near a blade will affect the blade due to the induced velocities caused by the strut tip. By reducing the gap distance (positioning the strut tip closer towards the blade) this downwash is stronger. Except the influence of the strut tip vortex on the blade, the reverse influence of the rotor blade tip vortex on the strut is also present. The strength varies based on the strut-blade attachment position on the rotor blade, with the downwash on the strut being the strongest when the strut is place towards the tip of the blade. Another parameter being varied is the tip speed ratio of the rotor. It shows that the optimal tip speed ratio for this VAWT is in the lower range which is in agreement with other studies on VAWTs. Finally, an inclination angle is introduced between the struts and blades. By doing so the loadings on the blades and struts change. Compared to a horizontal and unpitched strut, the inclined strut generate a load which in turn contribute to the torque in the rotor. The presence of the (inclined) struts in the turbine distorts the flow field in the wake and deflects the wake laterally based on the strength of the vortex strength on the struts. This relates to the inclination angle of the struts relative to the blades as this results in a increased angle of attack of the struts and thus a stronger bound vortex. As consequence the lifting load on the strut contributes to the torque generated by the turbine and the strut becomes an energy conversing body. But whereas the struts start to generate more torque with increasing inclination angle the main rotor blades' torque generating capacity deteriorates. Ultimately the energy conversing capability of the blades is transferred to the struts with increasing inclination angle of the struts. In this transfer a part of the rotor power coefficient is lost thus the net result is that the inclination of struts will lead to a reduced power conversing capability of the rotor.

CONTENTS

I

INTRODUCTION

RESEARCH BACKGROUND

WHY WIND ENERGY?

Due to climate change, governments are committed to create a more sustainable environment[19]. As wind turbines are becoming cheaper to implement, it becomes one of the alternatives for society to transit to a more sustainable energy production capacity. The abundance of wind energy[1] and its easy accessibility makes it a very promising candidate for reliable large scale power production. It could lead to a reduced dependency on fossil fuels and thus reduce carbon emissions. Although wind as a resource is free and abundant, it also has some other issues associated with. The first one is the higher upfront research and development costs than conventional power plants. Secondly the power production rate of the turbines are time specific instead of constant. Thirdly, public opinion does not always favour them in the neighbourhood due to the nuisance caused by the turbines[1]. Wind turbines and conventional power plants also have their operational costs. But once set up wind resources are free while fuel costs money. According to [20] wind energy production costs are now similar to conventional fossil fuel based costs. With more financial and time investment in wind turbines, its costs can be decreased severely due to the learning curve [20]. This makes wind energy as one of the prominent alternatives to fossil fuels.

(a) Typical horizontal axis wind turbine [1]

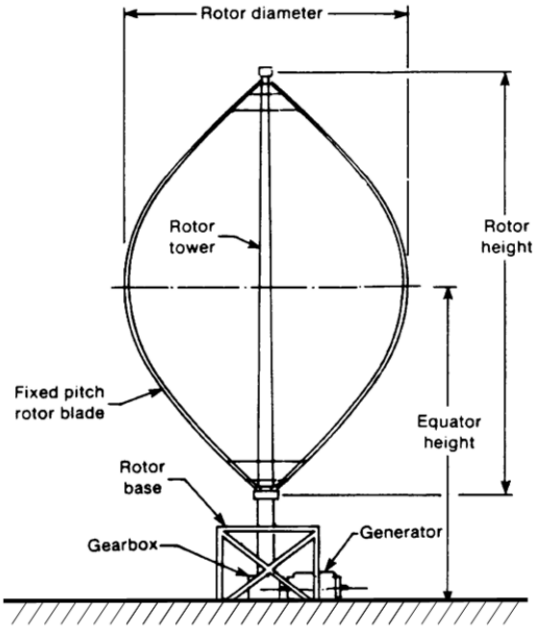

(b) Darrieus vertical axis wind turbine [21]

Figure 1: The two modern wind turbine types

WIND TURBINES

There are two main wind turbine categories: the horizontal axis wind turbine (HAWT) shown in figure 1a and the vertical axis wind turbine (VAWT) shown in figure 1b. Both categories have their own strengths and weaknesses[5]. While the standard for wind energy production are the horizontal axis wind turbine (HAWT) type, there is renewed interest in VAWTs. Specifically for applications in off-shore multi megawatt power generation due to the inherent features of the VAWT[21][22][23]. On the other hand small sized VAWTs are also mainly deployed in urban applications such as power generation on high-rise buildings[24]. But the standard of wind energy production wind turbines are of the HAWT type and the VAWT is a topic for which aerodynamic research has been lagging a bit behind compared to the HAWT[25]. Nowadays renewed interest is shown in VAWTs and its potential.

Most VAWTs have structural elements connecting blades to tower called struts, and these elements have impact on the performance of the VAWT. The goal is to create a better understanding of the aerodynamic effects of struts in a VAWT and its impact on performance. Thus this research deals with the (numerical) modelling of the struts in a vertical axis wind turbine using a 3D lifting line method and to assess the impact of strut geometry. Knowing how the presence of the struts and its geometry and topology relates to its aerodynamic

performances can have practical use for optimizing strut designs in a VAWT. In the end this can increase the efficiency of a VAWT and make it more feasible to produce them.

RESEARCH QUESTION, AIMS AND OBJECTIVES

This thesis report deals with the research on the aerodynamic effects of the struts in a vertical axis wind turbine. Similar studies by other researchers have been performed on this subject. Delphine[16] have performed a study on 2D VAWT rotor within another rotor using the actuator cylinder model. This inner rotor could represent a lift producing strut in 2D. Another study regarding struts is by Mendoza[14]. He has studied the wake deflection due to pitched struts in a VAWT, also using the actuator cylinder model. Hara et al [26] have also performed a study with CFD on pitched struts in the form of butterfly VAWTs, in which the struts are integrated to form closed loop blades.
A different approach of modelling is used in this research. The 3D lifting line solver called CACTUS is used in contrary to the above mentioned methods. In this research the main objective is to extend CACTUS to include the prediction of the effects of the struts on the aerodynamic performance of a H-Darrieus vertical axis wind turbine. The solver is modified such that the lifting line model itself is applied on the struts as well as this is not implemented by default. The original code only models the strut with minimal empirical relations. Thus the strut modelling is expanded upon in this work and allows to simulate the turbine with blades and struts in 3D.
The knowledge attained could be used to improve strut design in future VAWTs, leading to less losses. It is specifically noted that the analysis focuses on the 3D aerodynamic effects. Other considerations like structural or control aspects are outside of the scope of this research. The research question *How does the presence of struts in 3D affect the aerodynamic performance of a H-Darrieus Vertical Axis Wind turbine?* is a very broad question, thus it will be divided into smaller subquestions or goals. By answering all the subquestions, the main question will also be answered.
With the main research question and objective set, the next step is to consider which aspects must be taken into account. A framework is first presented to sketch the outline of this project which can be then used to solve this research problem. Based on the framework a set of subquestions can be made which is used to finally answer the main question.

SUBQUESTIONS

As mentioned earlier the main research question is still to broad, therefore this project is divided into smaller subproblems

1. *How to define and model the strut geometry in CACTUS?*
   (a) *How can we model our objective turbine into CACTUS?*
   (b) *How can the loadings (lift and drag) at the blade-strut intersection be modelled?*
   (c) *How can the loadings of the (inclined) struts be modelled?*
2. *How do the struts effect the VAWT performances?*
   (a) *What are the physical phenomena causing losses?*
   (b) *How and why does the sectional geometry of the strut affect the lift, drag, torque, power coefficient and velocity field?*
   (c) *How and why does the strut inclination angle affect the lift, drag, torque, power coefficient and velocity field?*
   (d) *How and why does topology of the struts relate to the performance of the VAWT?*
   (e) *What are the 3D secondary flow effects?*
   (f) *How and why do blade-wake interactions affect the struts?*
3. *How are the near and far wakes affected by the struts?*
   (a) *How is the velocity field downstream affected by the struts?*
   (b) *How is the shape of the wake affected by the struts?*

REPORT STRUCTURE

This report consists of two main parts. First part consists of the paper presenting the research and answering the research questions in the last section. The paper is a separate part of this report and is a full standalone document. The second part consists of supporting chapters which function as literature review on several topics of VAWTs. This part is divided into several chapters. In chapter 1 the theoretical background is presented for VAWTs including regular aerodynamic models. Chapter 2 continues with literature on unsteady aerodynamics common for VAWTs. Chapter 3 presents the literature related to modelling and research on struts by other researchers. Finally the support chapters are closed with a conclusion on the literature review and the research performed in the paper section. A few recommendations are also made in the concluding section.

II

RESEARCH PAPER

Aerodynamic modelling of support struts of a Vertical Axis Wind Turbine with CACTUS

W. Lu
Faculty of Aerospace Engineering, Delft University of Technology, Delft, the Netherlands

Supervisor: Dr. ir. C. J. Simão Ferreira
DUWIND, Faculty of Aerospace Engineering, Delft University of Technology, Delft, the Netherlands

Supervisor: ir. D.A.M. de Tavernier
DUWIND, Faculty of Aerospace Engineering, Delft University of Technology, Delft, the Netherlands

This thesis paper presents research on the modelling of struts of a vertical axis wind turbine and its effects on the wake and performance. The 3D non-linear lifting line solver CACTUS is extended to include the struts in the rotor as lifting bodies. This leads to the application of the lifting line theory on the struts and the vortices shed by the struts are considered. A case study is performed for different strut configurations in the rotor, with the focus set on the inclination angle of the struts. The results are studied and compared to the reference turbine excluding struts. The original version has a limited drag-only modelling of struts with empirical relations and assumes flat plate shape of the strut. The extended modelling of struts uses a more physics based approach and takes into account the strut geometry and the angle of attack of the strut with the flow. Limited aerodynamic interactions between strut and blade is possible with this method. The tip vortex from the blade creates a downwash on the strut and thus causes an increased bending load on the strut. On the other hand the effect of the inclined strut interference on the main rotor blade will have a relatively big impact as it causes deterioration in the blade loadings on the downwind pass. The consequence is that part of the torque generation by the blades is transferred to the struts. Finally it is found that the inclusion of the struts distorts the flow field in the wake, especially when the struts have a stronger bound vortex due to its inclination angle. The wake tends to expand and deflect more downstream then without the struts. The low velocity flow field as consequence deflects towards windward side, becomes turbulent and thus the flow deficit is lower than in the reference case.

Keywords: Vertical Axis Wind Turbines, VAWT, wake, struts, vortex method, lifting line method

Nomenclature

CACTUS	=	Code for Axial and Cross-flow TUrbine Simulation
CFD	=	Computational Fluid Dynamics
HAWT	=	Horizontal axis wind turbine
VAWT	=	Vertical axis wind turbine
AR_b	=	Main rotor blade aspect ratio $[-]$, $\frac{H^2}{S_b}$
B	=	Number of blades $[-]$
B_s	=	Number of struts $[-]$
c_b	=	Blade chord $[m]$
c_s	=	Strut chord $[m]$

C_D = Drag coefficient, $\frac{F_D}{0.5\rho S_e U^2}$ $[-]$
C_L = Lift coefficient of element, $\frac{F_L}{0.5\rho S_e U^2}$ $[-]$
C_N = Normal force coefficient, $\frac{F_N}{0.5\rho S_e U^2}$ $[-]$
C_T = Tangential force coefficient, $\frac{F_T}{0.5\rho S_e U^2}$ $[-]$
C_P = Power coefficient, $\frac{P}{0.5\rho S U_\infty^3}$ $[-]$
C_Q = Torque coefficient, $\frac{Q}{0.5\rho S R U_\infty^2}$ $[-]$
C_X = Loading coefficient in freestream direction, $\frac{F_X}{0.5\rho S U_\infty^2}$ $[-]$
C_Y = Loading coefficient perpendicular to freestream direction and out of plane of rotation, $\frac{F_Y}{0.5\rho S U_\infty^2}$ $[-]$
C_Z = Loading coefficient perpendicular to freestream direction and in plane of rotation, $\frac{F_Z}{0.5\rho S U_\infty^2}$ $[-]$
dt = Time step $[s]$
D = Turbine diameter $[m]$
H = Blade height $[m]$
k = Reduced frequency, $\frac{\Omega \cdot c}{2 \cdot U}$ $[-]$
L_s = Strut length $[m]$
P = Generated power by turbine $[W]$
Q = Turbine torque $[Nm]$
R = Turbine radius, $\frac{1}{2}D$ $[m]$
Re = Reynolds number, $\frac{\rho U_\infty R}{\mu}$ $[-]$
S = Rotor frontal surface area, $H \cdot D$ $[m^2]$
S_b = Blade planform area $[m^2]$
S_e = Element planform area $[m^2]$
S_s = Strut planform area $[m^2]$
U = Local flow velocity m^2
U_∞ = Freestream velocity $[m/s]$
α = Angle of attack $[^\circ]$
ϵ = Spanwise mounting point strut to blade as fraction of blade span $[-]$
λ = Tip speed ratio, $\frac{\Omega R}{U_\infty}$ $[-]$
μ = Viscosity, $[Pa \cdot s]$
ψ = Strut pitch angle $[^\circ]$
ρ = Air density $[kg/m^3]$
δ = Blade pitching angle $[^\circ]$
ϕ = Strut inclination angle against the x-z plane $[^\circ]$
ξ = Gap between attachment point strut-blade and the strut as fraction of radius R $[-]$
σ_b = Rotor blade solidity, $\frac{Bc_b}{2R}$ $[-]$
σ_s = Rotor strut solidity, $\frac{B_s c_s}{2H \cos\phi}$ $[-]$
θ = Turbine azimuth angle $[^\circ]$
ω = Vorticity $[1/s]$
Γ = Circulation $[m^2/s]$
Ω = Turbine angular velocity $[rad/s]$

I. Introduction

This paper focuses on the lift-based VAWT, called Darrieus turbine. The lift-based VAWT uses lifting bodies, to generate the required torque. The construction of the VAWT has a lower center of gravity and enhanced accessibility for maintenance. Due to the VAWT's independence of cylic gravitational loads[20][5], the VAWTs are more scalable compared to HAWT and are thus very suited for offshore applications[5]. However, the VAWTs have cyclic aerodynamic loads because of their continuously varying blade angle of attack and relative velocity, leading to increased susceptibility to fatigue. The rotor also deals with unsteady flow effects like dynamic stall and blade wake interaction[2]. The modelling of VAWTs introduces significant challenges as the blades uses carrying construction elements, struts, to carry the blades. These struts are part of the rotor and need to be accounted for when trying to model the performance of the full turbine.

To predict these aerodynamic performances and loadings, there are many different ways ranging from simple low fidelity momentum models like streamtube models to advanced CFD methods. Each method has their own benefits and limitations. Goude et al[4] have performed a parametric study on the influence of struts in a VAWT using the double-multiple streamtube method. They found out how the design parameters of struts are influencing the performance of the turbine. De Tavernier and Ferreira[1] show the application of the more improved 2D actuator cylinder model for use in an actuator-in-actuator concept. This could be used for the modelling of struts in their rotor in 2D or double bladed turbine as they demonstrated in their paper. Another research on this subject is performed by Siddiqui et al[15] in which they performed a 3D numerical study with CFD on a VAWT with and without struts and hub. It is concluded in the study that the extra profile drag and vortices caused by the struts impact the performance, especially at higher rotational speeds of the turbine. Marsh et al[10] have also performed a similar research but focused on the strut topology and the strut-blade joints. Finally Mendoza and Goude[11] study the effects of pitched struts in a VAWT on the wake deflection.
In all the previously mentioned studies the struts mainly served as structural elements in the rotor, and their inclusion are only analyzed for the loss of performance. But when the struts are shaped and inclined such that they can generate torque, the struts can become a power converting body. They could be integrated in such way that it could contribute to the rotor's power conversion. This research performed in this paper extends the previous studies by also including lift effects on the struts and analyzes how this would change the rotor performance. To model the VAWT with struts, a vortex-based method is used. This way a more extensive parameter study in 3D can be performed.

Goal of this research

The goal of this research is to a study the aerodynamic interactions between the struts and blades and its impact on the performance of the turbine. A parametric study is performed in which several design parameters of the struts and its topology are varied. Performing a parameter study with a high fidelity CFD code would take severe computational resources. While the low fidelity momentum methods are less computational intensive, they might not be accurate enough. The vortex method provides a mid-fidelity alternative. This method, sitting between CFD and momentum method, has a more physics based approach than momentum method while using less computational resources than CFD methods. Specifically the 3D lifting line code called *Code for Axial and Cross-flow TUrbine Simulation* (CACTUS) will be used for this purpose. The main research question is thus: *How does the presence of struts affect the flow and aerodynamic performance of a H-shaped Vertical Axis Wind Turbine?* The main goal with this thesis is to understand the aerodynamic relations between strut designs and blades of a VAWT. Following the main research problem, the thesis consists of the following research questions.

1) How to define and model the strut geometry in CACTUS?
2) How do the struts affect the performance of a VAWT?
3) How are the near and far wakes affected by the struts?

II. Methodology

To model and compare the effects of different strut configurations and its design parameters on the flowfield, multiple simulations are conducted with CACTUS. The reference VAWT is defined, modelled and simulated. Then several other cases, each with one varying parameter of the struts within the VAWT, are simulated. The results for the different configurations will be compared to each other with the goal to identify the effects of the design parameters.

A. Lifting line method: CACTUS

CACTUS is a 3D lifting line simulation tool originally developed and used for studying marine hydrokinetic turbine systems and wind turbine systems[12]. The opensource software is based on the VDART3 code[17], which was developed as a vortex method for Darrieus wind turbines[18]. The software is build for Linux systems and is published by Sandia National Laboratory. CACTUS has the ability to model arbitrary blade geometries in 3D and allows very limited strut modelling in the turbine. For the lifting surfaces, CACTUS uses the non-linear lifting line free vortex wake model and is considered a mid-fidelity method[12] being more capable than momentum methods but computationally cheaper than CFD methods.
This vortex method is based on the Weissinger Lifting line model[14]. A lifting body is modelled using blade elements where each element of the lifting body is modelled with a bound vortex Γ_b. The strength of this vortex can be computed

from the rewritten Kutta-Joukowski theorem given in equation 1.

$$\Gamma_b = \frac{1}{2} c U_{element} C_L \tag{1}$$

With $U_{element}$ being the local velocity of the blade element. To determine the C_L in the nonlinear lifting line model, the lift polar of an airfoil is used. The specific C_L value of the blade element can be extracted from the known polar if the local angle of attack α is known. This effective α can be determined by the local velocities on the airfoil. The system of vortices consists of the bound vortex Γ_b, its trailing vortices Γ_t and shed vortex Γ_s for each blade element in the lifting body. The trailing and shed vortices are the consequence of the varying vortex strength along the span of the lifting body. This system of vortices induces a velocity field $\mathbf{U}$ and can be determined using the Biot-Savart law in equation 2[21][8][14].

$$\mathbf{U} = \frac{\Gamma}{4\pi} \frac{\mathbf{r}_1 \times \mathbf{r}_2}{|\mathbf{r}_1 \times \mathbf{r}_2|^2} \mathbf{r}_0 \cdot \left(\frac{\mathbf{r}_1}{\mathbf{r}_2} - \frac{\mathbf{r}_2}{\mathbf{r}_1} \right) \tag{2}$$

$\mathbf{r}_1$ and $\mathbf{r}_2$ are respectively the position vector from the start and end of the vortex line to an arbitrary point in the field. $\mathbf{r}_0$ is the vector from start of the vortex line to its end. This can be done for every vortex line and their effects can be superimposed on every arbitrary point in space, therefore creating a velocity field. This velocity field can be used to calculate the angle of attack α on each element and this can be used again to determine the bound vortex strength Γ_b on the element. Furthermore all the blade element loadings can be derived using the polars and the angle of attack. The torque and power can then be derived from the loadings. Based on how the shed Γ_s and trailing Γ_t vortices are treated, the wake model is either a free wake model or a fixed wake model[22]. In the fixed wake model, the advection of the lattice points of the trailing and shed vortex points are prescribed. Thus the influence by the induced velocities from other wake elements are ignored. As consequence the wake structure stays constant downstream. The free wake model allows the mutual interference between the wake vortex elements downstream. Therefore the wake in a free wake model can deform substantially over time[22]. While this is more realistic than the fixed wake model, it requires substantially more computational resources.
In CACTUS, the nonlinear lifting line method has to be applied for every shift in azimuthal angle θ with the state of the previous θ becoming the new initial assumptions for the current computations. This will be done until a certain amount of rotations has been achieved or until the power coefficient C_P is converged. The viscous flow modelling is implied with the diverse set of airfoil polars for different Reynolds number Re. Furthermore, CACTUS contains a variety of extra models. It has the possibility to model dynamic stall using either Gormont model[3] or the indicial Leishman-Beddoes model[9] [12]. Other possibilities are the inclusion of blade pitch rate effects and corrections for compressibility effects. Finally CACTUS also gives the user the abilities to specify a model for the vortex core, a wall model for boundary conditions in a simulation, ground shear layer model and even a gust model[13].
As mentioned earlier, CACTUS has the possibility to include struts but this has its limitations. The original CACTUS does not represents the struts as lifting lines. Instead it is assumed that the α of the struts remains small[12]. Thus only the drag is modelled using empirical relations from Hoerner[7] based only on local Reynolds number and thickness to chord ratio of the strut elements[12]. These empirical relations determine the profile drag and the interference drag between the strut tip and blade. As consequence the strut elements do not contribute to the system of vortices and their influence on the velocity field in the near and far wake will be absent. For an uninclined and unpitched strut this model provides acceptable modelling as the assumption of the small α in [12] might be valid. But for struts with an inclination angle this model is lacking when investigating how the velocity field induced by the strut will contribute to the blade loadings and vice versa. Therefore an improved model is proposed where the struts will be modelled in the same way as the blades, with lifting lines. An airfoil is assigned for each strut element. By doing so, the strut could contribute to the rotor C_P output by inclining the struts. The previously mentioned empirical interference drag modelling of Hoerner is not used for the strut anymore in the extended CACTUS.

B. Reference turbine geometry

For this research a specific VAWT model ($P \approx 350kW$) inspired by the Arkom VAWT model (from the company Arkom Windpower) is used. The model, containing two main rotor blades, is a square shaped rotor with two struts supporting each blade. The struts are inclined relative to its rotational plane. Not much literature is available for standardized nomenclature of strut and rotor topology, thus an own definition is made partially extending the definitions in CACTUS. Table 1 states the values used to define the reference VAWT and figure 1 shows the schematic overview

of the turbine including the design parameters and topology. Note the three main directions given in the schematic view: X is positive in the direction of the freestream, Y is positive in the height direction of the rotor and Z is the rotor in-plane side direction. For the simulations the rotor will be rotating in clockwise direction. All turbines will start the simulation such that the rotor struts are fully aligned with the Z-axis and the main rotor blade chords are fully aligned with X-axis (freestream direction). The azimuthal angle at this position is the datum $\theta = 0°$. This is important due to the determination of the blade position relative to the freestream flow when analyzing the results.

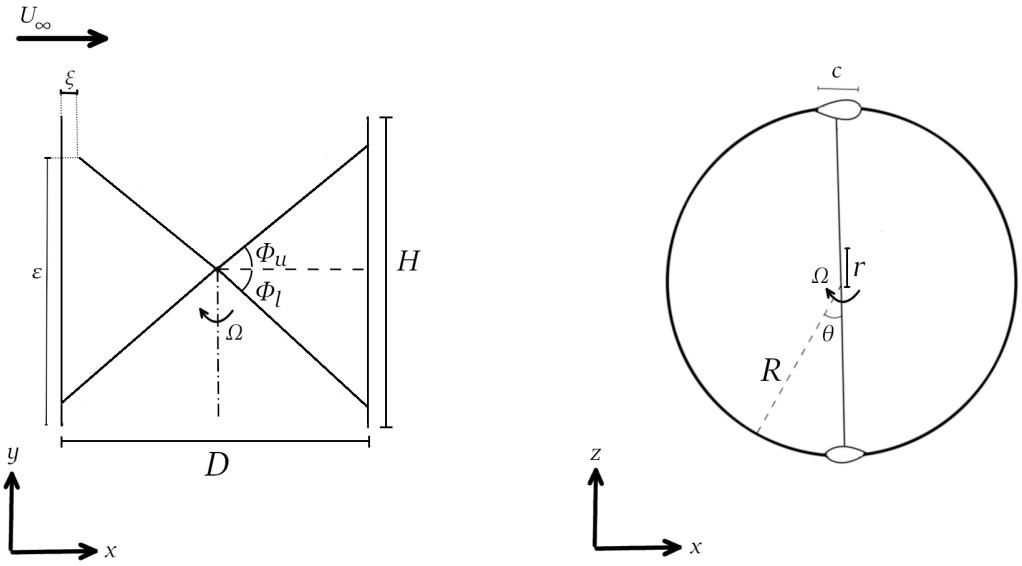

Fig. 1 Schematic view of turbine with design parameters

Table 1 Table containing design parameters of the reference turbine

Parameter	Value
H	28 m
D	28 m
c_b	1.19m
c_s	1.19m
λ	4.5
S	784 m^2
σ_b	0.085
Airfoil type	NACA 0018
δ	0°

The VAWT general geometry can be described by the variables stated in figure 1. Some of these variables are dependent on other variables. To model the full VAWT in CACTUS most of the parameters are expressed relative to rotor radius R. There are many variables required to model the full VAWT, but in this research it is specifically aimed at the struts. Thus some of these parameters, not related directly to the struts, will be chosen to be constant. This way a base model for the VAWT is created in which only the parameters for the strut can vary. Finally the aerodynamic shape of the blade is modelled using blade elements along the span of the blade. The blade elements are modelled

using airfoils which have known aerodynamic behaviour. Two airfoil types are used, the flat plate and the NACA0018 airfoil. The upper and lower struts can have different inclination angles but it is assumed that the strut inclination is axi-symmetric. Although the geometry was described with struts, the reference configuration is strutless.

C. Simulation of test cases

With the reference configuration for the VAWT defined, table 2 shows the different test cases used in this parametric study. All the test cases are an extension of the reference case including struts. In the table it can be seen that some of the cases have subcases as two phenomena can actually influence each other. Based on an earlier grid convergence study it was determined that one revolution will consist of 72 timesteps. Furthermore each blade and strut will be modelled with 15 elements in a cosine distribution. All simulations in table 2 will run for 20 revolutions. These settings lead to a simulation with acceptable results while still maintaining a reasonable simulation time.

Design vector $\bar{X}$ will contain the following variables of interest:

$$\bar{X} = \{\lambda \quad \phi_{l,u} \quad \xi \quad \psi_{r,t} \quad \epsilon\} \tag{3}$$

In each of the cases in table 2, specific design variables from eq. 3 are varied to test its effect on the rest of the configuration. Besides the given design vector there are some dependent variables, the surrogate variables. These variables which are not needed in the design vector, but are derived from it. These are given in eq. 4. A Python script is used to derive necessary information from the design vector and translate into a suitable input geometry file for CACTUS. All of the cases will be simulated under nearly standard sea level conditions stated in table 3. No ground shear layer model is used, so U_∞ is constant along the height of the turbine. The default vortex core model in CACTUS is used which gives a finite constant velocity in the core. All the simulations are performed on a high performance computer.

$$\bar{Y} = \{\sigma_s \quad AR_{strut}\} \tag{4}$$

Table 2 Test cases

case	λ	$\phi_{l,u}$	ξ	$\psi_{r,t}$	ϵ
A	4.5	NA	NA	NA	NA
B	4.5	0°	$0R$, $0.01R$, $0.05R$, $0.1R$, $0.3R$, $0.5R$	±10°	$0.0H$; $1.0H$
C	3:0.5:6	0°	0	±10°	$0.0H$; $1.0H$
D	4.5	0°	0	0°	$0.5H$: 0.1 : $1.0H$ $0.0H$: 0.1 : $0.5H$
E	4.5	0:5:45°	0	0°	$0.5H$: 0.1 : $1.0H$ $0.0H$: 0.1 : $0.5H$

Table 3 Simulation freestream and operational conditions

Symbol	Description	Values
ρ	Air density	1.225 kg/m^3
μ	Viscosity	$1.7902 \cdot 10^{-5}$ $Pa \cdot s$
T	Temperature	$293K$
Ω	Turbine angular velocity	3.87 rad/s (37 rev/min)

D. Performance parameters

The performance parameters are used to compare the different cases in table 2 to the reference case. These parameters are primarily the blade elements loading coefficients $C_L(\alpha)$, $C_D(\alpha)$, $C_N(\alpha)$ and $C_T(\alpha)$ during a revolution (change in

azimuthal angle θ) of the VAWT. Based on the loading coefficients the torque coefficient C_Q can be determined by the contributions of the tangential forces of each blade and strut. Finally as λ is known and C_Q can be determined from the loadings on the blades, $C_P = C_Q \cdot \lambda$ can be computed. Besides these parameters, the 3D wake of each case at the end of their simulation are visualized together with the velocity field in the wake (U/U_∞, V/U_∞ and W/U_∞). This can give insight on how the wake has developed for each case. All rotors in the cases will have the same projected turbine surface area S so all rotors can be compared to each other.

III. Results and discussion

A. Reference case

Rotor and blade analysis

As reference case this will be the baseline to which the other cases will be compared to. With the standard $\lambda = 4.5$ and $\Omega = 3.87 rad/s$ ($37 RPM$), freestream velocity $U_\infty = 12.05 m/s$. Furthermore a reduced frequency of $k = 0.0425$ was calculated. This indicates that the flow can still be described with quasi-steady aerodynamics. Directional loading coefficients (C_X, C_Y and C_Z) are referred using figure 1. The revolution averaged performance and loading data are plotted in figure 2a and shows the convergence of the C_P and C_Q over time. Both plots adhere to $C_P = \lambda \cdot C_Q$ and converges very quickly within 10 revolutions. Then figure 2b shows the revolution averaged directional loading coefficients of the rotor. In the spanwise direction $C_Y = 0$, which is expected as the blades are symmetrically loaded. The thrust coefficient C_X and lateral loading coefficient C_Z are converged at the end of the simulation. All the plots and values discussed look reasonable for a typical 2 bladed VAWT without any struts although the power generated by the turbine is a bit higher than expected for its typical size, around 400 kW which is around 80% of its theoretical limit. The theoretical limit should be approximately 500 kW based on the Betz limit.

The plots in figure 3 show the instantaneous performance indicators throughout one full revolution by the rotor or per blade which is averaged over span. Only the last revolution is taken for this time dependent plot as figure 2 shows that the solution is converged sufficiently at the last revolution. Figure 3a shows the time dependent loading coefficients along one full rotation. In addition figure 3b also shows the instantaneous rotor torque coefficient which is split up into the contributions caused by each blade. Immediately it is seen that in the case with only two blades the torque contribution of the blades are the same including its time dependent pattern meaning high rotor torque contribution caused by the blade in the upwind and low torque in the downwind region. The torque contribution plots are shifted with 180° relative to each other. This is expected as the blades are indeed spaced 180°.

Going into detail analysis of the blade loadings itself, the plots of figure 3c show the net loadings in the three main directions of each blade during a full revolution. Once again it can be seen that the blade loadings of each blade lags half a revolution as expected with zero spanwise loadings detected. This means that the flow leads to a symmetric distribution of forces on the blade. Furthermore the loadings of the blades individually create the rotor loading pattern of figure 3a. These loadings contributes to the total rotor torque with the peak torque on the upwind part and low torque on the downwind part.

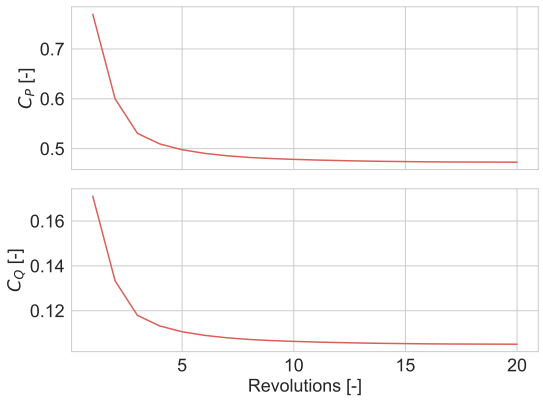

(a) The power C_P and torque C_Q coefficients as they are converging during the simulation.

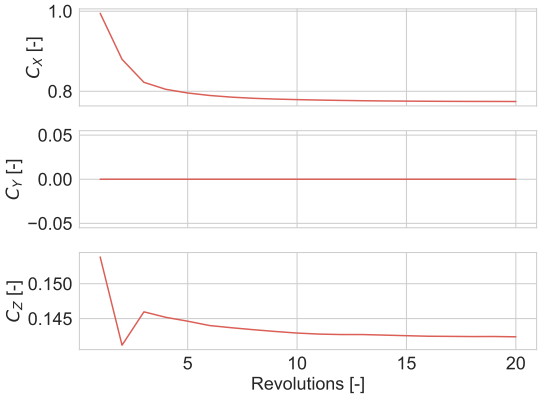

(b) Rotor loading coefficients C_X, C_Y and C_Z averaged over all blades.

Fig. 2 Revolution averaged results of the rotor for the reference case.

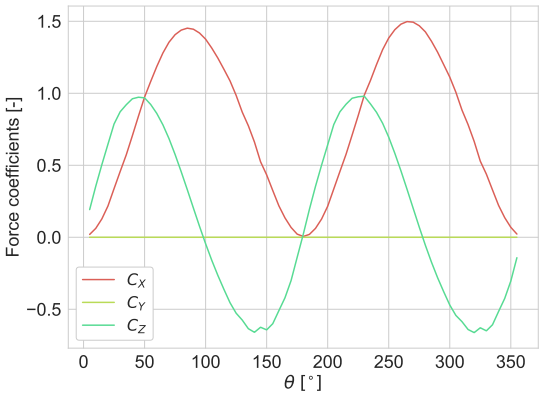

(a) Instantaneous loading coefficients C_X, C_Y and C_Z of rotor.

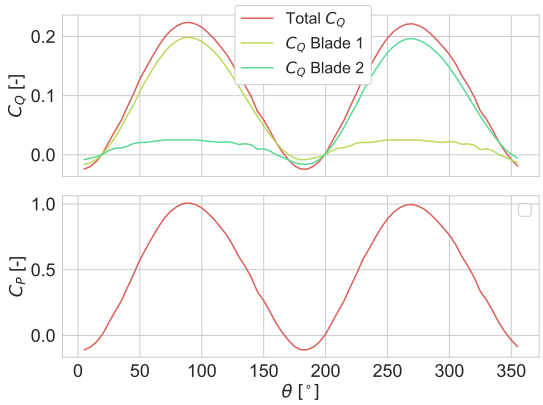

(b) Instantaneous C_Q contribution by blade and C_P by rotor.

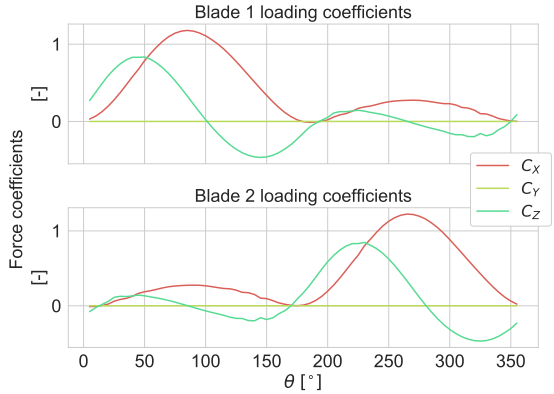

(c) Instantaneous loading coefficient C_X, C_Y and C_Z of blade 1 and 2.

Fig. 3 Plots showing instantaneous C_X, C_Y, C_Z and C_Q values of last revolution (reference case).

Diving deeper into the C_Q generation by a blade, figure 4 plots the rotor C_Q contribution along the blade. This is done element specific and across the full blade span. The blade spanwise coordinate in CACTUS are normalized such that the lower tip of the rotor blade is $Y/H = -0.5$, midspan $Y/H = 0.0$ and the upper tip $Y/H = +0.5$. As the blade elements along the blade span are placed with a cosine distribution. The blade elements at the tips have a smaller planform area S_e than midspan. As C_Q is normalized with reference to the frontal surface area S of the rotor instead of each element, the highest C_Q contribution is at midspan where the blade element is also the biggest. When going towards the tips, the C_Q contribution values drop.

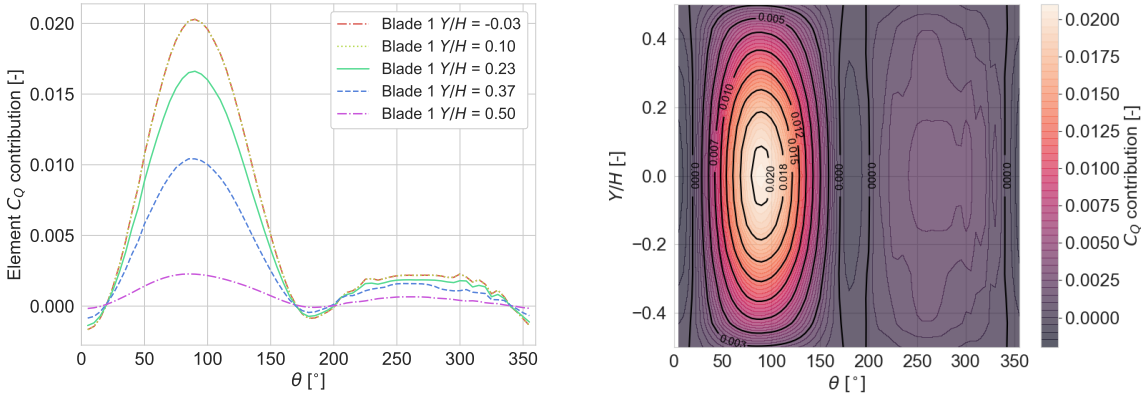

(a) The C_Q contribution per specific element.

(b) The C_Q contribution along blade span.

Fig. 4 C_Q contribution of the rotor blade along one revolution. Blade locations are defined such that $Y/H = \pm 0.5$ are the lower and upper tips and $Y/H = 0.0$ mid span. Note that the C_Q contribution is normalized to rotor frontal surface area instead of element surface area.

In figure 5, the loading coefficients on the span of the blade are specified in more detail. The C_L, C_D, C_T and α are shown. Note that the loading coefficients are normalized with respect to the blade element surface area. Typical for VAWTs are its varying α and loading coefficients as the blade make one full revolution. As expected due to the definition of α of the blade the loading coefficients and α are positive on the upwind part ($\theta = 0 - 180°$) and negative on the downwind part ($\theta = 180 - 360°$). In all plots of figure 5 the magnitude at the tips of the blade is larger than at the root. This is most notable at the downwind pass. This is due to one of the effects in 3D, the tip vortices which are generated at the tips. These vortices will lead to a higher absolute lift coefficient, but also causes induced drag effects. When the shape of the plot in figure 5c is compared to the one in figure 4b, it is expected that the increased C_T value at the tips would also lead to a larger C_Q at the tips. But this is not the case due to the way C_T and C_Q is defined. Although relatively seen, the C_Q should be larger at the tips but with the smaller size of the element at the tips, the total rotor C_Q value contribution by that element is small in absolute sense. If the C_Q contribution would be normalized with respect to the planform area of the element S_e instead of the frontal rotor surface S, the shape of figure 4b would match the one of figure 5c.

One remarkable effect to mention is the very slightly negative drag coefficient at the downwind pass of the blade. This would imply that instead of being a drag force, it becomes a small assisting force on the blade in the rotating direction, thus implying a slightly increased torque. While it is not expected, it is possible due to unsteady flow phenomena like dynamic stall as the drag force could become a small propulsive force when certain conditions are met[9]. Leishman and Beddoes discovered similar phenomena due to unsteady pressure drag with a helicopter rotor at the downstroke of their blade, when the angle of attack decreases quickly. The Mach number is similar to the turbine at the lower range. Similar events happen at the VAWT as in figure 5d the gradient on α is very high on the transition from upwind to downwind path. When using a flat plate airfoil ($c_l = 2\pi \sin\alpha$ and $C_D = 0$) with all unsteady effects turned off, $C_D = 0$ as expected with a flat plate airfoil in potential flow. One noticable effect is that the lift induced drag is not directly modelled by CACTUS. Even with $C_{D0} = 0$, one would expect a $C_{Di} \neq 0$ especially at the tips but this is not the case and can also not been found in the code. The drag seems to be fully dependent on the prescribed drag of a airfoil section and on effects due to unsteadiness.

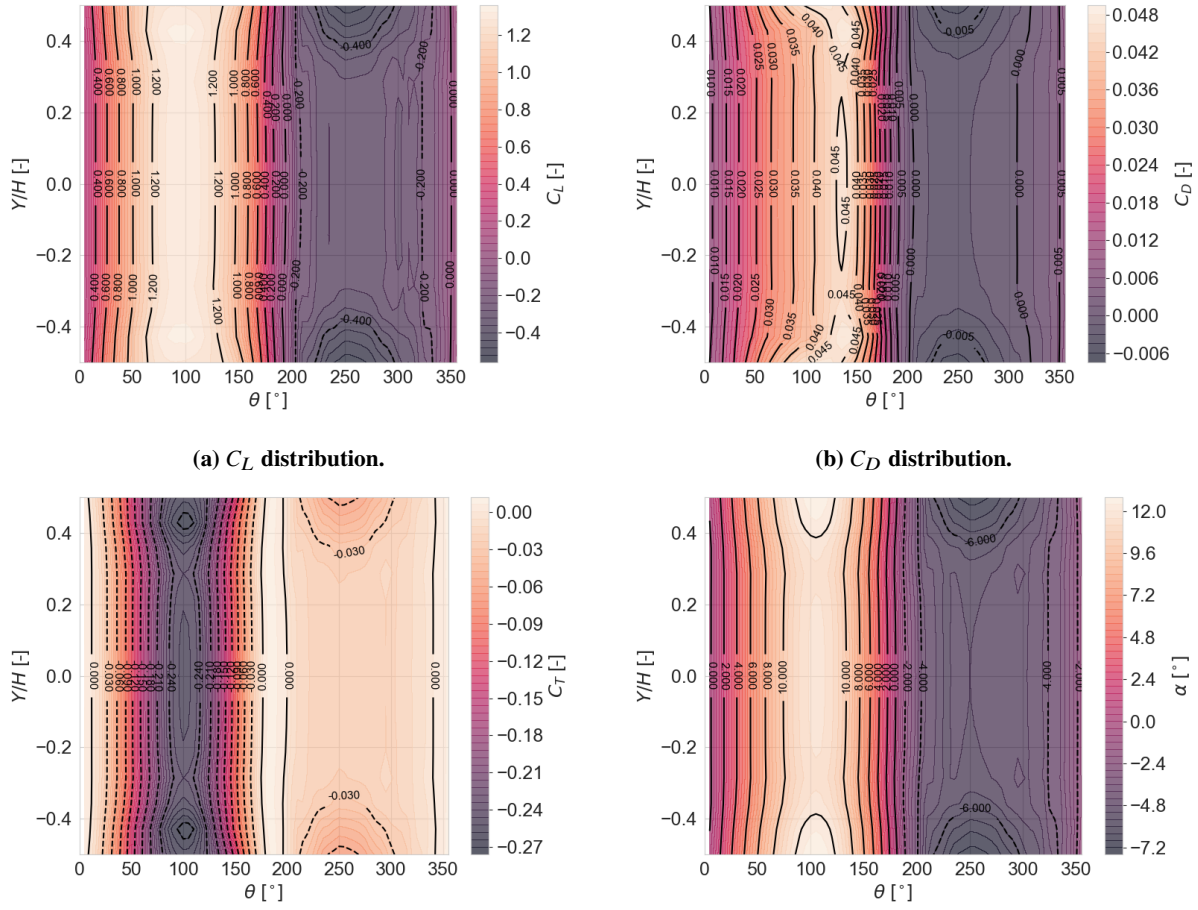

(a) C_L distribution.

(b) C_D distribution.

(c) C_T distribution.

(d) α distribution at quarter chord of blade.

Fig. 5 Blade spanwise C_L, C_D, C_T and α distribution along azimuthal position θ. Blade locations are defined such that $Y/H = \pm 0.5$ are the lower and upper tips and $Y/H = 0.0$ mid span.

Wake and velocity field

For this simulation the free wake has developed to 25 rotor radii downstream in the X-direction, but only part of the wake is shown for visibility reasons. Figure 6 shows the wake development from the blades with the black dashed lines marking the projected area of the rotor. As can be seen from figure 6a the rotor blade tips are at a position of $Y/R = 0$ and $Y/R = 2$ with midspan position being at $Y/R = 1$. From the topview perspective of figure 6b the tower is positioned at $(X/R, Z/R) = (0, 0)$. Finally a front view looking downstream is also shown in figure 6c. The wake is in 3D, but for the sake of clarity only the wake of one blade is plotted in different 2D perspectives. The plots from figure 6 show that the near wake is only symmetric in the Y-axis direction. The trajectories of the shed vortices in the wake are marked with different colors. The vortices formed at the tip of the blades (indicated with blue and orange) do not stay planar but expand in Y and Z directions. This causes the whole wake to expand downstream, becoming twice as large as the initial stage. Further downstream the shed vortices from the other elements start to interfere and mix with it, thus becoming fully turbulent. The tip vortices on the retreating side of the rotor are dispersed more than at the advancing side. These vortices at the tips cause the increased loading coefficients at the blade tips as found in figure 5. The wake trajectories of the midspan elements behave two dimensional and stay planar, expanding only laterally in the Z direction. When considering only the midspan wake trajectory in figure 7, the shape is comparable to the midspan wake simulated with the vortex method in the thesis of Tescione[19]. The midspan wake bends towards the advancing side of the rotor after several rotor radii meaning that the thrust of

the rotor is not fully aligned with the X-axis. Finally from figures 6b and 7 it is seen that the blades intersect its own wakes.

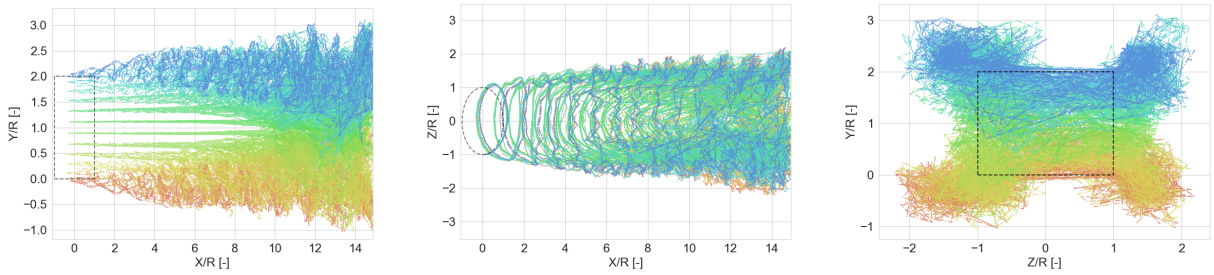

(a) Side view (X-Y plane). **(b) Topdown view (X-Z plane).** **(c) Front view (Y-Z plane).**

Fig. 6 Plot of the wake development by main rotor blade (reference case). All blade elements are indicated with different colors.

The velocity fields are presented for several planes of the 3D wake in figures 8 to 10. Each of the figures consists of three fields with velocities in the X, Y and Z directions indicated respectively by U, V and W. Figure 8 shows a slice in the $X-Y$ plane of the wake velocity field at $Z/R = -0.1$ near the center of the turbine, figure 9 shows the $X-Z$ plane at $Y/R = 0.89$ which is almost midplane of the rotor and 10 shows the $X-Z$ plane at $Y/R = 1.95$ which is at the tip of the rotor.
It can be clearly seen that the wake has a lower U velocity downstream of the turbine as the kinetic energy has been extracted from the flow. Figure 8 shows that the V and W velocities are not significantly affected until near $X/R = 7.5$ at which the V and W velocities will start to become significant while the low U area will start to contract. This indicates that the flow from the tips have mixed with the flow from the center of the rotor. Based on the positive and negative velocity patterns adjacent to each other it seems the far wake is fully turbulent from $X/R = 12$.

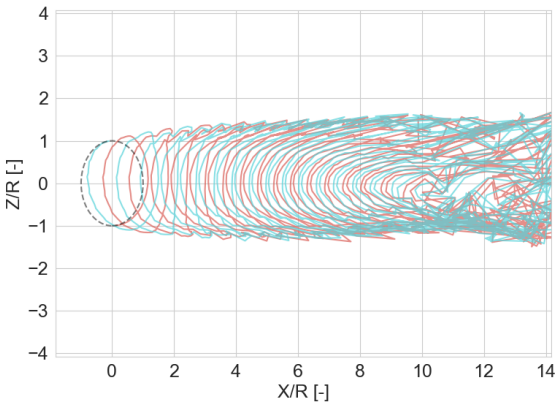

Fig. 7 Shed vortex trajectories mid span of both blades.

The velocity field in figure 9 showing the V component (velocity in Y direction) in the midplane is zero m/s. In the near wake at the rotor there are only significant U and W components. Thus there should be no spanwise flow in the mid span of the blades, therefore the flow behaves two dimensional in the midplane. From figure 10 the induced velocities caused by the tip vortices can be readily identified. To compare to figure 9, the blades' tips in figure 10 show a C-shaped area in the rotor where the V velocity component is positive in the outer part of the C-shape and negative in the inner part of the C-shape. This is the tip vortex generated by the blade as it is rotating. The velocity field W in direction Z shows that the wake expands laterally and is in accordance which what was observed in figure 6. Based on figure 9 the low velocity wake zone although expanding due to the decrease in velocity, do seem to pull towards right side based on freestream direction in accordance with what is found in figure 7. This is especially notable when looking at the tips of the rotor in figure 10 as the wake is recovering it deflects to the advancing side ($Z/R \leq 0$). This could be the characteristic of a clockwise rotating VAWT where the thrust vector is not fully aligned with the freestream. This is explained via figure 3a where the rotor C_Z is only zero at $\theta = 90°$ or every multiple of it. This indicates that there will be a non-zero force vector in Y direction and as consequence the resultant loading direction will not be fully aligned with the freestream.

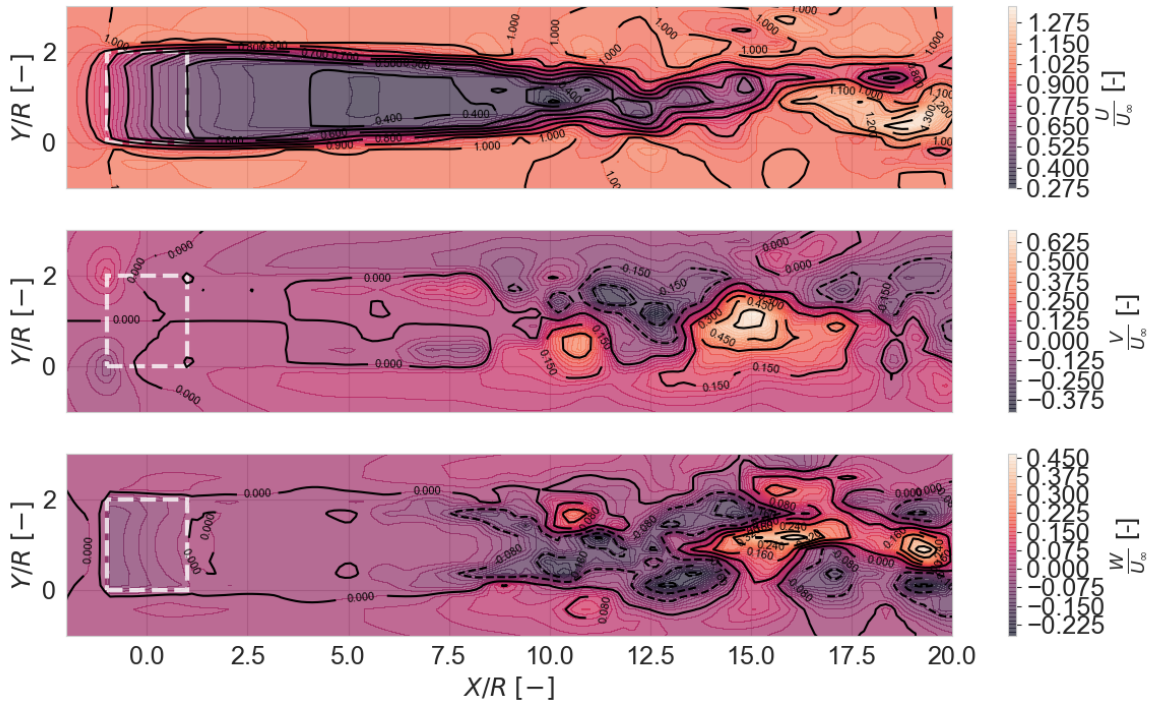

Fig. 8 **2D plot in $X-Y$ plane of the U, V and W velocity fields at $Z/R = -0.1$. Velocities are normalized with respect to U_∞.**

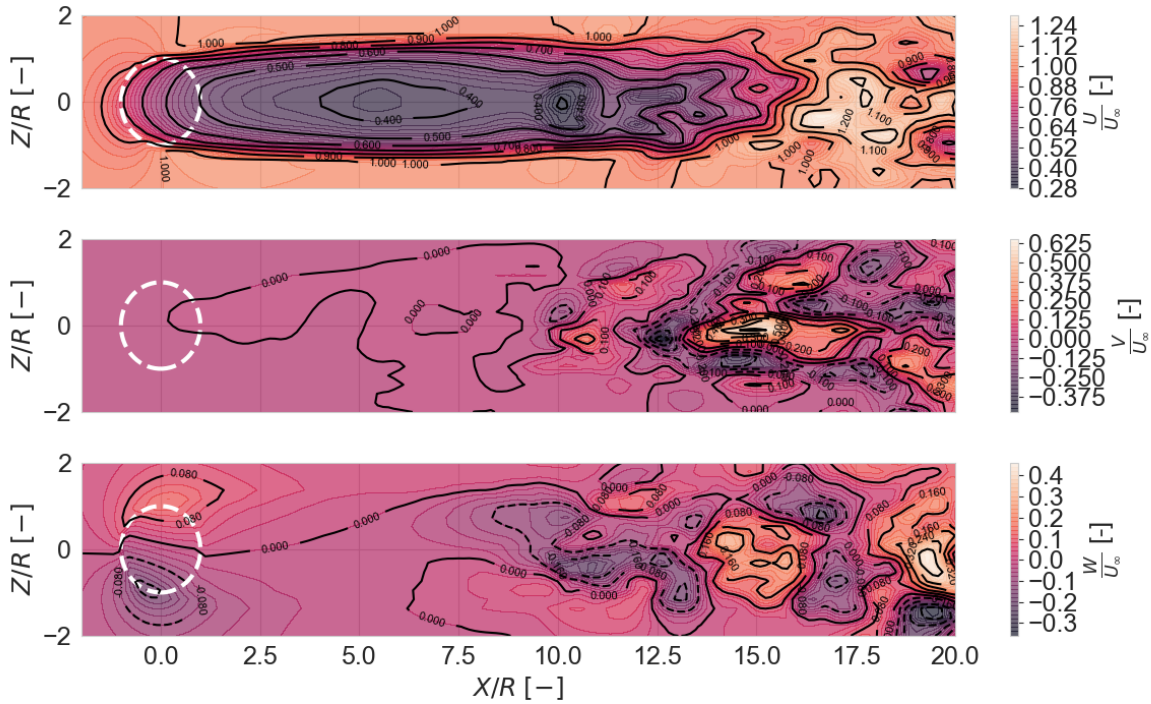

Fig. 9 **2D plot in $X-Z$ plane of the V and W velocity fields at $Y/R = 0.89$ (mid plane). Velocities are normalized with respect to U_∞.**

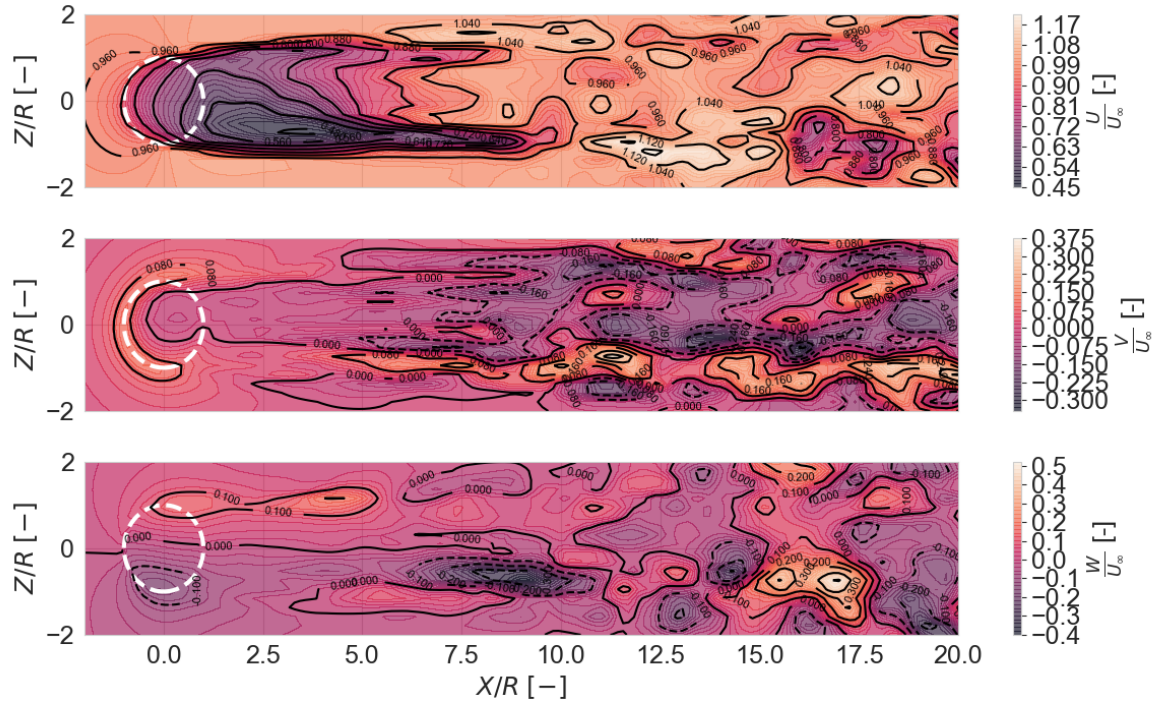

Fig. 10 2D plot in th $X-Z$ plane of the V and W velocity fields at $Y/R = 1.95$ (upper rotor tip). Velocities are normalized with respect to U_∞.

B. Effect of the strut tip vortex due to strut-blade gap distance

In the last section, tip vortices from the blade are seen in the results. This is a 3D effect and with the extended strut modelling, the struts should also shed tip vortices. These tip vortices can interfere with the main rotor blades and function as strut-blade junction interference. Therefore it is of interest to see if and how the tip vortices of the struts interfere with the rotor blades in their vicinity and how they affect the performances of the blades. The strut tip vortices should have the strongest effect when placed in the direct vicinity of the blades and vice versa. The same rotor of the reference case and its operating parameters were used again. But this time the struts are included with a gap ξ introduced between the tip of the strut and the attachment points at the lower and upper tips ($\epsilon = 0.0H$ and $\epsilon = 1.0H$) on the main rotor blade. By decreasing the distance between the strut's tip and blade, it can be seen what happens when the tip vortex generated by the strut is brought closer to the blade. It is expected that the induced vortex from the strut's tip interferes with flow on parts of the blade. The struts attachment point to the blade will be on the tips of the blade, therefore an influence of the blade's tip vortex is to be expected on the strut. The struts are uninclined and have a constant pitching angle ψ of $\pm 10°$ depending on whether the struts are on the top or bottom of the rotor. This is to artificially increase the bound vortex strength of the strut and thus it becomes easier to analyse the variations in ξ. Figure 11 shows the relative distance of this gap and consequently the decrease in rotor C_Q, C_X, C_Y and C_Z with decreasing ξ. Note that these values are normalized to the (strutless) reference case and that the gap is indicated as fraction of the rotor radius R. Remarkable observation is that $C_Q/C_{Q,ref} > 1.0$ at $\xi \geq 0.38R$ and this is not expected as this means that a small unattached strut body near the vicinity of the tower would improve the performance compared to a strutless turbine. Figure 11b indicates that this could be due to the increase in thrust coefficient C_X. Note furthermore that at $\xi = 0.0R$ the $C_Q/C_{Q,ref} = 0.85$ implying that the attached struts are causing a loss of 15%. But this value is in reality lower because the struts' pitching angles are artificially increased with 10°. With unpitched struts, the bound vortex strengths of the struts were to small to notice anything. The rotor components are split up into struts and blades for which the C_X, C_Z and C_Q are plotted in figure 12. The plots in the figure show that strut C_Q becomes more negative with smaller ξ or higher strut aspect ratio, stating basically that the strut is just a drag body deteriorating power generating capacity of the rotor. It is interesting to see though that at $\xi = 0.5R$ the $C_Q \approx 0$ and that this decrease is non-linear towards $\xi = 0$. This could either mean that the aspect ratio affects this non-linear decrease in C_Q

or it is the blades' tip vortices interaction with the strut. A more in-depth analysis will be conducted to determine the cause.

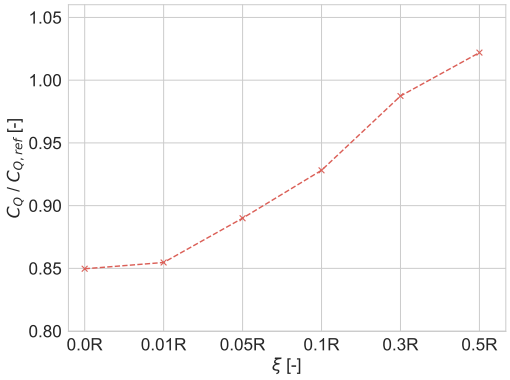

(a) Revolution averaged torque C_Q coefficient normalized to reference case

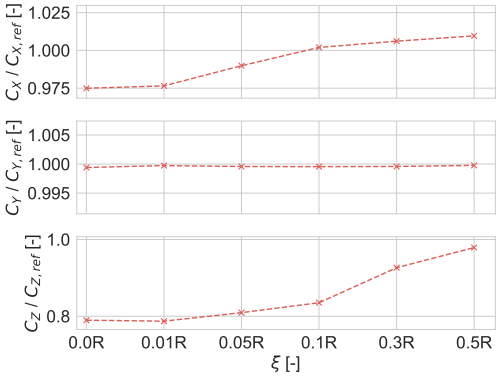

(b) Revolution averaged loading coefficients C_X, C_Y and C_Z normalized to reference case

Fig. 11 Rotor C_X, C_Y, C_Z and C_Q comparison for varying ξ

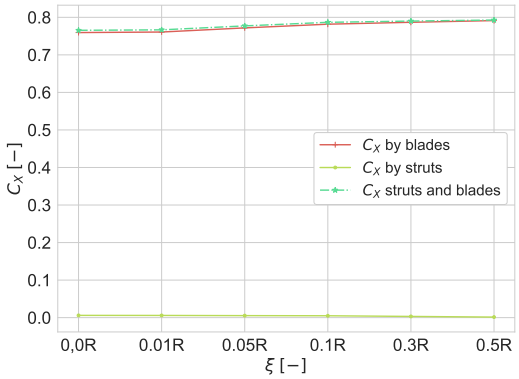

(a) C_X. Note that the red and cyan lines overlap each other.

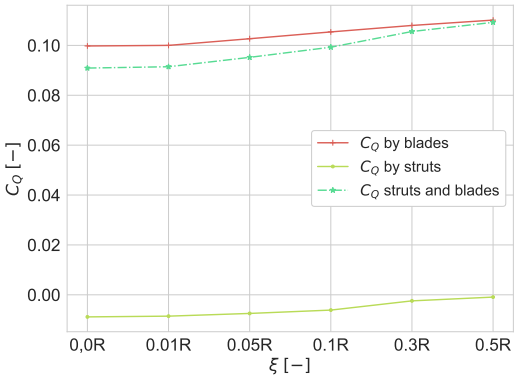

(b) C_Q

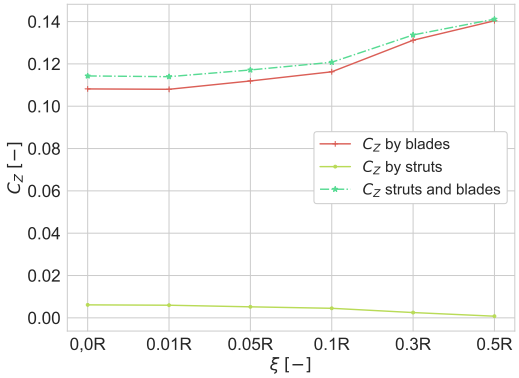

(c) C_Z

Fig. 12 Loading coefficient contributions by strut and blade for varying ξ

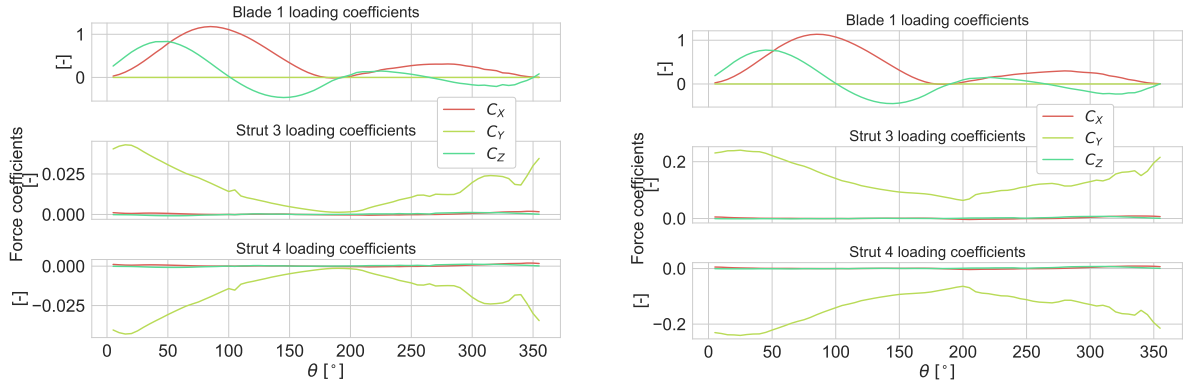

(a) $\xi = 0.5R$ **(b)** $\xi = 0R$

Fig. 13 Blade or strut loadings of last revolution at $\xi = 0.5R$ and $\xi = 0.0R$

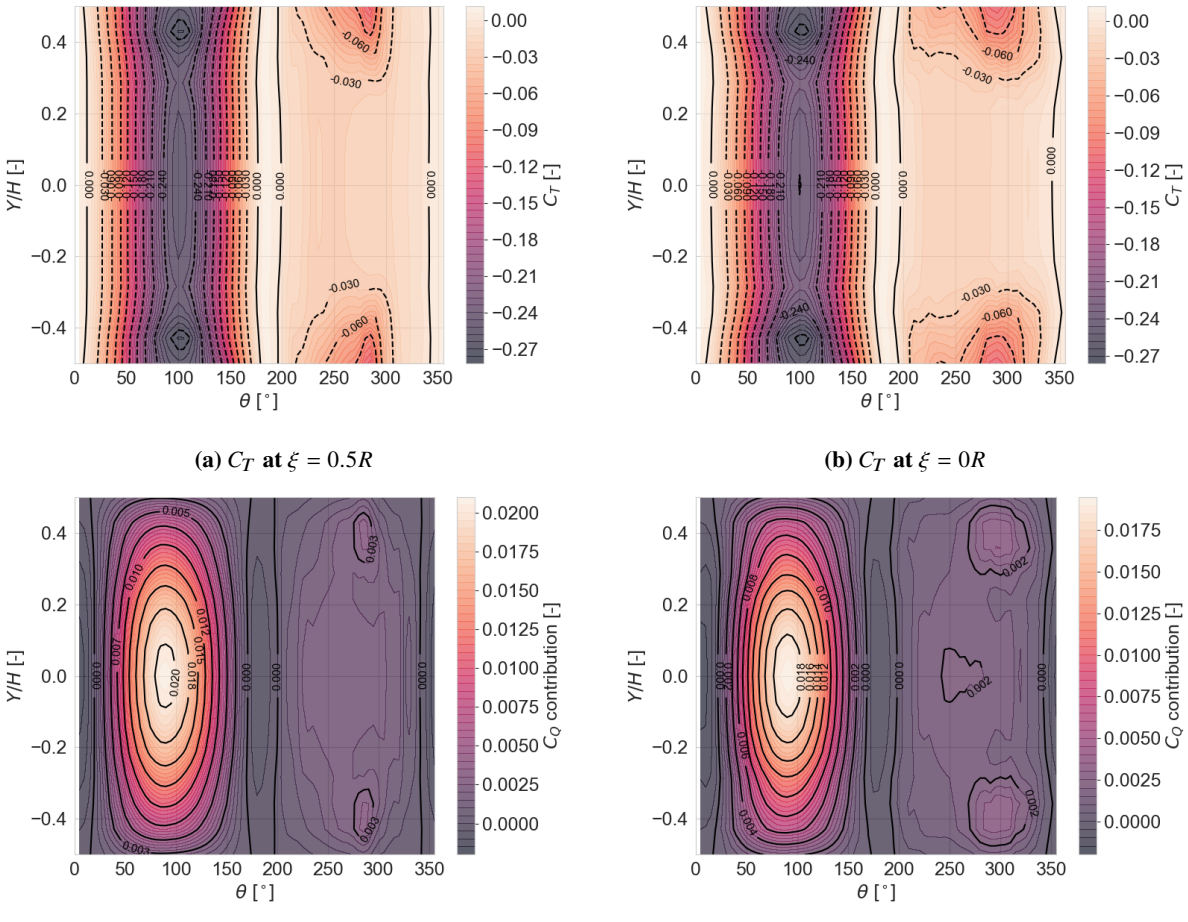

(a) C_T **at** $\xi = 0.5R$ **(b)** C_T **at** $\xi = 0R$

(c) C_Q **at** $\xi = 0.5R$ **(d)** C_Q **at** $\xi = 0R$

Fig. 14 C_T and C_Q distribution along blade span against θ. Blade locations are defined such that $Y/H = \pm 0.5$ are the lower and upper tips and $Y/H = 0.0$ mid span.

For the main rotor blades it is clear that the cause of variations in C_X, C_Z and C_Q must be due to the struts' tip vortices interfering with the blade. No other design or operational parameter of the blade changes, only the strut length is varying. As the gap ξ closes, the blades' C_X, C_Z and C_Q decrease slowly between $\xi = 0.5R$ and $\xi = 0.1R$. But between $\xi = 0.1R$ and $\xi = 0R$ the drop rate increases. The induced velocity field from the tip of the strut starts to interfere more with the blade as expected. Only once the gap ξ is smaller than 10% of the turbine radius the interference becomes noticeable. These blade strut interference as consequence lead to lower C_X, C_Y and thus lower C_Q for the blade. The struts' C_X and C_Y increase due to the increased aspect ratio of the strut, but in the net impact is negative on its C_Q. These variations in all kind of loadings besides the C_D indicate that the application of the lifting line model on the struts functions as the original model of struts in CACTUS should not be able to shed vortices.
The blade and strut C_X, C_Y, C_Z along one revolution are plotted in figure 13 for few ξ values. The blades' C_X and C_Z drops from figure 12 are too small to be visible on this scale as the drop in C_X amount to approximately $4-5\%$ between $\xi = 0R$ and $\xi = 0.5R$. Only the variation of C_Y can clearly be seen, but this is only non-zero for the struts. Figure 14 shows the blade's C_T and C_Q distributions. The struts interference with the blade is mainly in the downwind pass at the tips. Note that the C_T variations at the tips is still mainly due to its own blade induced tip vortex. With the strut closing in at the blade, the area affected in the plots expands. While the trends are visible, the C_T and C_Q values do not change much. This can be due to the strut's configuration, but the main point is that blade strut interaction with the method functions.

C. 3D effects with varying tip speed ratio λ

In the last section it was found that the strut can be effectively modelled using the same lifting line method already applied to the main rotor blades. In this section the full rotor is modelled with the struts spanning the full radius of the rotor and with a pitching angle of $\psi = 10°$ introduced for the struts. The full rotor will be subjected to varying tip speed ratios λ beside its default $\lambda = 4.5$. As the angular velocity is kept constant to 37 RPM, this means that the freestream velocity and Reynolds number will change up to factor 2 for varying λ. For clarity these operational parameters are given in table 4.

Table 4 Operational parameters

λ	3.0	3.5	4.0	4.5	5.0	5.5	6.0
U_∞	18.08 m/s	15.50 m/s	13.56 m/s	12.05 m/s	10.84 m/s	9.86 m/s	9.04 m/s
Re	17.3E6	15.0E6	13.0E6	11.5E6	10.4E6	9.4E6	8.7E6

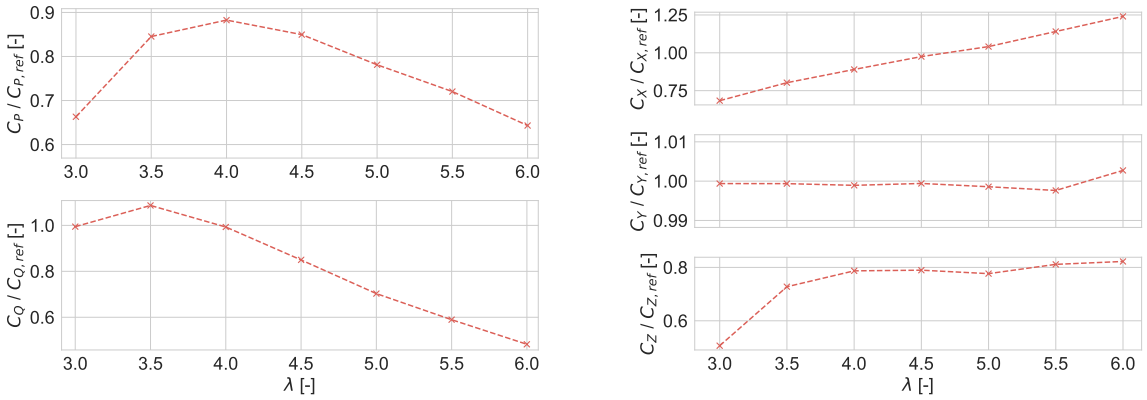

(a) Power C_P and torque C_Q coefficients along λ, normalized to reference case.

(b) Revolution averaged loading coefficients in X,Y and Z direction. Coefficients are normalized to reference case.

Fig. 15 Average performance data comparison between all subcases of case C.

In figure 15 the performance indicators are compared for different λ. Notice at figure 15a the typical $\lambda - C_P$ curve

of an VAWT with the plot normalized to the reference case at $\lambda = 4.5$. It seems that the C_Q drop is large at higher λ. The lowest C_P loss compared to the reference case would be at a tip speed ratio of $\lambda = 4.0$ with a loss of around 12% from figure 15a. Thus the optimal tip speed ratios for cases including struts would still be at lower λ values. The C_X and C_Y contributions of the struts are negligbly small throughout the whole simulated λ range with only the side loading C_Z increasing, and this coincides with the eventual decrease in C_Q by the struts based on figures 16b and 16d. The wake can also be expected to be more skewed at higher λ.

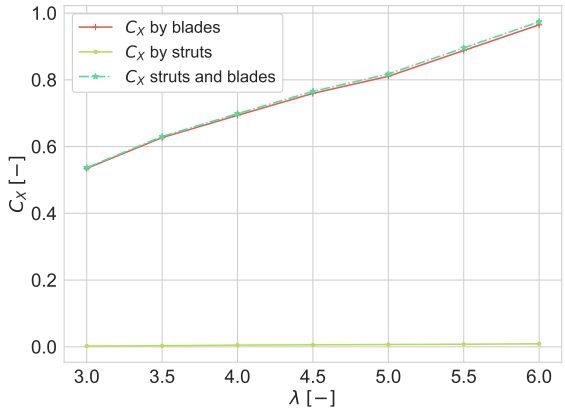

(a) C_X contribution by blade and strut against λ. The cyan and red lines overlap as the contribution is mainly from the blades.

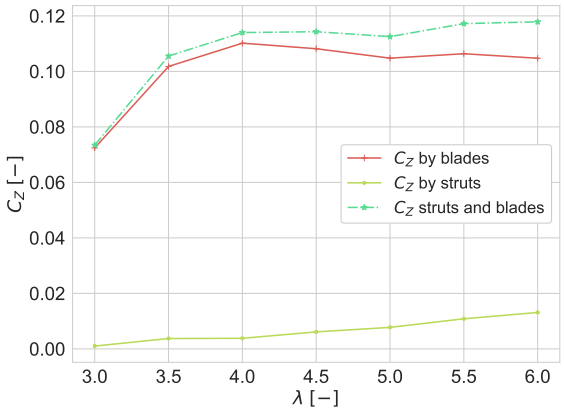

(b) C_Z contribution by blade and strut against λ.

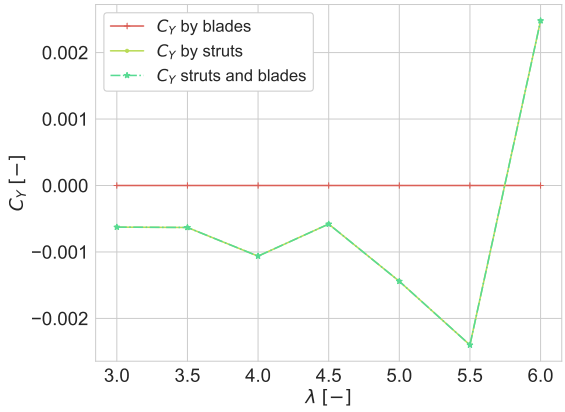

(c) C_Y contribution by blade and strut against λ. The cyan and green lines overlap as the contribution is mainly from the struts.

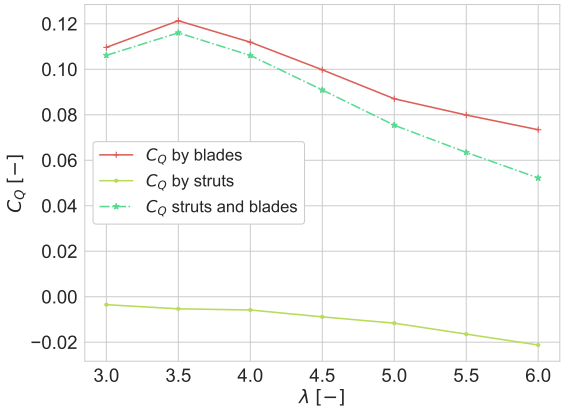

(d) C_Q contribution by blade and strut against λ.

Fig. 16 Separated blade and strut C_X, C_Y, C_Z and C_Q contributions for varying λ.

Higher tip speed ratio also makes the simulation more unstable to converge on C_P. Figure 17 shows the instantaneous C_Q of one blade and one strut for different λ values. The other blade and struts have the same trend but with a phase shift of 180°. A lower λ will give a more slender C_Q peak in the upwind phase (0°-180°) for the blade but also a moderate C_Q peak along the whole downwind phase (180°-360°). As the λ increases, the maximum C_Q peak value in the upwind phase decreases and the C_Q peak widens along the whole upwind phase. In the downwind phase the overall torque generating capacity will be lower and in the strut's case becoming more negative. Most of the torque generated will then be focused in the upwind part. Torque generation will also become (more) negative at the transition points between upwind and downwind and vice versa.
For the struts the instantaneous C_Q will be slightly negative along the whole revolution for low λ but with the increments

in λ the downwind phase of the struts starts to generate more negative torque in the downwind pass. The shape of the C_Q cycle remains similar along all λ values, but the difference in C_Q can be a factor 3.75 between $\lambda = 3.0$ and $\lambda = 6.0$ in the downwind phase. Coupled with lower C_Q values at the downwind phase for a blade, the strut design can become very dominant for the performance of the full rotor. The C_Q value of the strut is initially very low relative to the blade C_Q but at higher tip speed ratios the C_Q contribution from the strut can be as high as 25% of the blade. Thus at higher λ the struts cannot be neglected in the design of a VAWT.

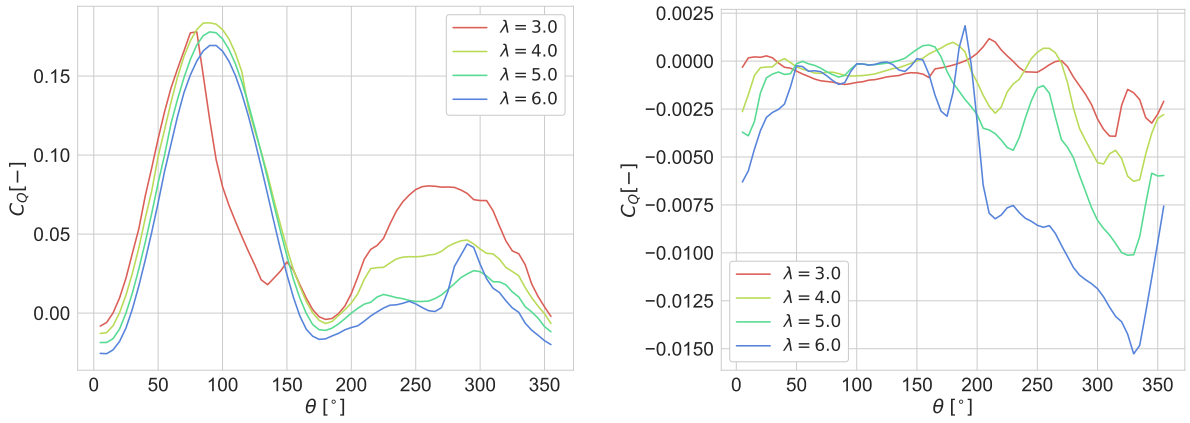

(a) Blade C_Q. **(b) Strut C_Q.**

Fig. 17 Instantaneous blade and strut C_Q contributions for varying λ.

D. Effects due to varying strut-blade interconnections

In the fourth case the focus will be put on the position of the strut. From case B it was inconclusive how the blade's tip vortices would affect the struts. Thus in this case the focus would be put on the consequences of interference effects on the strut. Until now the struts were always attached at the tip of the blades. But it is of interest to understand what will happen when the strut will be positioned more towards the root of the main rotor blade. As such the strut attachment position to the blade ϵ will be varied between $\epsilon = 0.5H$ (root) and $0H$ or $1.0H$ (lower or upper tips) based on whether its the lower or upper struts. The struts are neither inclined or pitched, thus the bound vortex strength on the strut should be very low. But it is expected that if the struts are shifted towards from the root to the tip of the blade, the induced velocities from the blade's tips will actually create a down or upwash on the strut and thus a change in its angle of attack α therefore some loadings should be detected on the struts.

From figure 18 it can be shown that the contribution to the rotor C_Q by the struts is marginal, which was expected. But nonetheless it does show based on figure 18 that the shift of the struts towards the tip does something to the struts performance although the effects are not significant. The strut's tip vortex strength should be very small thus any change to the struts loading should be caused by the blades. The strut's C_X, C_Y and C_Z are analyzed for different ϵ values in figure 19. The C_X and C_Z do not change but with the decrease in ϵ (shift of the struts towards blade tips), the induced velocites from the blade tip vortex causes a loading in the Y direction. Thus the downwash should be causing an induced angle of attack on the struts. Please note that the plots, especially at higher ϵ, show numerical errors as the values are really small. This can be seen by the strange unexpected peaks for example at $\epsilon = 0.5H$ the C_Y is expected to be zero but some numerical errors can be seen in the peaks. Furthermore note that with the subcase of $\epsilon = 0.5H$, the upper and lower struts of each blade is replaced by a single strut midspan of the blade. Thus struts 3 and 4 from figure 19a are the only struts in the rotor.

The effects of the downwash on the struts by the blades can be seen by the angle of attack α distribution on the struts for varying ϵ. In figure 20 these α distributions of $r/R \geq 0.3$ are plotted for the same four situations of figure 19. Note that the Y/H position of the strut matters as the angle of attack is different for every ϵ. As expected at $\epsilon = 0.5$ in the center between the two tips, the α on the strut is zero. As the strut are positioned towards the tips, the downwash starts to cause an induced angle of attack on the strut. At $\epsilon = 0.1$ the angle of attack is on the order of $\pm 1^\circ$ and at will be at a maximum at $\epsilon = 0.0$. The angle of attack is not uniformly distributed along the blade but varies along the full span and also for

each azimuthal angle θ.

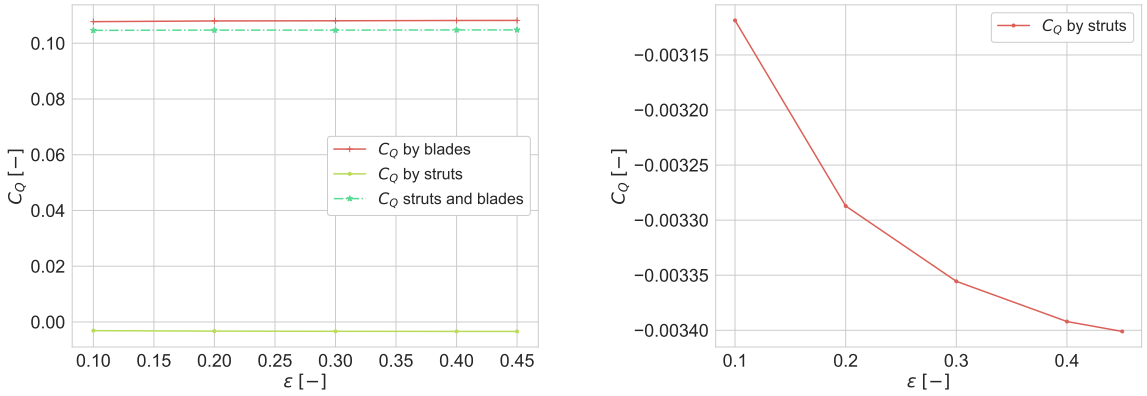

(a) Blade C_Q. **(b) Strut C_Q.**

Fig. 18 Instantaneous blade and strut C_Q contribution for varying ϵ.

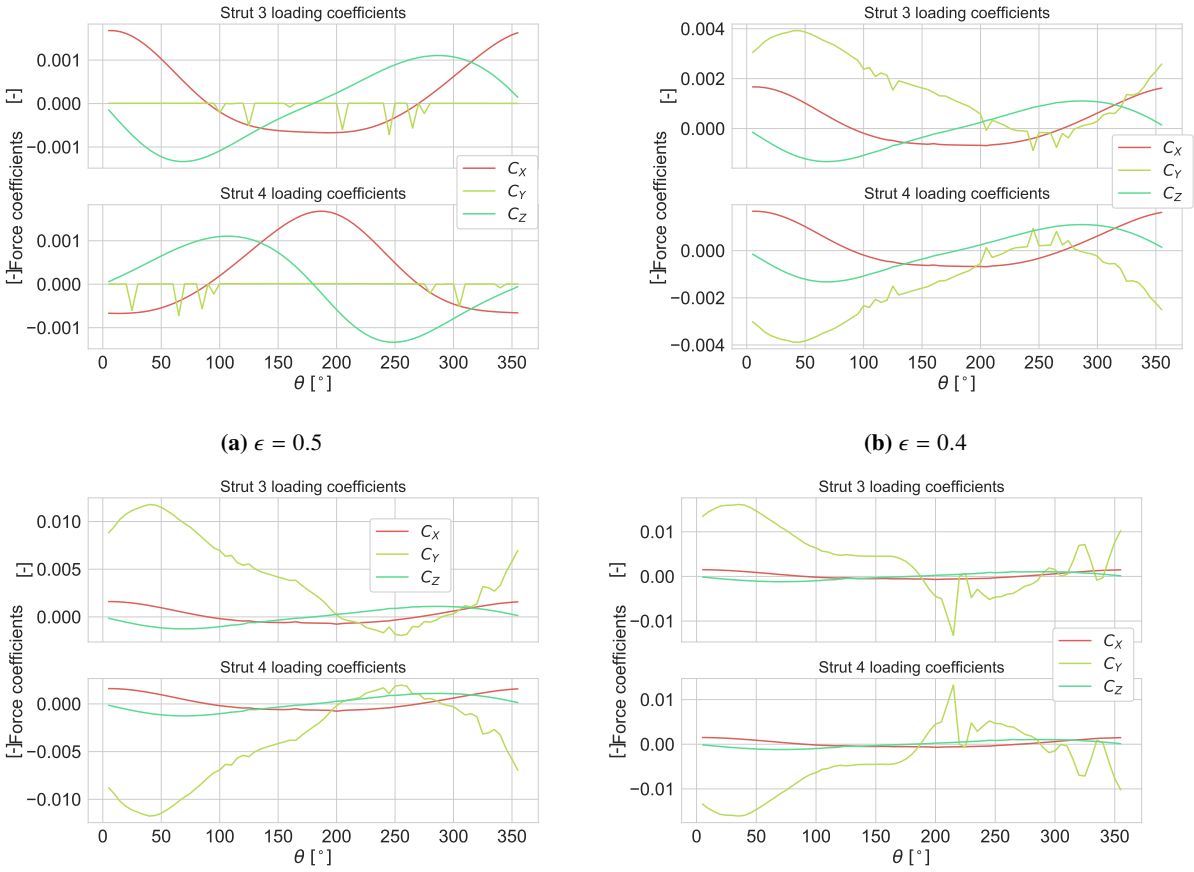

(a) $\epsilon = 0.5$ **(b) $\epsilon = 0.4$**

(c) $\epsilon = 0.2$ **(d) $\epsilon = 0.1$**

Fig. 19 Strut C_X, C_Y and C_Z values against θ for different ϵ.

In general it can be observed that this angle is the highest upwind and lowest or even slightly negative downwind. The main rotor blades' vortex strength is the highest upwind and thus induces the strongest downwash at that phase. This is also supported by observations from figure 19 where the C_Y is positive upwind and near zero downwind. All the lift generated from the strut is not used effectively for power generation this way as the lift vector is pointed towards the blade's spanwise direction Y. Therefore the low C_X and C_Z of the struts do not really benefit the rotor's torque generating capacity. But for the application of the lifting line model on the struts these plots show that CACTUS can model the interference of the main rotor blades on the struts.

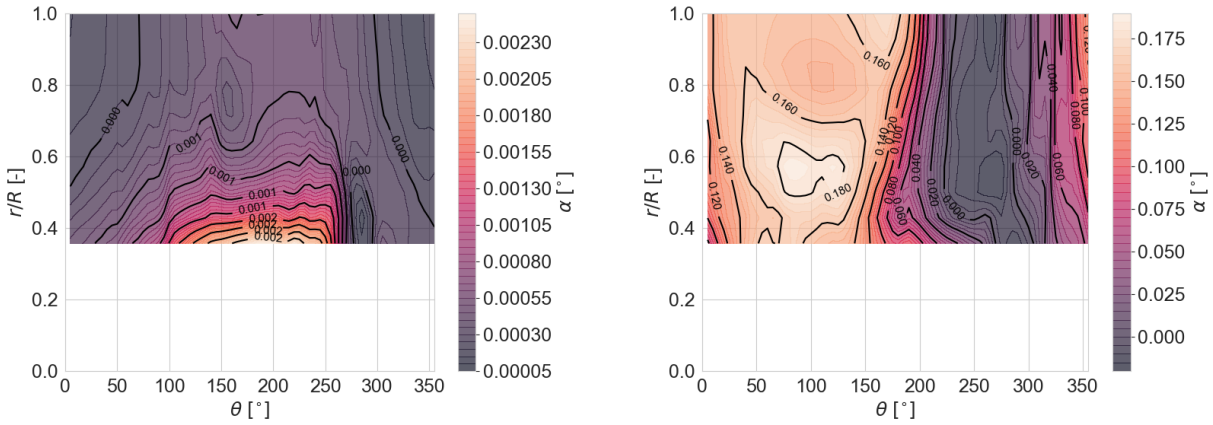

(a) $\epsilon = 0.5H$

(b) $\epsilon = 0.4H$

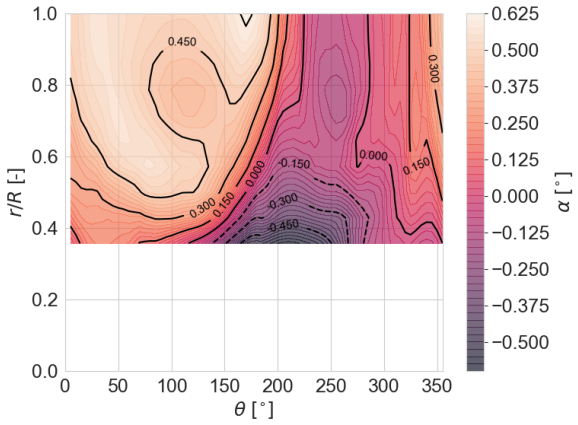

(c) $\epsilon = 0.2H$

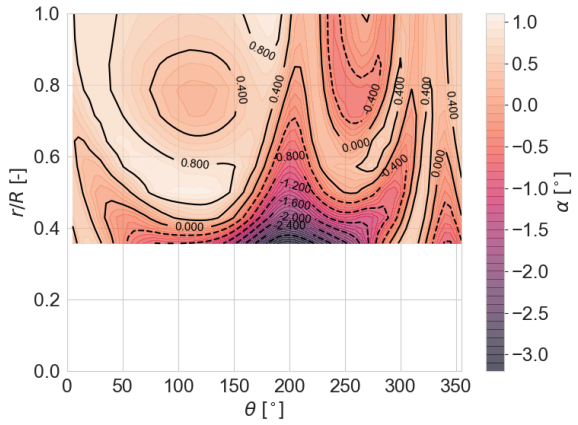

(d) $\epsilon = 0.1H$

Fig. 20 α **distribution along strut span against** θ **for different** ϵ**. Strut locations are defined such that** $r/R = 0.0$ **is at the root of the strut and** $r/R = 1.0$ **at the tip.**

E. Varying the inclination angle ϕ

Rotor and blade analysis

This section has the goal to gain understanding in how struts contribute to the rotor performance as they are placed under an inclination relative to the blades. In theory this leads to an increased α of the struts and generate meaningful lift, which can lead to positive torque contributions by the struts. It is therefore of interest to compare the average performance values of VAWT with different (symmetrical) inclination angles settings described in table 2 and is shown in figure 21. All the simulations have been performed at $U_\infty = 12.05m/s$ and $\lambda = 4.5$. The Reynolds number of the turbine is approximately $Re = 11E6$ for all cases. The set of simulations with varying ϕ was ended after twenty revolutions and the dynamic stall model was based on the Leishman-Beddoes model. Another set of simulation was made without the use of dynamic stall modelling and using flat plate airfoil in a inviscid flow. In earlier trials it could be seen that all simulations tend to converge in 10 to 12 revolutions. The average rotor loadings also takes into account the loadings caused by the struts as seen in figure 21b. It seems that with a higher inclination, the torque and power coefficients drop while the rotor loadings increase. This drop is at first low for small angles but at higher ϕ the drop in torque and performance becomes non-linear with ϕ shown in figure 21a. In the viscous case, an odd anomaly is found at and around $\phi = 15°$ where the C_P suddenly drops before recovering. Furthermore the thrust coefficient C_X seems to not increase at that same point. This anomaly disappears again at higher ϕ. In the same figure the same comparison is made but with a flat plate blade profile and without any dynamic stall modelling. Here the C_P also drops with greater ϕ but the decline is smaller, due to the exclusion of any form of drag. Also the anomaly found at specific angles is not present anymore. Compared to results seen in the paper of Siddiqui et al[16], the drop in performance in the case of using the NACA0018 airfoil is low when the struts are uninclined. Of course the situation here is different as the airfoil is thinner than the one used in [16] and the solidity is also lower. Also in their research, the simulation method is has a higher fidelity and includes more flow effects than the vortex method would do. This could explain why their comparison between the inclusion and exclusion of struts leads to a difference of 6% in C_P while in this paper it is less than 1%.

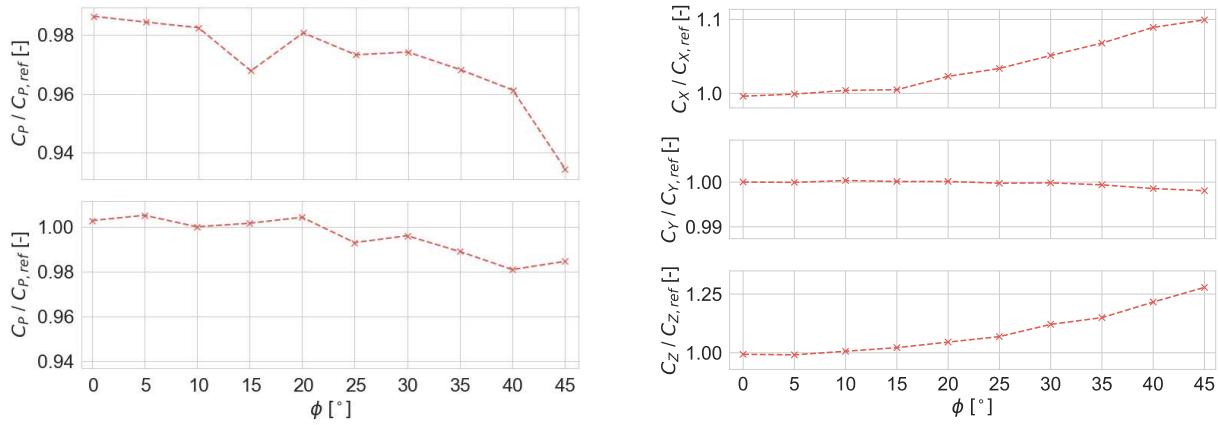

(a) C_P coefficients with varying ϕ: version using Leishman-Beddoes Dynamic stall and using NACA0018 (above) and inviscid case without dynamic stall (below). Normalized to reference case 0.

(b) Rotor loading coefficients in X,Y and Z direction (version using dynamic stall and NACA0018 airfoil).

Fig. 21 Average C_P, C_X, C_Y and C_Z comparison with varying ϕ.

Figure 22 shows the C_X,C_Z and C_Q coefficients against varying ϕ. The plots' total C_X, C_Z and C_Q contributions by all struts and blades should have the same shape as in figure 21. Please note that the coefficients are not normalized in the figure, so the values are the absolute values. The total loading coefficients (C_X, C_Z or C_Q) are split up in the contribution by the blades only and contribution by the struts only. For the case in figure 22a which uses a NACA0018 airfoil, with $\phi = 0°$ the C_Q contributions of the struts are slightly negative due to the profile drag of the struts. This is expected as these struts are just drag bodies counteracting the torque generating rotor blades. With increasing ϕ the

struts are actually producing positive torque contribution but at the same time the C_Q contribution by blades falls by a similar margin, thus counteracting the benefits of the inclined struts. Eventually the gain in C_Q contribution by the struts with inclination is lower than the loss by the blades. As consequence the total C_Q contribution (and thus C_P) by all blades and struts just drop slightly with increasing ϕ. The increase in strut C_Q contribution must be caused by the small extra angle of attack α of the strut introduced by the inclination. The strut has a lift vector inclined by ϕ relative to the rotational plane of the struts. Only a part of this lift vector is aligned with the lift vector of the main rotor blade. This part will positively contribute to the extra torque for power generation. Figures 22c and 22d indicate that the increase in rotor C_X and C_Z is fully caused by the struts. The C_X and C_Z contribution by the main rotor blade actually drops up to 0.13 respectively 0.015 at an ϕ of 45°. This while the total rotor C_X and C_Z still increase because the contributions by the struts increases severely by 0.21 and 0.058. Based on these values the conclusion would be that the thrust vector of the rotor would be less aligned with the freestream due to the presence of the struts. This will result in a more deflected wake and less effective power producing struts.

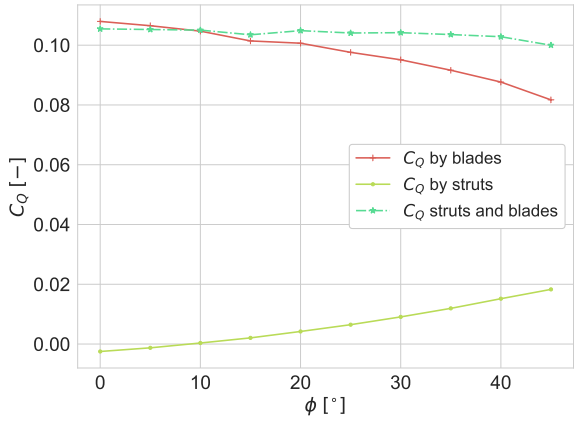

(a) C_Q with varying ϕ using NACA0018 airfoil.

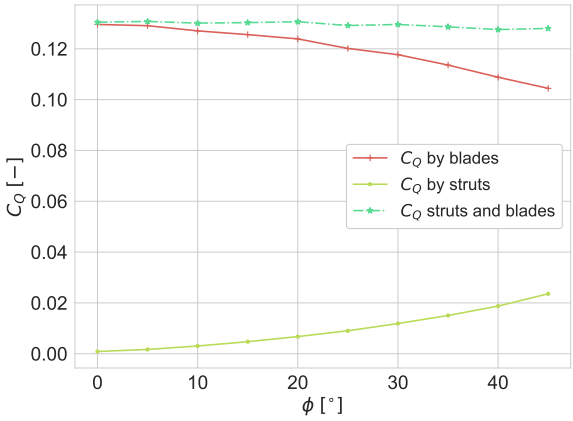

(b) C_Q with varying ϕ using flat plate airfoil.

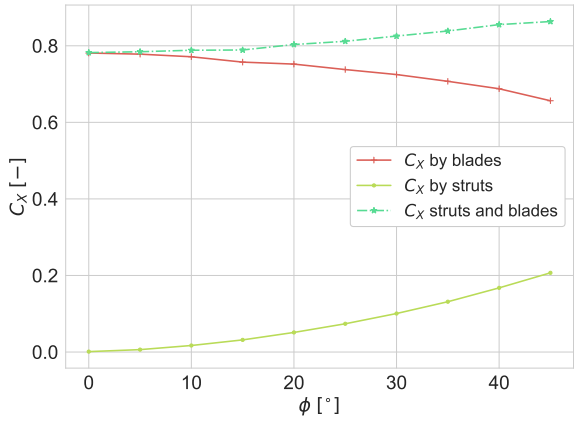

(c) C_X with varying ϕ using NACA0018 airfoil.

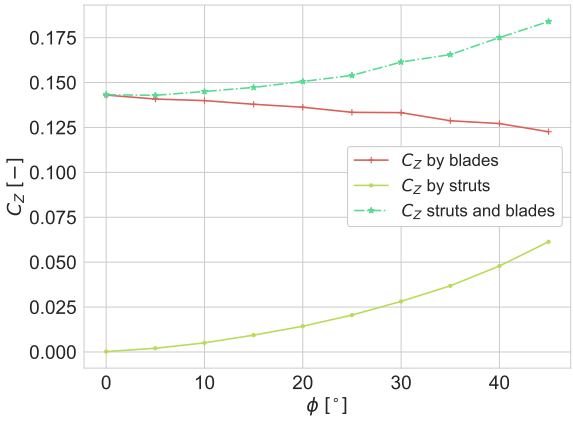

(d) C_Z with varying ϕ using NACA0018 airfoil.

Fig. 22 C_X, C_Y or C_Q contribution by parts with varying ϕ.

The instantaneous loadings of the last 360 degrees are plotted in figure 23 as this can show exactly where the decrease or increase in torque (and thus power) occurs. As seen in the figure, the increase in the amplitude of the loadings are mainly at the peaks where the instantaneous power coefficient is also on its highest point. How all these changes affects the torque and the power can be concluded from figure 24. In the same figure it can be seen that the increase in strut inclination, which leads to the increase in strut C_Q contribution, is only visible in the upwind phase of

the rotation. Only the first blade and the adjoint upper and lower struts are shown here for clarity purposes. On the downwind side the C_Q due to the strut is negligibly small. What also happens due to the interference of struts is the drop in C_Q by the blade in the upwind and downwind phase. Especially in the downwind phase the second torque peak of the rotor blade collapses and the shape of the plot changes severely compared to the upwind part. This explains the lower C_P peaks of figure 23b and also why the rotor blades itself will have lower C_Q at higher ϕ (figure 22).

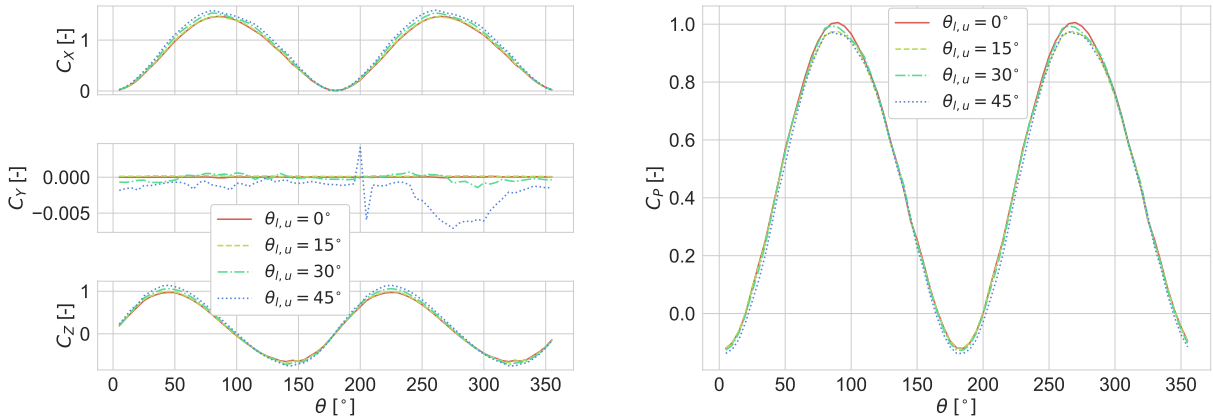

(a) Rotor loading coefficients C_X, C_Y and C_Z.

(b) Instantaneous C_P by rotor

Fig. 23 Instantaneous C_X, C_Y, C_Z and C_P plot for varying ϕ.

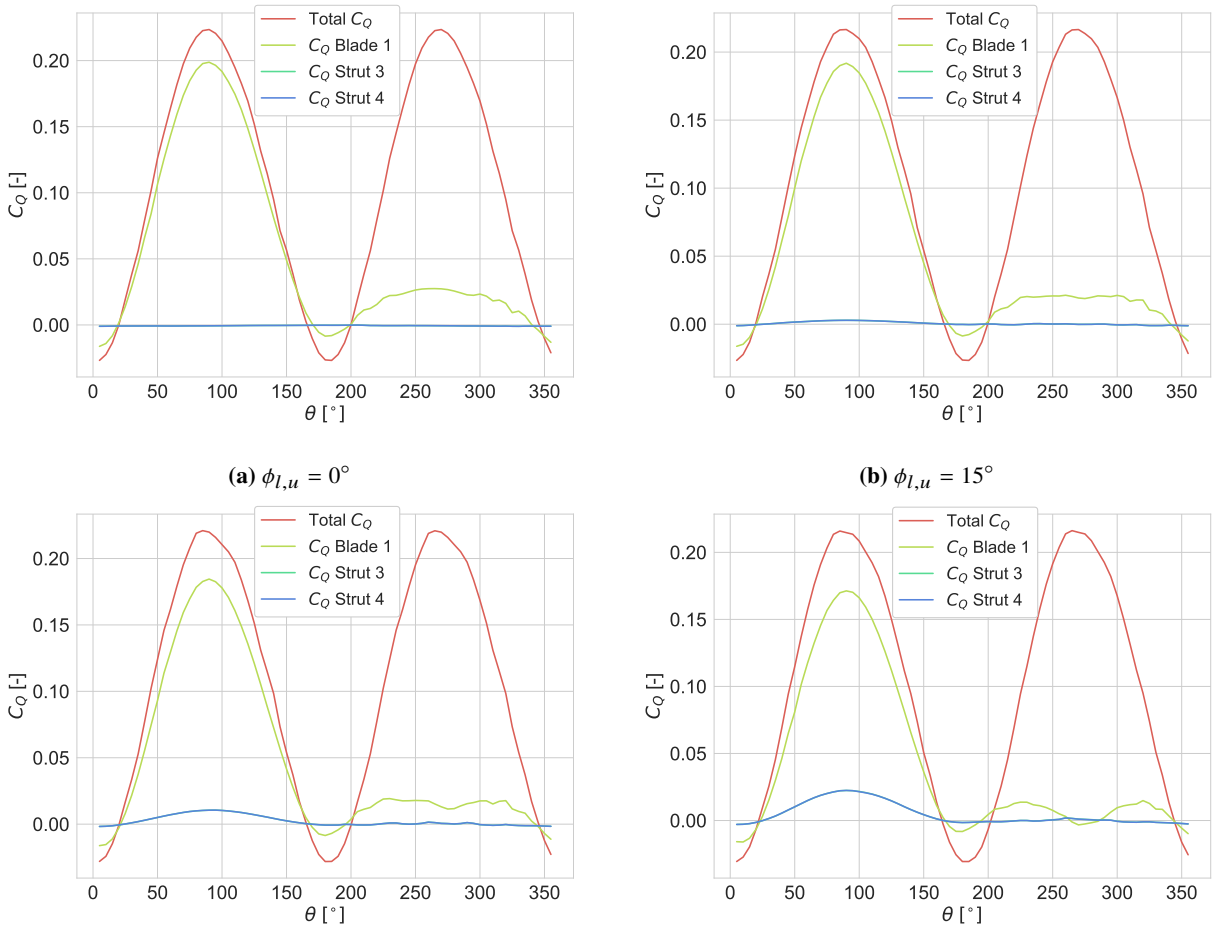

(a) $\phi_{l,u} = 0°$ **(b)** $\phi_{l,u} = 15°$

(c) $\phi_{l,u} = 30°$ **(d)** $\phi_{l,u} = 45°$

Fig. 24 Blade and struts contributions to instantaneous rotor C_Q of case A. Note that the upper and lower struts C_Q (cyan and blue lines) overlap each other.

Figures 25a to 25d show the loadings of the different blades and struts in different configurations of case A. Only blade one and the connected upper and lower struts are shown. Notice that the upper and lower struts always show opposite loadings in the Y direction as the struts are inclined. With the main rotor blade loading in Y direction also being zero, the net loading in rotor spanwise Y direction should be near zero. For the struts in general, the loadings are small compared to the main rotor blades. But the in-rotor plane loadings like C_X and C_Z do increase by a large margin with rise in inclination θ during the upwind pass. This means that the struts are contributing to power generation in the upwind pass. For the main rotor blade, the loading curves seem very typical for a 'strutless' rotor. But the influence of the struts becomes noticeable at the downwind part of the revolution, while in the upwind part the rotor blades does not seem to be affected in a way it is notable. The thrust coefficient C_X starts to collapse at the apex of the downwind pass between $\theta = 250°$ and $\theta = 300°$, especially at higher inclination angles. The same occurs for the other blade but shifted 180°, and thus the rotor performance as whole is affected during the full revolution as was seen in figure 23.

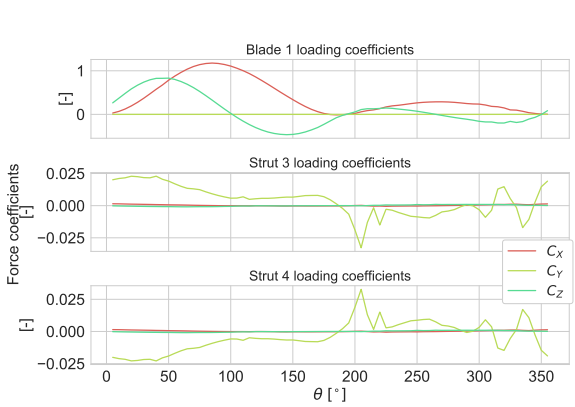

(a) $\phi_{l,u} = 0°$

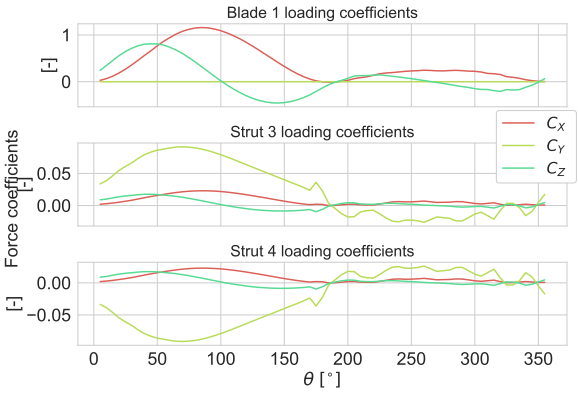

(b) $\phi_{l,u} = 15°$

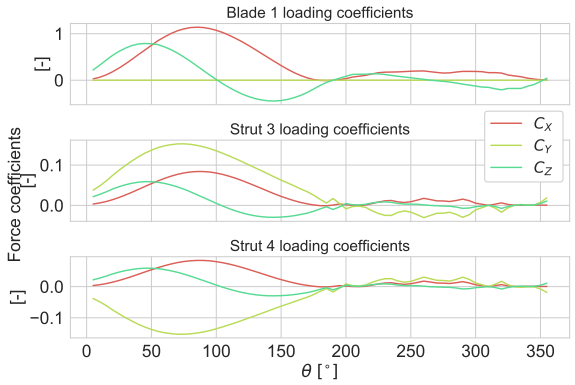

(c) $\phi_{l,u} = 30°$

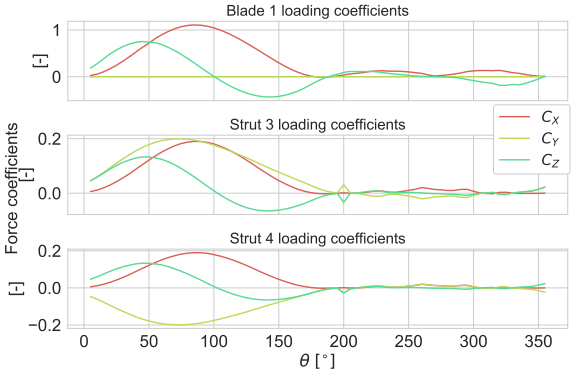

(d) $\phi_{l,u} = 45°$

Fig. 25 Blade or strut loadings of last revolution for varying $\phi_{l,u}$.

Until now only the rotor or blade specific performances and loadings are shown. Taking a more in depth look at the rotor blade loadings, the full spanwise blade C_T along a full revolution is plotted in figure 26 for different ϕ. The plots show how the blade's aerodynamic performances is influenced due to interference with the strut. Only C_T is shown but this is of course based on C_L, C_D and α. Note that the C_T in CACTUS is defined such that a negative C_T means a positive contribution to torque and a positive means a negative contribution. It seems that the decrease in absolute C_T values on the blade starts getting affected in the region 15% of its span from the tips of the blade and only in the downwind pass. With further increments in ϕ the region on the blade in which absolute C_L deteriorates, expands towards the root of the blade. It is also remarkable that the deterioration zone starts when the main rotor blade reaches the $\theta = 270°$ but with increase in ϕ it expands to the rest of the blade. Thus severely hampering the C_P capacity as implied in figure 24. This observation confirms what was found in the CFD simulation of Hara et al[6] on double bladed VAWT which they called 'torque dip'. In their case the presence of a tower did shift the torque dip. In the reference case no similar effect is found in figure 3b, thus the dip cannot be caused by the vortices shed from the main rotor blades with the given operational parameters. Also figure 24 shows that uninclined strut bodies do not cause the dip in the torque as the struts lack the generation of lift and thus the vortex shedding. Only with a higher inclination when the struts shed the vortices, then the dip in C_Q can be seen in the downwind pass. It seems that the main rotor blade passes the vortices discharged from the strut in the downwind pass as these vortices are convected downstream. In the upwind pass this should not be possible as these vortices get convected downsteam, away from the rotor blade. These phenomena are also observed in the paper of Hara et al[6].

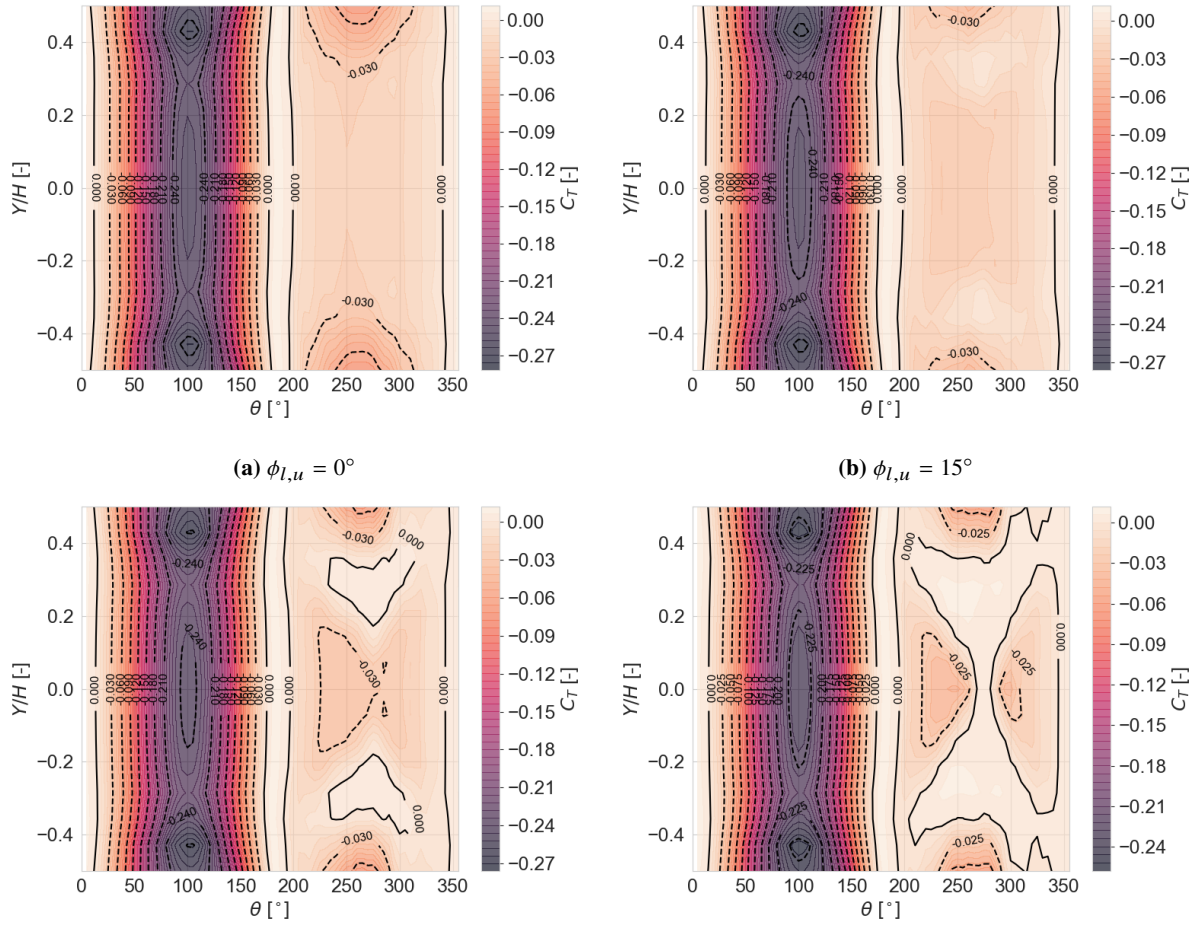

(a) $\phi_{l,u} = 0°$ **(b)** $\phi_{l,u} = 15°$

(c) $\phi_{l,u} = 30°$ **(d)** $\phi_{l,u} = 45°$

Fig. 26 Comparing C_T distribution along span for every azimuthal position (blade 1). Blade locations are defined such that $Y/H = \pm 0.5$ are the lower and upper tips and $Y/H = 0.0$ mid span.

Figure 27 show the blade C_Q distribution for $\phi_{l,u} = 0°$ and $\phi_{l,u} = 45°$ of the struts. For an improved view on the surface from the side, an elementwise C_Q contribution plot have been placed beside the related surface plot. As expected the blade's spanwise contribution is similar to that of the reference case. So the midspan of the blade has a larger contribution to the total C_Q of the rotor than the blade's tips. The pattern at the downwind is similar to that of what is happening to figure 26, the decrease in C_T on certain parts of the blade causes the same effects in the C_Q distribution. On the upwind part the C_Q contribution is still higher at the midspan than at the tips, but the values in general will be a bit lower with increasing ϕ as shown in figures 27b and 27d.

Strut analysis

Compared to the blades, the strut acts a bit different as it functions like an rotorcraft rotor with constant angular velocity but with different rotational speeds along its radius. With a constant inclination angle one can compare it to the introduction of an extra partial inner turbine[6][1]. Figure 28 shows the distribution of the tangential force coefficient C_T along the strut. Although there are four struts in this case, only one is shown as the upper and lower strut of one blade are symmetrical. The strut loadings of the other blade are shifted 180° relative to the analyzed blade. As can be seen in the figures, only the loading distribution is plotted from $r/R \geq 0.3$ where $r/R = 0$ is the root of the strut and $r/R = 1$ being the tip. At the root of the strut, the angle of attack is very large and as such the tangential loadings are very high at small regions near root. For plotting purposes the high loading coefficient at the root are too dominant such that distribution

along the mid span and tip of the strut cannot be seen any more. While the loadings are high at root, the contribution to the total torque of the strut are an order of magnitude smaller then at mid span or tip due to the near zero velocity at the root.

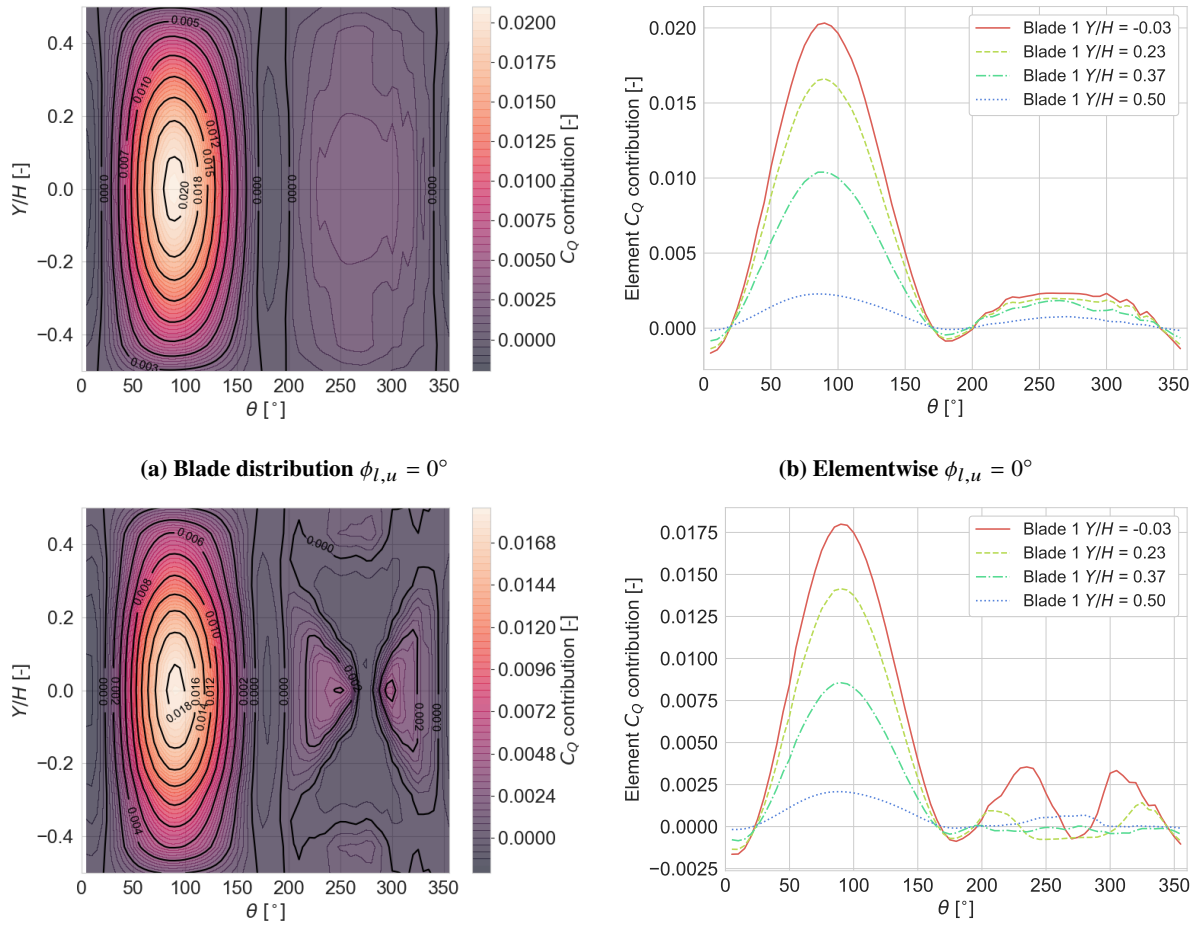

(a) Blade distribution $\phi_{l,u} = 0°$

(b) Elementwise $\phi_{l,u} = 0°$

(c) Blade distribution $\phi_{l,u} = 45°$

(d) Elementwise $\phi_{l,u} = 45°$

Fig. 27 Blade spanwise C_Q contribution for $\phi_{l,u} = 0°$ and $\phi_{l,u} = 45°$. Blade locations are defined such that $Y/H = \pm 0.5$ are the lower and upper tips and $Y/H = 0.0$ mid span. Note that the C_Q contribution is normalized to rotor frontal surface area instead of element surface area.

Figures 28 shows different C_T distributions along the strut span for varying ϕ. An uninclined strut shows a positive albeit very small C_T along the whole strut with the exception of the root. Towards the root of the strut, C_T can become very large but its contribution to torque is negligible thus the contribution to torque of the strut are almost purely viscous effect (Re is in the order of millions) of the strut profile which correlates to the profile drag coefficient of the NACA0018 airfoil. The strut is now a streamlined drag body which reduces drag as much as possible. With increasing $\phi_{l,u}$ the C_T distribution in the upwind part of the rotation becomes negative and contributes to the torque generation of the turbine, although in the downwind part the C_T is not really affected by inclination except at the root and tip of the struts. The C_T values at high inclination angles are pretty high and combined with the fact that each side has two struts one should expect that inclined struts would be beneficial for the power coefficient of a turbine. Somehow this is not the case, as figure 21 shows that the increase of $\phi_{l,u}$ actually leads to a lower turbine C_P. Note that interference effect at the junction between the strut and blade are not accounted for. This could be a extra drag effect and as consequence affects the torque contribution negatively.

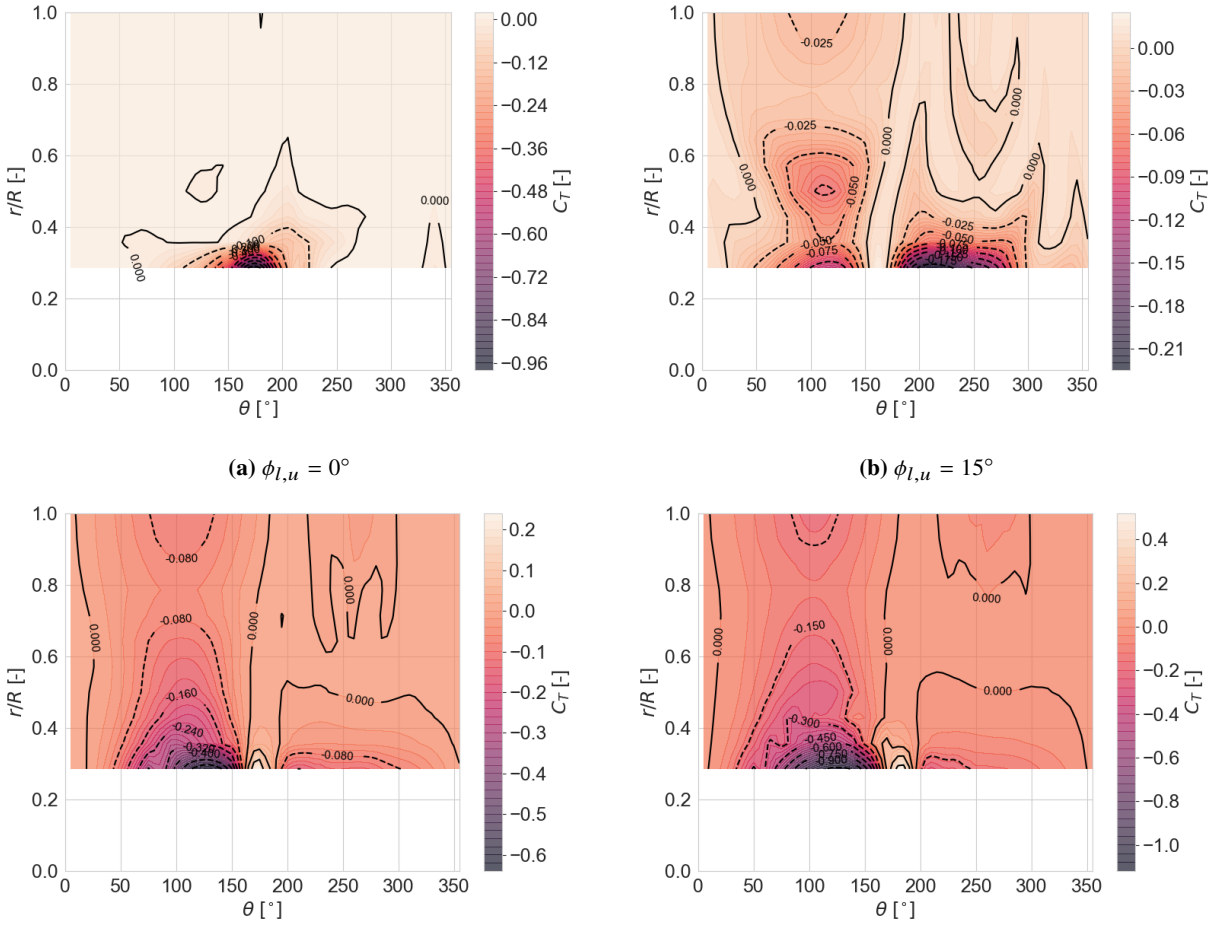

(a) $\phi_{l,u} = 0°$ **(b)** $\phi_{l,u} = 15°$

(c) $\phi_{l,u} = 30°$ **(d)** $\phi_{l,u} = 45°$

Fig. 28 Strut C_T distribution for varying $\phi_{l,u}$. Strut locations are defined such that $r/R = 0.0$ is at the root of the strut and $r/R = 1.0$ at the tip.

Figure 29 shows the spanwise C_Q contribution of the strut C_Q seen in figure 24. Note that the struts are also modelled with a cosine distribution for the elements like the blades. At $\phi = 0°$ the torque is very slightly negative throughout the up- and downwind phase. With increasing ϕ the increasing torque generated by the struts are focused in the upwind phase as already known from figure 24. As the C_Q contribution is normalized to the rotor frontal surface rather than the element specific surface, it indicates that the C_Q generation towards the tips of the struts is relatively large compared to mid span. It also shows that the torque generated is mostly focused on the sections between mid span and the tips. Especially at higher ϕ this becomes more concentrated on that specific section in the upwind phase.

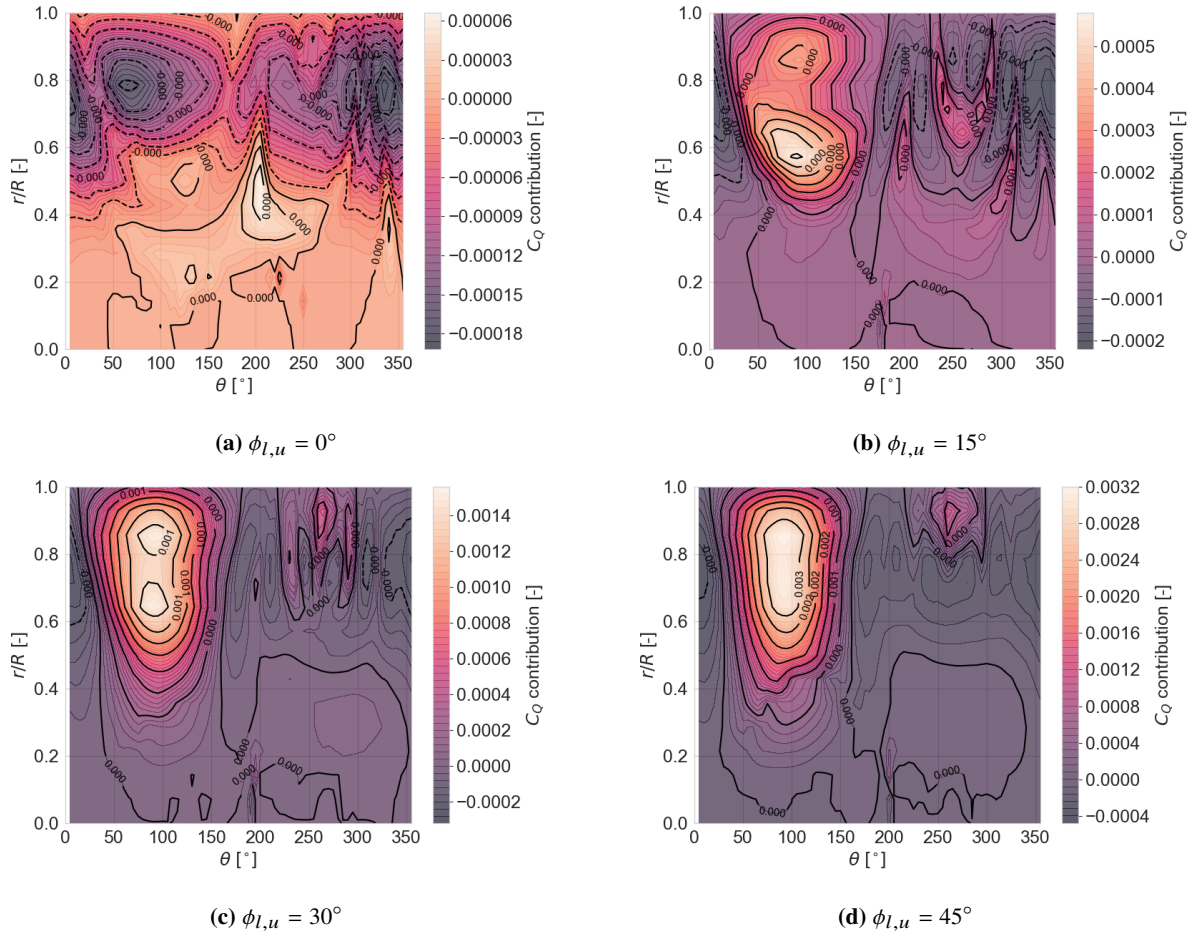

(a) $\phi_{l,u} = 0°$

(b) $\phi_{l,u} = 15°$

(c) $\phi_{l,u} = 30°$

(d) $\phi_{l,u} = 45°$

Fig. 29 Strut C_Q distribution for several subcases. Strut locations are defined such that $r/R = 0.0$ is at the root of the strut and $r/R = 1.0$ at the tip. Note that the C_Q contribution is normalized to rotor frontal surface area instead of element surface area.

Wake and velocity field

An interesting issue is to compare the wake field of the inclined strut cases with the reference case. So multiple wake trajectory plots of the main rotor have been made. Figure 30 shows that as the inclination angle ϕ increases, the vortex structure in the near wake alters. The increased inclination angle leads to a higher angle of attack and thus to the increased strength of the vortices shed by the strut. The vortices shed by the strut interact with the vortices shed by the blades and causes the wake to deflect. The far wake tends to deflect upward with higher inclination similar to [11], although it was expected that the wake would just expand as there is no net loading in Y direction. Compared to the reference case where the rotor wake expands vertically and horizontally, with the addition of the struts the wake does not necessarily expand vertically. The wake will instead, as it is observed from figure 30, also contract or make an sweeping motion. However the more inclined strut causes a higher rotor C_Z and this is seen in the wake it expands more laterally in the far wake of figure 30f.

When the wake trajectory of a strut is added into the figure, one can see from figure 31 that a secondary wake is created. The shed vortices from the strut are not strong so the effect of the main rotor blade wake will probably be dominant. The wake trajectories of the strut indicate that the wake merges with the wake of the main rotor blade after 2 rotor radii. Furthermore it seems that downstream the strut wake will bend towards the advancing side of the rotor. With $\phi = 45°$ a triangular shaped wake enveloped by the wake of the outer rotor but merged with a significant part of it. For $\phi = 0°$ The wake structure is fully mixed and turbulent at $X/R \leq 7.5$ while at $\phi = 45°$ the wake structure directly outside the rotor periphery is fully turbulent. Another observation based on the strut wake trajectory of figure 31b is that the main rotor

blade crosses the wake caused by the struts downstream. Which is expected as in the last section blade loadings were affected with varying ϕ.

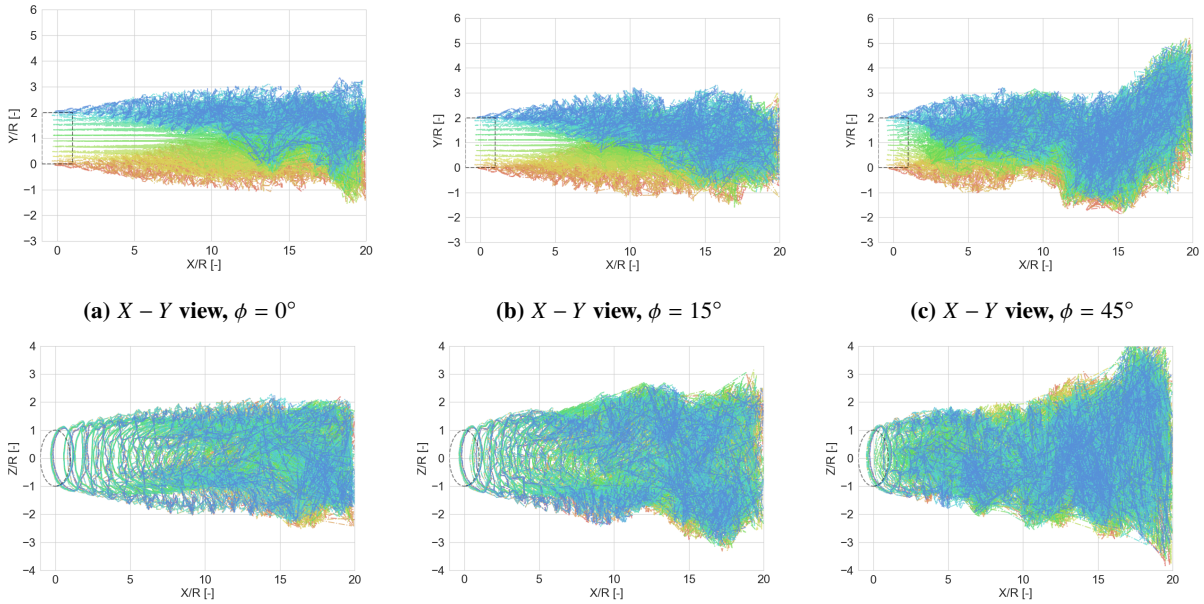

(a) $X-Y$ **view,** $\phi = 0°$ **(b)** $X-Y$ **view,** $\phi = 15°$ **(c)** $X-Y$ **view,** $\phi = 45°$

(d) $X-Z$ **view,** $\phi = 0°$ **(e)** $X-Z$ **view,** $\phi = 15°$ **(f)** $X-Z$ **view,** $\phi = 45°$

Fig. 30 Wake of the rotor blade 1, all blade elements are indicated with different colors.

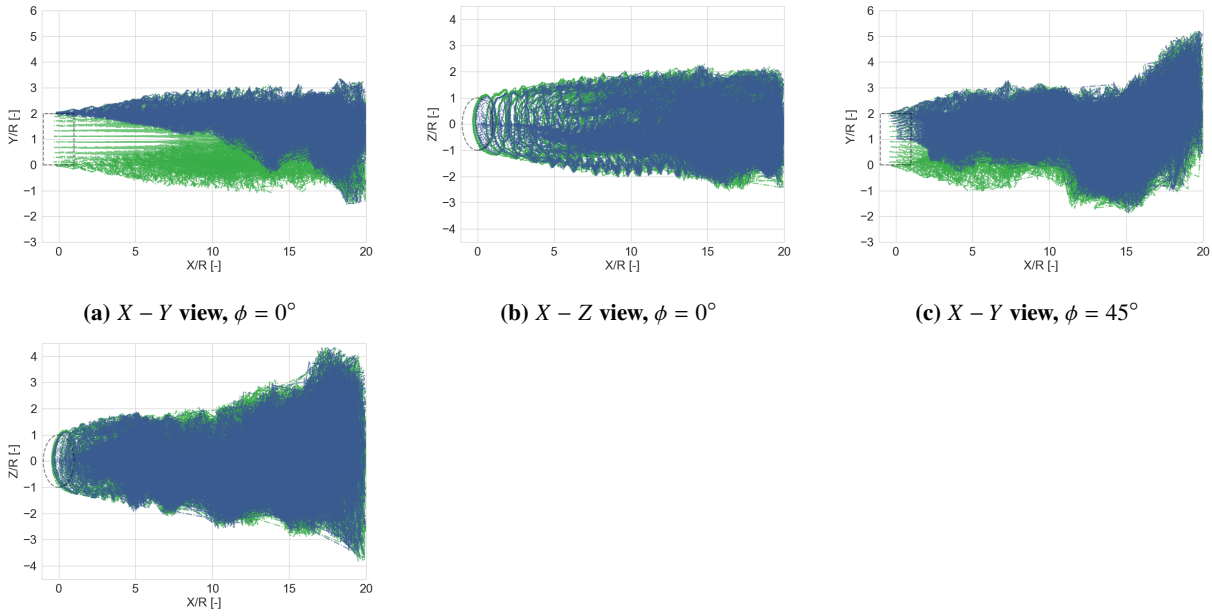

(a) $X-Y$ **view,** $\phi = 0°$ **(b)** $X-Z$ **view,** $\phi = 0°$ **(c)** $X-Y$ **view,** $\phi = 45°$

(d) $X-Z$ **view,** $\phi = 45°$

Fig. 31 Wake trajectory of the rotor blade 1 (green) and upper adjacent strut (blue). Color distinction used for clear differentiation between vortex trajectories of blade and strut.

The following plots in figures 32 to 37 show the velocity fields of the wake for the different subcases. The mid plane of the rotor and the upper tip plane are taken for comparison as the mid plane act as a 2D version of the rotor while at the tip it will show any 3D effects as well. As $\phi = 0°$ the velocity field is pretty similar to the reference case although at the tips in figure 34 the velocity deficits due to the strut's wake are noticable.

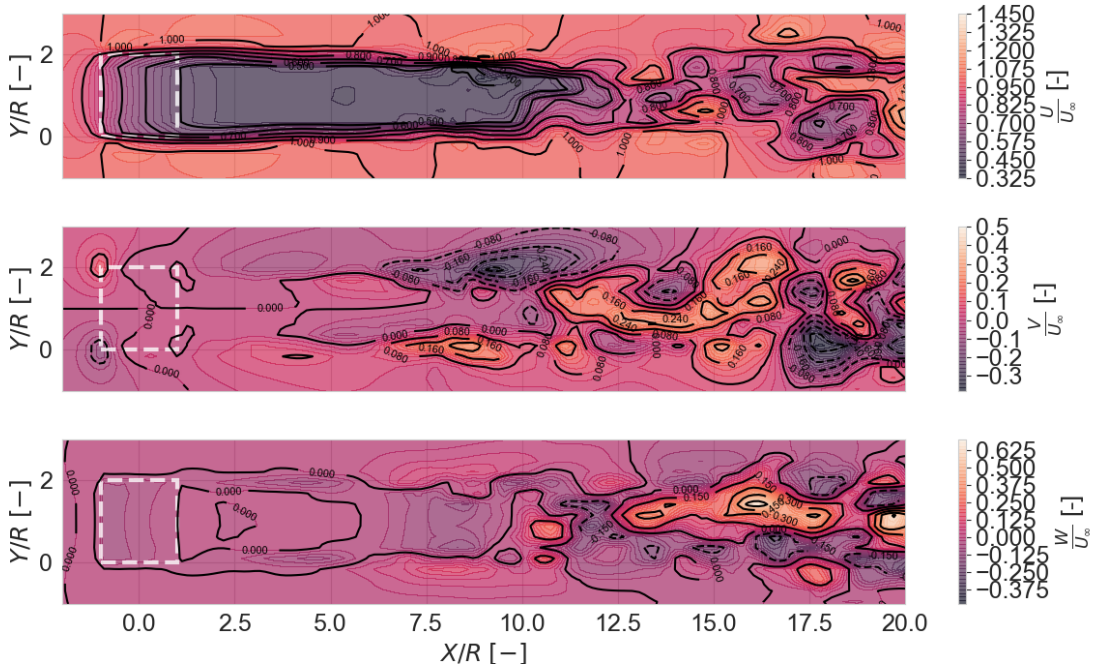

Fig. 32 $\phi = 0°$**, 2D plot in X-Y plane of the velocity field at Z/R=-0.1. Velocities are normalized to** U_∞**.**

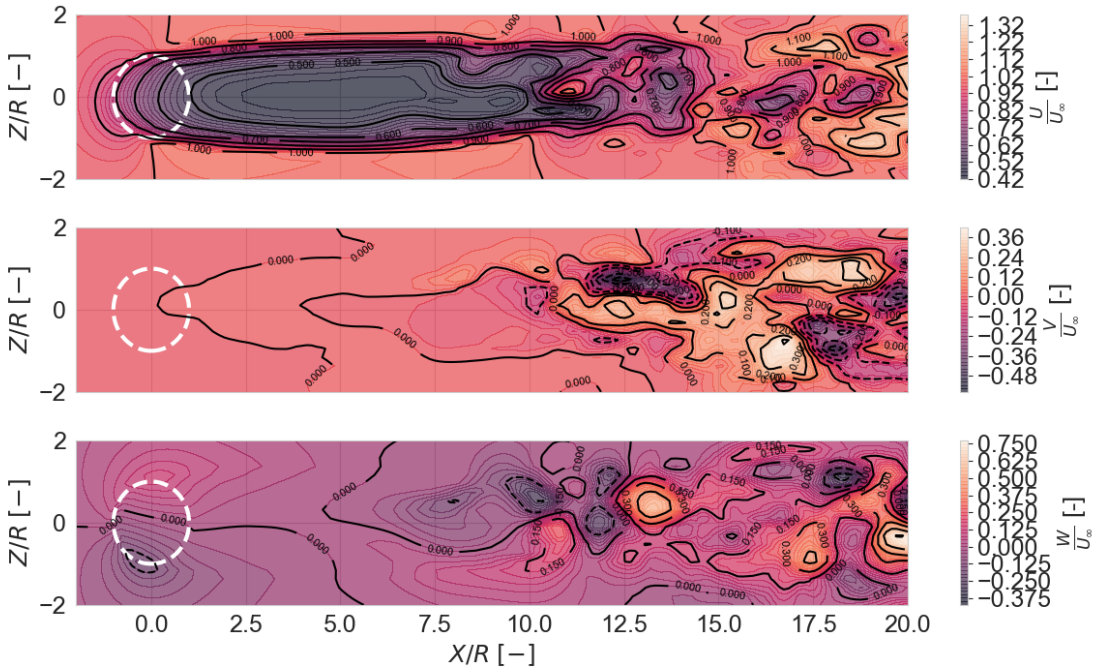

Fig. 33 $\phi = 0°$**, 2D plot in X-Z plane of the velocity field at Y/R=0.89 (mid plane). Velocities are normalized to** U_∞**.**

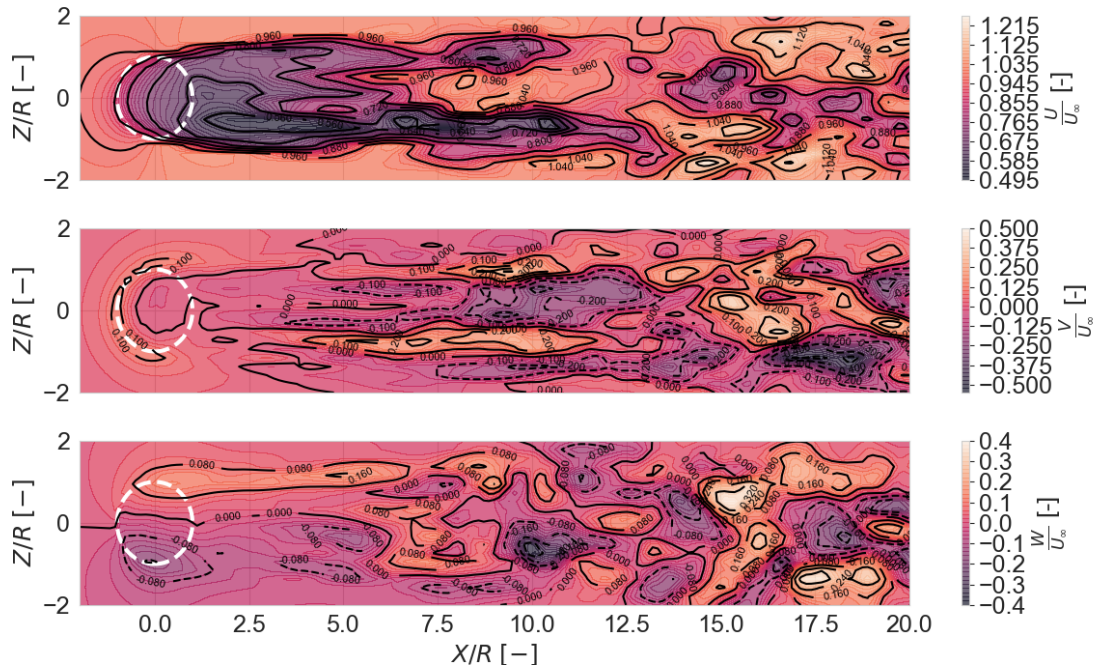

Fig. 34 $\phi = 0°$**, 2D plot in X-Z plane of the velocity field at Y/R=1.95 (upper rotor tip). Velocities are normalized to** U_∞**.**

Then with inclined struts from figures 35 to 37 the flow just becomes fully mixed and turbulent as mentioned earlier. This is clearly seen in the velocity fields as the U, V and W velocities are very unsteady.

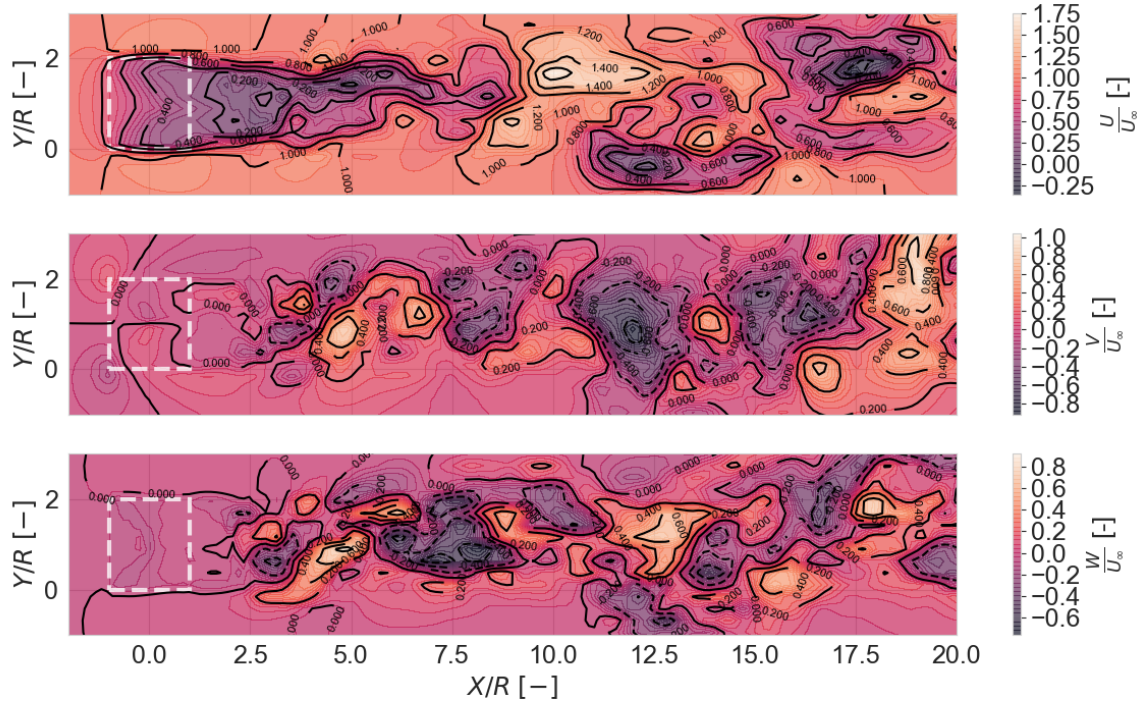

Fig. 35 $\phi = 45°$**, 2D plot in X-Y plane of the velocity field at Z/R=-0.1. Velocities are normalized to** U_∞**.**

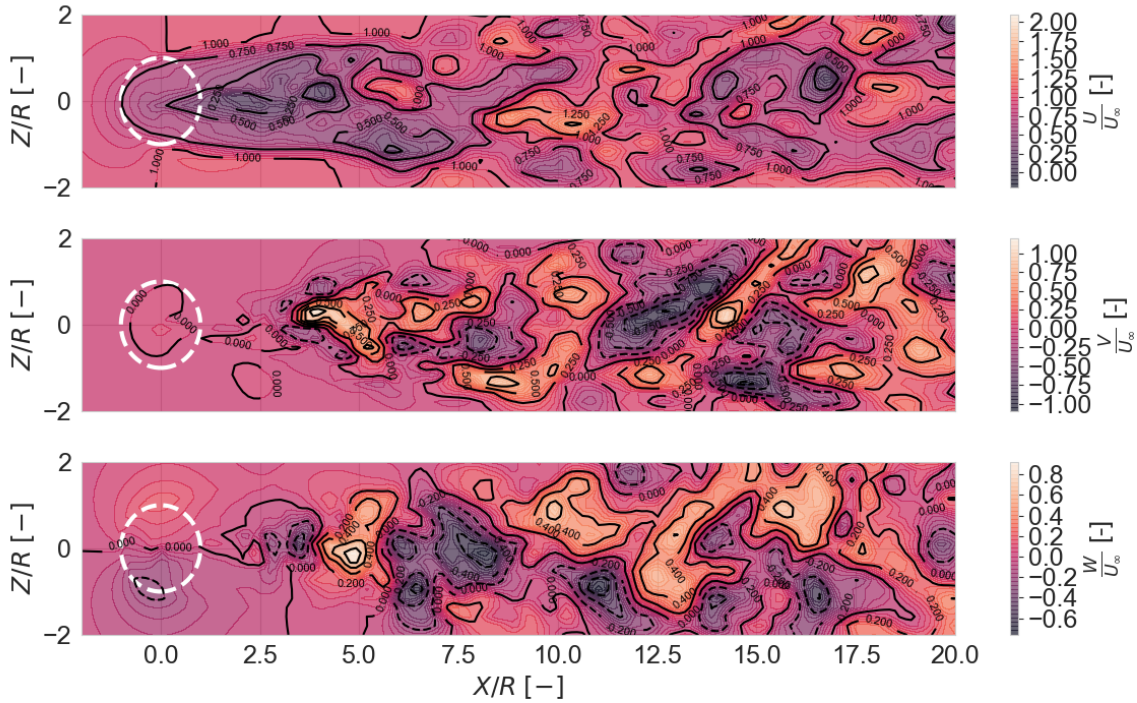

Fig. 36 $\phi = 45°$**, 2D plot in X-Z plane of the velocity field at Y/R=0.89 (mid plane). Velocities are normalized to** U_∞**.**

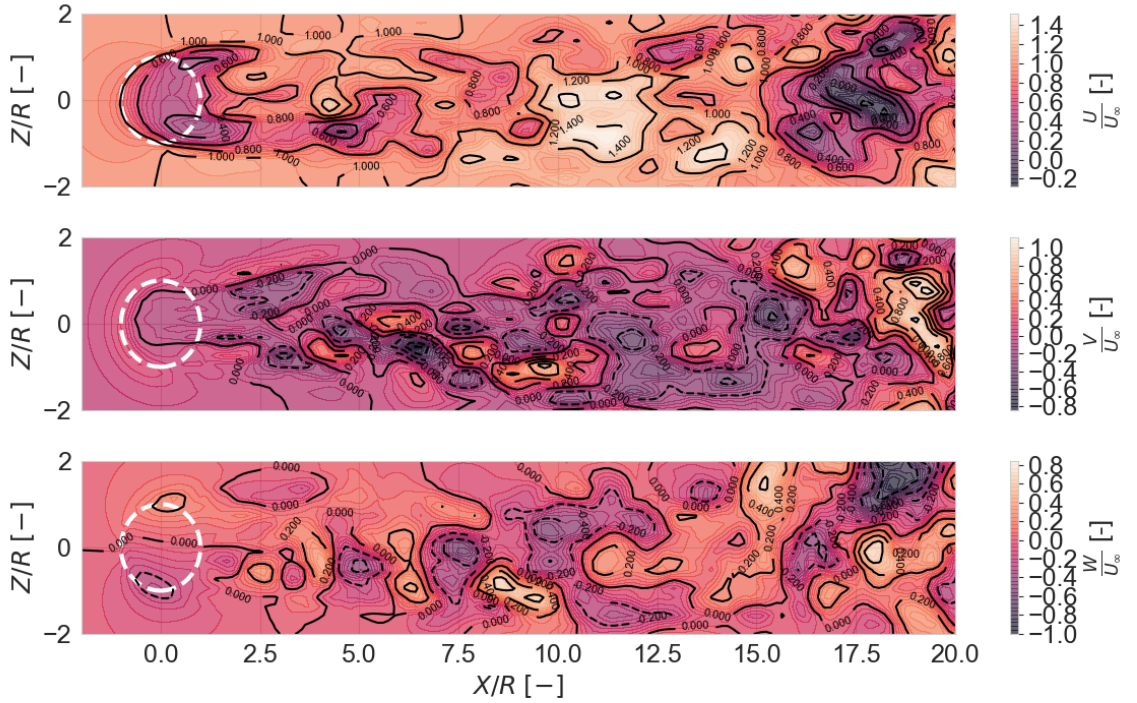

Fig. 37 $\phi = 45°$**, 2D plot in X-Z plane of the velocity field at Y/R=1.95 (upper rotor tip). Velocities are normalized to** U_∞**.**

IV. Conclusion

In this paper the CACTUS software is extended to allow the application of non-linear lifting line free vortex wake model on the struts. This extension makes it possible to model different geometries of the struts in a rotor and to model it in a more fundamental way than using empirical relations only. With the extended model, the struts are now able to produce lift and shed vortices which can interfere with the main rotor blades. This model was then used for a case study for varying parameters of a strut in the rotor. The variations in inclination angle, strut-blade attachment positions, tip speed ratio and the strut tip to blade gap are studied for their effects on the rotor performance and its wake. With the tip of the struts closing in on the strut-blade interjunction point, the tip vortex of the strut functions as part of the strut-blade interference effects. This can cause a drop up to 15% of the C_P relative to a strutless turbine. With varying tip speed ratio λ it was shown that the optimal λ was relatively low at around $\lambda = 3.5$. At low tip speed ratios the C_Q contribution by the strut was negative but small. At higher λ this negative torque contribution by the strut could add up to a decent proportion of 25% the torque contribution by blade. Most of it caused by the downwind phase of the strut.
It was shown that the position of the strut blade interjunction has significant effect on the strut itself due to the downwash induced from the tip vortices of the main rotor blade. This downwash will cause a loading in Y direction (spanwise of rotor blades). As consequence a small induced angle can be detected on the struts. While in this case its effect on the loading generated by the strut is small, but it can be expected that this can have a more significant effect with inclined struts.
Finally the lifting line model on the struts was applied in combination with an inclined strut. This way the strut can produce actual torque and contribute to the power conversion of the rotor. But doing so has an negative effect on the main rotor blade due to the shed vortices from the struts which interferes with the blades downwind. By inclining the struts, the torque is redistributed from the blades to the struts. However, there is still a net loss of power. This loss can be up to 5% depending on the inclination and approximately up to 7% relative to a strutless rotor. Furthermore the inclination of the struts deflects the wake and also causes it to become turbulent in after a few rotor radii as the wake from the struts and blades start to mix. The applied model for struts shows it is able to model the extra effects caused by the struts which would not have been possible in the original version of CACTUS.

V. Recommendations

The main goal to model the struts with a lifting line method and to perform a study with was achieved. However there were some issues which were not treated in this research. The modification of CACTUS to allow the struts to be modelled using the non-linear lifting line theory is a first step. But by doing so, the model of Hoerner[7] for strut-blade interference drag was not used any more as it was not compatible with the current implementation. Therefore the interconnection between strut and blade could not be modelled, but instead are just placed together with a zero gap between the strut's tip and the blade attachment point. While this does give some interactions between the strut and blade, some of the interference effects are not accounted for. Also the model of Hoerner was not completely implemented in the original CACTUS version, thus the original drag only strut bodies were always hardcoded to be uninclined. It is therefore advised to revise and reimplement this model again for future research.
While CACTUS itself has been validated with higher fidelity method[12], and shows good agreement with experiments. It is still advised to repeat this research with a higher fidelity method like CFD to verify the current results or compare it to results from other aerodynamic models. Finally the original plan was to also include a three-bladed version of the rotor and asymmetrical positioned struts, but due to time constraints this could not be done any more. It is recommended to test for these cases as well to get an even better overview.

Acknowledgements

This paper is part of a thesis for the curriculum of MSc Aerospace Engineering at Delft University of Technology. The first author would like to thank Delphine de Tavernier and Carlos Simão Ferreira for their unconditional support as supervisors during the thesis. Furthermore the advice on the use of CACTUS and the following discussion with Bruce LeBlanc are greatly appreciated. Finally the author would like to thank the Faculty of Aerospace Engineering and Paulus Schoutsen for their provision of high performance computing resources for this thesis.

References

[1] Delphine De Tavernier and Carlos Ferreira. An extended actuator cylinder model: Actuator-in-actuator cylinder (AC-squared) model. *Wind Energy*, 2019. ISSN 10991824. doi: 10.1002/we.2340.

[2] Eduard Dyachuk and Anders Goude. Simulating dynamic stall effects for vertical axis wind turbines applying a double multiple streamtube model. *Energies*, 8(2):1353–1372, 2015. ISSN 19961073. doi: 10.3390/en8021353.

[3] Ronald Gormont. A Mathematical model of unsteady aerodynamics and radial flow for application to helicopter rotors. pages 1–91, 1973.

[4] Anders Goude, Staffan Lundin, and Mats Leijon. A parameter study of the influence of struts on the performance of a vertical-axis marine current turbine. *Proceedings of the 8th European Wave and Tidal Energy Conference*, pages 477–483, 2009.

[5] Brian Hand and Andrew Cashman. Aerodynamic modeling methods for an offshore vertical axis wind turbine : a comparative study (Unpublished research). *Renewable Energy*, 129:12–31, 2017. ISSN 18790682. doi: 10.1016/j.renene.2018.05.078. URL https://doi.org/10.1016/j.renene.2018.05.078.

[6] Yutaka Hara, Takafumi Kawamura, Hiromichi Akimoto, Kenji Tanaka, Takuju Nakamura, and Kentaro Mizumukai. Predicting double-blade vertical axis wind turbine performance by a quadruple-multiple streamtube model. *International Journal of Fluid Machinery and Systems*, 7(1):16–27, 2014. ISSN 18829554. doi: 10.5293/IJFMS.2014.7.1.016.

[7] S. F. Hoerner. *Fluid Dynamic Drag*. 1965. ISBN 9993623938.

[8] Joseph Katz and Allen Plotkin. *Low-Speed Aerodynamics , Second Edition*. Cambridge University Press, 32 Avenue of the Americas, New York, NY 10013-2473, USA, 2nd editio edition, 2010. ISBN 9780521665520.

[9] J. G. Leishman and T. S. Beddoes. A Semi-Empirical Model for Dynamic Stall. *Journal of the American Helicopter Society*, 34 (3):3–17, 1989. ISSN 21616027. doi: 10.4050/JAHS.34.3. URL http://openurl.ingenta.com/content/xref?genre=article{&}issn=2161-6027{&}volume=34{&}issue=3{&}spage=3.

[10] Philip Marsh, Dev Ranmuthugala, Irene Penesis, and Giles Thomas. Three-dimensional numerical simulations of straight-bladed vertical axis tidal turbines investigating power output, torque ripple and mounting forces. *Renewable Energy*, 83:67–77, 2015. ISSN 18790682. doi: 10.1016/j.renene.2015.04.014. URL http://dx.doi.org/10.1016/j.renene.2015.04.014.

[11] Victor Mendoza and Anders Goude. Improving farm efficiency of interacting vertical-axis wind turbines through wake deflection using pitched struts. *Wind Energy*, 22(4):538–546, 2019. ISSN 10991824. doi: 10.1002/we.2305.

[12] Jonathan Murray and Matthew Barone. The Development of CACTUS, a Wind and Marine Turbine Performance Simulation Code. *49th AIAA Aerospace Sciences Meeting including the New Horizons Forum and Aerospace Exposition*, (January):1–21, 2011. doi: 10.2514/6.2011-147. URL http://arc.aiaa.org/doi/abs/10.2514/6.2011-147.

[13] Jonathan C Murray and Matthew Barone. CACTUS User's Manual. pages 1–24, 2013.

[14] D. Owens. Weissinger's model of the nonlinear lifting-line method for aircraft design. 2013. doi: 10.2514/6.1998-597.

[15] M. Salman Siddiqui, Naveed Durrani, and Imran Akhtar. Numerical Study to Quantify the Effects of Struts and Central Hub on the Performance of a Three Dimensional Vertical Axis Wind Turbine Using Sliding Mesh. *Volume 2: Reliability, Availability and Maintainability (RAM); Plant Systems, Structures, Components and Materials Issues; Simple and Combined Cycles; Advanced Energy Systems and Renewables (Wind, Solar and Geothermal); Energy Water Nexus; Thermal Hydraul*, (March 2016):V002T09A020, 2013. doi: 10.1115/POWER2013-98300.

[16] M. Salman Siddiqui, Naveed Durrani, and Imran Akhtar. Quantification of the effects of geometric approximations on the performance of a vertical axis wind turbine. *Renewable Energy*, 74:661–670, 2015. ISSN 09601481. doi: 10.1016/j.renene.2014.08.068. URL http://dx.doi.org/10.1016/j.renene.2014.08.068.

[17] J. H. Strickland. The Darrieus Turbine: A performance prediction model using multiple streamtubes. Technical report, Sandia Laboratories, Albuquerque, 1975.

[18] J. H. Strickland, B. T. Webster, and T. Nguyen. A Vortex Model of the Darrieus Turbine: An Analytical and Experimental Study. *Journal of Fluids Engineering*, 101(4):500, 1979. ISSN 00982202. doi: 10.1115/1.3449018.

[19] Giusceppe Tescione. *On the aerodynamics of a vertical axis wind turbine wake*. 2016. ISBN 978-94-6299-462-1. doi: https://doi.org/10.4233/uuid:86ac7352-46b8-4c2d-9014-817472d80174.

[20] Willy Tjiu, Tjukup Marnoto, Sohif Mat, Mohd Hafidz Ruslan, and Kamaruzzaman Sopian. Darrieus vertical axis wind turbine for power generation II: Challenges in HAWT and the opportunity of multi-megawatt Darrieus VAWT development. *Renewable Energy*, 75:560–571, 2015. ISSN 18790682. doi: 10.1016/j.renene.2014.10.039.

[21] Oliviu Şugar Gabor, Andreea Koreanschi, and Ruxandra Mihaela Botez. A new non-linear vortex lattice method: Applications to wing aerodynamic optimizations. *Chinese Journal of Aeronautics*, 29(5):1178–1195, 2016. ISSN 10009361. doi: 10.1016/j.cja.2016.08.001.

[22] Bofeng Xu, Tongguang Wang, Yue Yuan, Zhenzhou Zhao, and Haoming Liu. A simplified free vortexwake model of wind turbines for axial steady conditions. *Applied Sciences (Switzerland)*, 8(6), 2018. ISSN 20763417. doi: 10.3390/app8060866.

Appendix: Grid convergence study

This section discusses the convergence study for CACTUS simulations. As with all numerical methods, it is important to evaluate how the solver and geometry discretization affects the simulation results and to make sure that the error becomes independent of the grid used. Therefore the main goal with these tests is to find the settings of the CACTUS simulation for which the simulation results are not affected significantly to variations in spatial (blade elements) and temporal grid (timesteps). It is furthermore important to keep the numerical resources used for the simulations manageable. Of course the grid could use an extreme high number of blade elements or timesteps, but with increasing the amount of elements or timesteps the computation time increases non-linearly. An optimum is reached when a grid size is found for which the error of the results becomes sufficiently low while maintaining a reasonable simulation time. What reasonable errors and simulation times are depends on the type of simulation.

Convergence on timesteps

The turbine in the simulation will not rotate continuously but in discrete steps. These are called timesteps N and are spaced evenly. They can be related to a discrete shift of azimuthal angle $\Delta\theta$ during rotation and is defined as $\Delta\theta = 360/N$. The two bladed H-shaped rotor without struts is simulated up to 20 revolutions or until a C_P convergence of 0.001 is reached. The design parameters of this turbine are given in table 5. This turbine also represents the turbine modelled in the paper. 20 blade elements were used to model each blade during the convergence test with timesteps.

Table 5 Main design and operating parameters of the turbine

Design parameters	
Number of blades B	2
Turbine radius R	14 m
Turbine height H	28 m
Blade chord c	1.2 m
Airfoil type	NACA0018
Tip speed ratio λ	4.5
Dynamic Stall model	Leishman-Beddoes

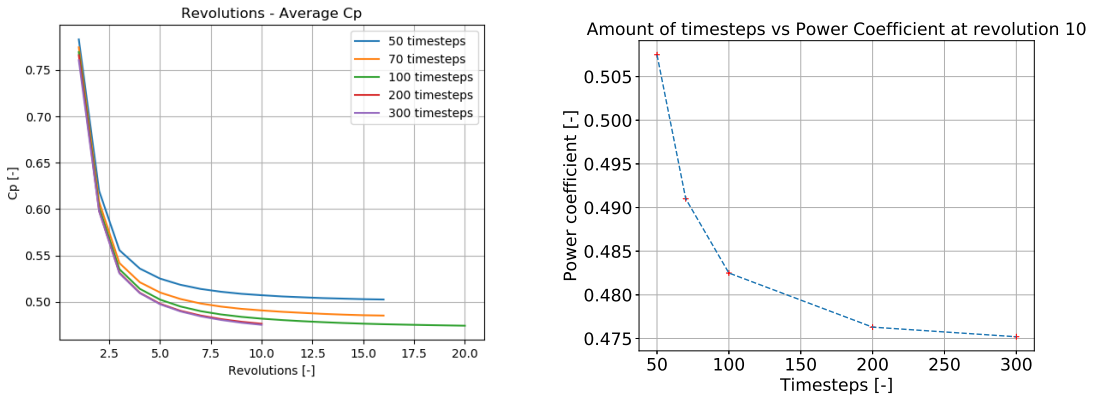

(a) Plots showing the convergence of C_P value with different timesteps. The simulations in the plot converges when the error in C_P is minimized or if a certain number of revolutions has been reached.

(b) Comparison of C_P values at revolution 10 for cases with different timesteps N. Note that small increments in the lower timestep range leads to drop in C_P value.

Fig. 38 Results of convergence test with varying timesteps N of the VAWT described in table 5.

Different situations of the turbine are tested in which the amount of timesteps varies exclusively. In theory a greater

amount of timesteps could capture effects which are missed with insufficient timesteps. The trade-off is that the increase in timesteps leads to more computations and thus increase in simulation time. The timesteps value N is varied between 50 and 300, translating to a $\Delta\theta$ between 7.2° and 1.2°. The convergence of the C_P value will be compared for different N values. The results of the increments in timesteps on the power C_P coefficients can be found in figure 38. From figure 38a it can be concluded that the simulations follow the same trend. When increasing the timesteps, the C_P converges on a smaller value while maintaining the trend. This indicates that the simulation results indeed depend on the timestep size. At a number of 200 timesteps or greater the error becomes less than 1% with the error between 200 and 300 timesteps being 0.2%. Another point is while figure 38a shows the trend of the plots with different timesteps, it can be deduced that after 10 revolutions or so the average C_P value of the 200 and 300 timesteps cases fluctuate less than 0.4% and after 16 revolutions this fluctuation becomes less than 0.1%. The reduction in error above 100 timesteps is negligible but leads to unacceptable computation time. Although not shown in the plots, the time to finish each simulation varied between few hours and more than a full week. As computational time increases non-linearly it is only feasible when keeping N small. For the simulations in the paper a $N = 72$ is used which amounts to a phase angle of $\Delta\theta = 5°$. While $N = 100$ would be more optimal, time wise it becomes impractical for $N \geq 72$.

Convergence on blade elements

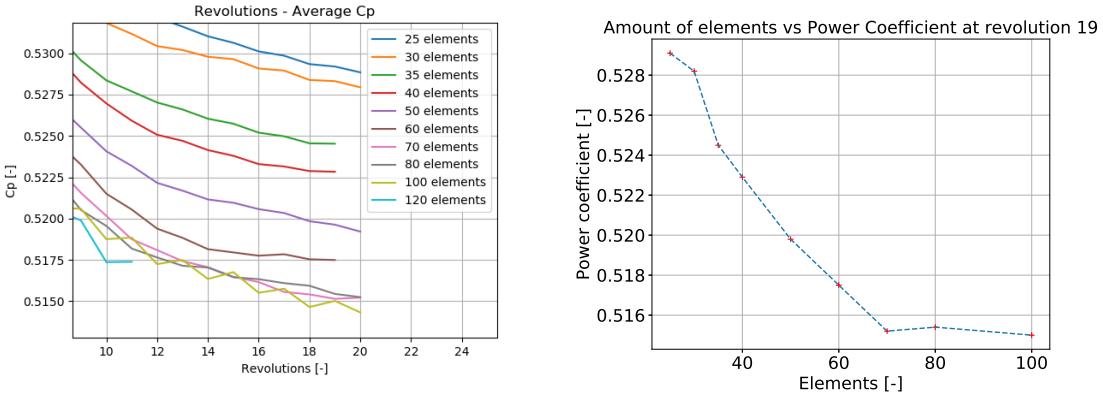

(a) Comparison of the *Revolutions* − C_P with different amount of blade elements.

(b) C_P − *elements* at revolution 19.

Fig. 39 Convergence test with blade elements of a two bladed VAWT.

The study was performed with 25 to 120 elements per blade distributed linearly and used 30 timesteps for all simulations. Figure 39a shows the C_P against its revolutions plots for all cases. Figure 39b shows the convergence of the C_P from 70 elements per blade on. Increasing the number of elements further does not seem to have effect anymore. The variation in C_P between the use of 70 and 100 elements is only approximately 0.03%. It can be concluded that the use of 70 elements per blade should lead to sufficiently accurate simulation results based on a linear blade element distribution along the blade.

In reality the flow field around the tip is more complex than mid span of the blade thus the number of elements used can be reduced by refining the element density locally instead of globally. Also note that the difference between 25 elements per blade and 70 elements per blade is approximately 2.7%. Also the effects of timesteps on the C_P seems to be more influential than the amount of blade elements, while they both increase the simulation time non-linearly. Thus by using a non-linear blade element distribution where the density of elements is focused on the tip area, this difference can be made much smaller and as such the amounts of elements can be lowered. This can easily reduce the simulation time by a large margin while still maintaining sufficient accuracy. As such, a cosine distribution is applied on the blade and only a number of 15 elements per blade is used. Unfortunately no extra convergence study could be conducted anymore, but the results from the (similar) reference case in the paper indicate that the cosine distribution leads to a similar C_P value of what was achieved here with less elements.

III

SUPPORT CHAPTERS

1

THEORETICAL BACKGROUND FOR VERTICAL AXIS WIND TURBINES

1.1. WIND TURBINE AERODYNAMICS AND POWER

To produce power, wind turbines turn the momentum of the flow into electricity. The power contained in the flow crossing a specific section S with freestream velocity U_∞ is described as $P_{flow} = \frac{1}{2}\rho U_\infty^3 S$. The efficiency of a wind turbine can be defined with the power coefficient $C_P = \frac{P}{P_{flow}} = \frac{P}{0.5\rho U_\infty^3 S}$. This is one of the performance indicators of a wind turbine. The power P generated from the flow itself is based on the torque and rotational speed $P = Q_{total}\Omega$ of the turbine or non-dimensionalized as $C_P = C_Q\lambda$. The total torque Q_{total} generated by the turbine are the torque contributions by blade Q_{blade}, struts Q_{strut} and possible other secondary effects Q_i influencing the torque $Q_{total} = Q_{blade} + Q_{strut} + Q_i$ [23]. Q_{blade} and Q_{strut}, are determined from integration of all the tangential loading on each blade and strut if applicable. Thus from Mendoza[27] and [23] the revolution averaged torque of a blade in one revolution should can be given as equation 1.1. Basically the tangential loading distribution should be integrated along the blade span and then averaged over one revolution. Similar equation can be given for the struts in equation 1.2, but this time the term for the interference (or interjunction) drag between strut and blade has to be taken into account as well if there is a connection between strut and blade (there should be one). Besides the tangential loading there is also a normal loading on the blade perpendicular to the direction of the tangential loading and chord. This loading does not contribute to the rotor torque. In numerical methods the blade is modelled at discrete points, thus the loading distribution will not be integrated but instead it is summed over the amount of elements used to model a blade or strut.

$$Q_{blade} = \frac{1}{2\pi}\int_0^{2\pi}\int_0^{H} BR(s)F_T(\theta,s)dsd\theta \tag{1.1}$$

$$Q_{strut} = \frac{1}{2\pi}\int_0^{2\pi}\int_0^{R_{strut}} B_s R(r)F_T(\theta,r)drd\theta + \frac{1}{2\pi}\int_0^{2\pi} B_s RF_{interference}(\theta)d\theta \tag{1.2}$$

The tangential loading of the blades and struts have to be determined to compute the torque contributions. This loading depends on the lift and drag of the bodies, which are then related to the flow conditions and geometry of the lifting body.

1.2. VERTICAL AXIS WIND TURBINES

As this thesis is about vertical axis wind turbines (VAWTs), a small introduction about them will be given in this section. These wind turbines are defined by having the axis of rotation perpendicular to the freestream direction instead of being aligned like the horizontal axis wind turbines (HAWTs). The lifting or drag bodies of a VAWT are connected to the tower by supporting structure or struts and with a different axis of rotation changes the dynamics of the turbine in many ways. The VAWTs consist of two subcategories, the drag based Savonius turbines and the lift based Darrieus turbines. The thesis will solely focus on the lift based turbines. Due to the different alignment of the axis of rotation this will give some benefits of the VAWTs compared to

its horizontal variants. First one is the omnidirectionality of the turbine, thus no need for yawing mechanism to align the turbine to the freestream direction. Secondly, the drive train and generator can be placed at the base of the tower instead of on top. This will lead to a lower center of gravity which leads to better stability of the turbine, and is one of the reasons why VAWTs are considered as a great alternative for offshore wind turbines[5]. With lower tip speed ratio λ in general compared to the regular HAWTs, the noise of the turbine can be reduced compared to the horizontal axis types[28]. In some cases a VAWT can also be easier and cheaper to manufacture, having only simple straight blades without different airfoil section distribution along its span due to aerodynamic requirements[28].
On the other hand VAWTs also have some inherent traits which are less beneficial like its inherent cyclic blade loadings due to the way the turbine spins. This means that the torque and power generation of the turbine are not constant along its azimuthal rotation in contrary to a HAWT. Also the cyclic loadings means these kind of turbines can be more prone to fatigue than HAWTs. Another issue of the VAWT is the poor self starting capability[15][2]. One challenge that VAWTs creates is the different aerodynamic situation due to how the turbine rotates. As the blades and struts passes the wake generated earlier upwind, they will interact with the wake and cause all kinds of unsteady phenomena.
The 2D view projected view of a vertical axis wind turbine is seen in figure 1.1a and the cross sectional view of this turbine is shown in figure 1.1b. The tangential (or chordal) velocity of the turbine blades in this case can be described by $V_t = \Omega R + V_a \cos\theta$ and the normal component $V_n = V_a \sin\theta$, with V_a being the induced velocity. An important parameter, the tip speed ratio can then be defined as the ratio of blade tangential velocity and freestream velocity $\lambda = \frac{\Omega R}{V_\infty}$. Given the above information, the relative inflow velocity at the blade is then described by $W = V_\infty \sqrt{\sin^2\theta + (\lambda + \cos\theta)^2}$. The angle of attack α used to determine the aerodynamic loading on the airfoil section is dependent on the azimuthal angle θ and λ. In contrary to a more constant α on a HAWT, the VAWT describes α as equation 1.3.

$$\alpha = tan^{-1}\left(\frac{\sin\theta}{\lambda + \cos\theta}\right) \tag{1.3}$$

The azimuthal range of the turbine's upwind part is from $0° \leq \theta \leq 180°$ while the downwind part is between $180° < \theta \leq 360°$. This definition will be kept for all subsequent sections in this report. The angle of attack for the blade of a VAWT is dynamic and dependent on the azimuthal position and the tip speed ratio. As consequence the loadings on the blade are dynamic and the instantaneous torque is not constant but fluctuating.

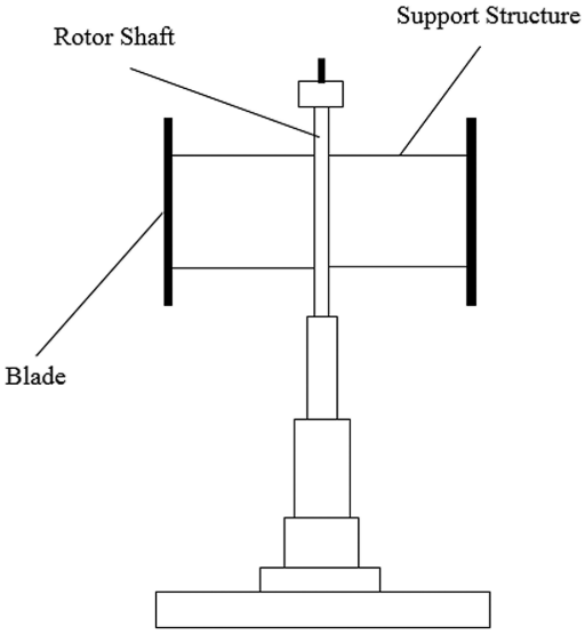

(a) 2D schematic view from the side[29]

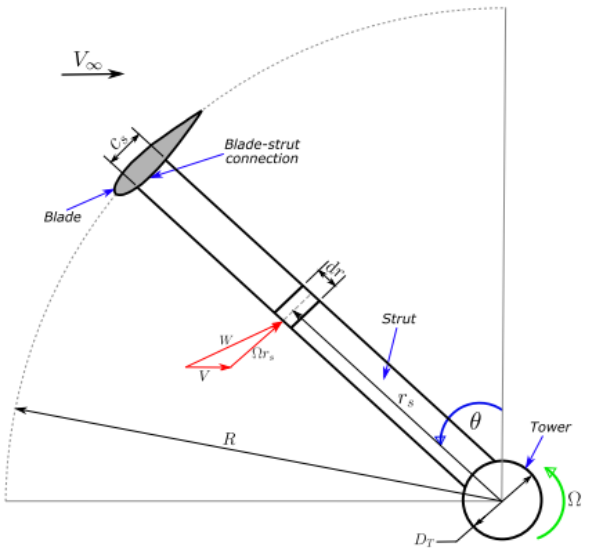

(b) 2D cross sectional view of the VAWT[23]

Figure 1.1: A vertical axis wind turbine

1.3. NUMERICAL METHODS FOR WIND TURBINES

To design and optimize a VAWT as good as possible it is essential that the behavior of the VAWT can be predicted. There are multiple numerical methods available, but each of them have different degrees of accuracy and their own strengths and weaknesses. They vary widely in accuracy and required (computational) resources. Not all of them are equally useful for design of an wind turbine due to its long computation time. In the preliminary stage of design the numerical methods are the most accessible. Some important characteristics concerning the numerical methods are that they should be as accurate as possible, while also maintaining a short computation time. These two are often contradicting. The following points are important characteristics which the computational methods should have according to Islam et al[2]:

1. Calculations of local relative velocities and angle of attacks at different tip speed ratios and azimuthal positions.
2. Calculation of ratio of induced to freestream velocity considering the blade-wake interaction.
3. Mathematical expressions based on different approaches (Momentum, Vortex or Cascade principles) to calculate normal and tangential forces.
4. Airfoil characteristics at different Reynolds numbers;
5. Post-stall models for stall development and fully stalled flow.
6. Finite aspect ratio consideration due to tip vortices.
7. Models to account for dynamic stall.
8. Flow curvature model for the circular blade motion.

Some popular methods in use are the momentum models (Single streamtube model, Double-Multiple Streamtube model, Actuator Cylinder model) and vortex models[2]. CFD is also available but for preliminary design purposes this might not be the most practical form of numerical study yet. In the following sections some of the mentioned models will be discussed.

1.4. BLADE ELEMENT THEORY

The blade element theory describes a lifting body (a blade) by dividing it into a segments called blade elements. These elements can then be modelled using known airfoil polar data and its forces can be determined based on the flow conditions and its angle of attack α. Figure 1.2 shows an example of the (induced) velocity components and the loadings on one blade element.

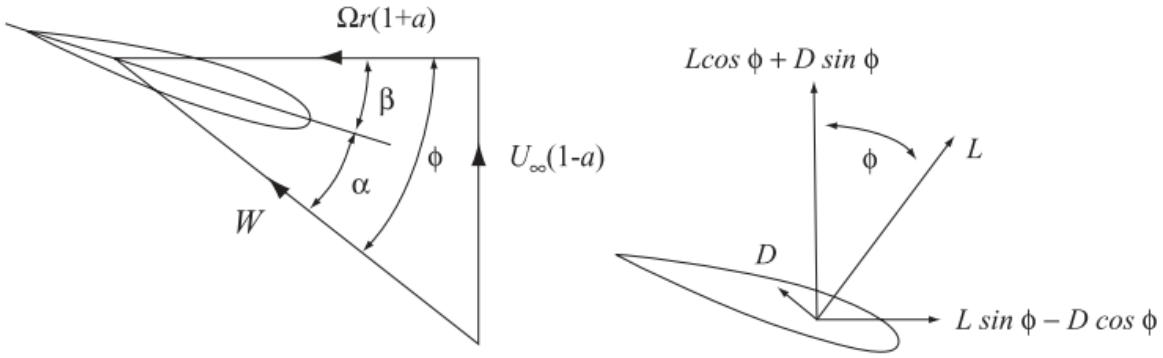

Figure 1.2: The blade element showing on the left side the relative velocity W, freestream velocity U_∞ and rotational speed Ωr. The induced velocity factor a is also given. On the right picture the lift component L and drag component D of the element are shown. [1]

The velocity components based on the rotation of the blade element and the freestream determines the relative velocity $W = \sqrt{U_\infty(1-a) + (\Omega r)^2(1+a')^2}$ on the blade element. This relative velocity W has a certain inflow angle Φ and together with the pitching angle β are used to determine the angle of attack $\alpha = \phi - \beta$. Finally with this angle of attack known, the lift and drag forces of this blade element can be determined

using equations 1.4 and 1.5. The tangential load on the blade element is then $dF_T = dL\sin\phi - dD\cos\phi$ and the normal load $dF_N = dL\cos\phi + dD\sin\phi$. This must be repeated for each element and when all the blade elements are computed it can be integrated along the blade span to determine the full blade loading F_T and F_N. These loads can then be used in equations 1.1 or 1.2 to determine the torque of the rotor. The blade element theory can be combined with the momentum models or the vortex models to determine the induction coefficient a in an iterative process.

$$dL = c_l \frac{1}{2}\rho W^2 c dr \tag{1.4}$$

$$dD = c_d \frac{1}{2}\rho W^2 c dr \tag{1.5}$$

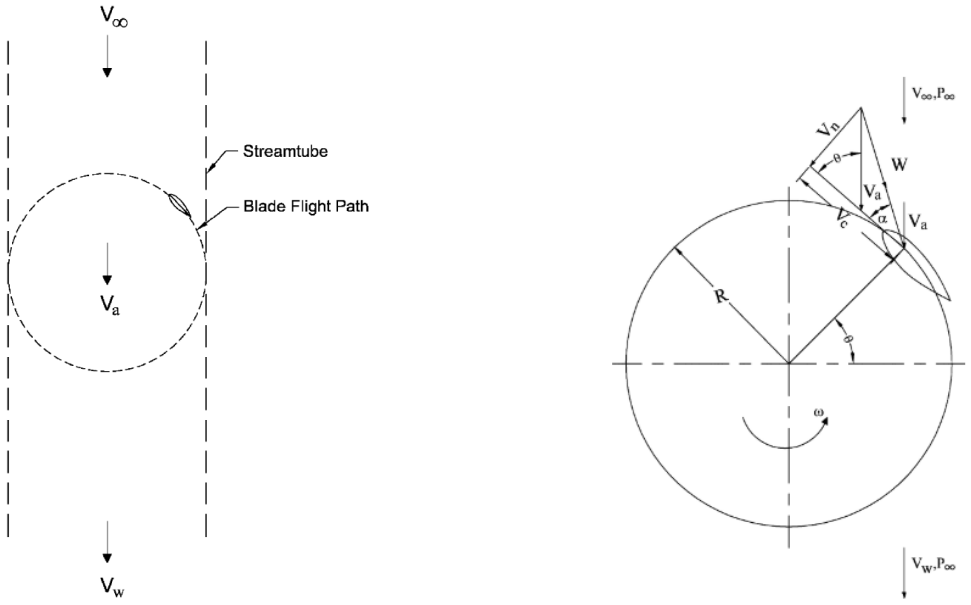

(a) Single streamtube with V_∞, V_a and V_w

(b) Velocities on blade in a VAWT

Figure 1.3: schematic overview single streamtube momentum model [2]

1.5. MOMENTUM MODELS

The momentum theory is based on the calculation of stream velocity through turbine by equating the aerodynamic forces on the blades (calculated with the blade element theory) with the rate of change of momentum of the flow. The aerodynamic forces are calculated using the blade element theory and then multiple iterations are performed for the induced velocity calculations until it converges to one consistent solution. This combination of the blade element theory and the momentum theory is the blade element momentum theory (BEM). In the following sections this will be referred as momentum models and some variants of the momentum models will be discussed, each extending the previous one. The main assumption in all momentum models is that the loadings on a blade element is solely responsible for the change of momentum of a steady flow which passes through a certain actuator surface[1]. While this is a simple method, the drawback of the momentum models is that it does not capture all the effects like blade tip losses or unsteady effects without additional modelling.

1.5.1. SINGLE STREAMTUBE MODEL

The most basic version of the momentum model is a single streamtube passing through a actuator disk. In the original blade element momentum theory (BEM), the disk represented a propeller or the rotor of the horizontal axis wind turbine. Templin modified and applied this model for VAWTs[5]. Figure 1.3 shows a schematic overview of the the single streamtube model and the kinematics of the VAWT. The rotor in the figure rotates in counter-clockwise direction, and α will be positive in the upwind part of the streamtube and

negative in the downwind part. The actuator disk is positioned in the center of the turbine. Most applications use this technique as it is quick and rather accurate in specific range. As this model uses only one actuator disk for the whole rotor, the induction factor a for the upstream and downstream parts of the rotor stay constant. The mass flow rate is constant along the whole streamtube[1]. This model can become inaccurate or even invalid for large tip speed ratios or high solidities [2] and can overpredict the power coefficient due to inaccurate stall modelling [5]. Based on figure 1.3, with freestream velocity V_∞ the wake velocity is derived as $V_w = (1-2a)V_\infty$ and the velocity at the actuator disk is $V_a = \frac{1}{2}(V_\infty + V_a)$ or $V_a = (1-a)V_\infty$. The drag D can be given as $D = 2\rho S V_a(V_\infty - V_a)$ with S being the surface area of the disk. Then the disk drag coefficient C_{DD} is given as

$$C_{DD} = \frac{D}{0.5\rho V_a^2 S} \tag{1.6}$$

and substituting D into C_{DD} gives $C_{DD} = 4(\frac{V_\infty}{V_a} - 1)$ or $\frac{V_\infty}{V_a} = 1 + \frac{1}{4}C_{DD}$. This disk drag coefficient can then be converted to a normal drag coefficient via $C_D = \frac{D}{0.5\rho V_\infty^2 S}$ and equation 1.6. Substituting and rewriting gives equation 1.7, and relates the C_{DD} to C_D.

$$C_D = \frac{D}{0.5\rho V_\infty^2 S} = C_{DD}\frac{V_a^2}{V_\infty^2} = \frac{C_{DD}}{(1+\frac{1}{4}C_{DD})^2} \tag{1.7}$$

1.5.2. MULTIPLE STREAMTUBE MODEL

The multiple streamtube model extends the single streamtube model from the last section. In contrary to use of one main streamtube, this streamtube is now split into several independent smaller streamtubes. Figure 1.4 shows how one of these streamtubes is modelled. For each of the streamtube the momentum theory will be applied on like with the single streamtube model. That is for each streamtube, the momentum exchange equals the forces on the blade passing through that specific streamtube [5]. Due to the use of multiple streamtubes the variation of the wind velocity field can be accounted for[3]. Although this model uses multiple streamtubes, there is still one actuator plane at which the induced velocity is calculated and treats the rotor like it is a flat actuator disk. There are two main implementations of the multiple streamtube model besides the several small modified versions. First one is by Wilson and Lissaman and the second one is by Strickland which is an improved model of the first one and also includes more effects like windshear.

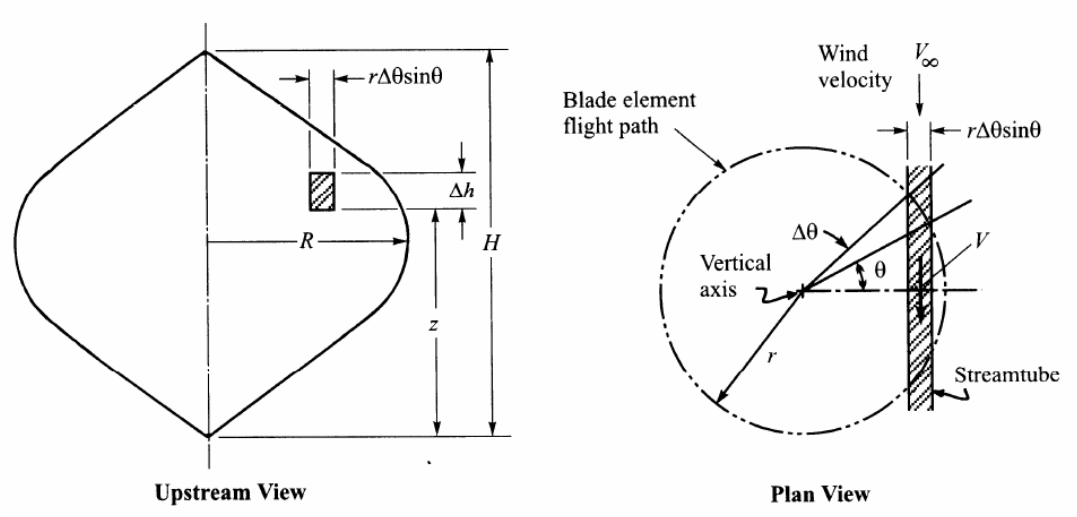

Figure 1.4: Schematic overview of the multiple streamtube model from Strickland [3]

According to Islam et al[2] the main difference between the Wilson and Strickland aerodynamic models is that Wilson used the theoretical lift force only in the calculation of induced velocity while Strickland added the effect of drag force as well for the similar calculation. This means that the model of Wilson is fast and the model of Strickland is more accurate but will lead to an increase in computation time.

1.5.3. DOUBLE-MULTIPLE STREAMTUBE MODEL

The idea of using two actuator discs in tandem is first developed by Lapin but is refined by Paraschivoiu[5][30]. It was introduced as the double-multiple streamtube model which expands the multiple streamtube model by using two actuator disks in tandem for each streamtube to model the upstream and downstream halves of the rotor separately. The single and multiple streamtube models assume one constant induced velocity throughout the rotor with one actuator disk. With the extension of using two actuator disks this method allows the calculation of two different induced velocities along each streamtube. This variation of the induced velocities can account for larger loadings on the upstream part of the rotor and smaller loadings in the downstream part. In the double-multiple streamtube method the downstream induction velocity is dependent on the upstream induction velocity. The velocities in a streamtube at can be computed with equations 1.8a to 1.8d. The equations state that the induced velocities keep decreasing along the streamtube in downstream direction. a_1 and a_2 are the induction factors of the actuator disk at upstream side respectively the downstream side of the rotor. $V_{\infty i}$ is the inflow velocity at a streamtube, V_{au} is the induced velocity upstream, V_{ad} is the induced velocity downstream, V_w is the wake velocity downstream and V_e is the induced equilibrium velocity at the center between the up- and downstream phases.

$$V_{au} = a_1 V_{\infty i} \tag{1.8a}$$

$$V_e = (2a_1 - 1) V_{\infty i} \tag{1.8b}$$

$$V_{ad} = a_2 V_e = a_2 (2a_1 - 1) V_{\infty i} \tag{1.8c}$$

$$V_w = (2a_2 - 1)(2a_1 - 1) V_{\infty i} \tag{1.8d}$$

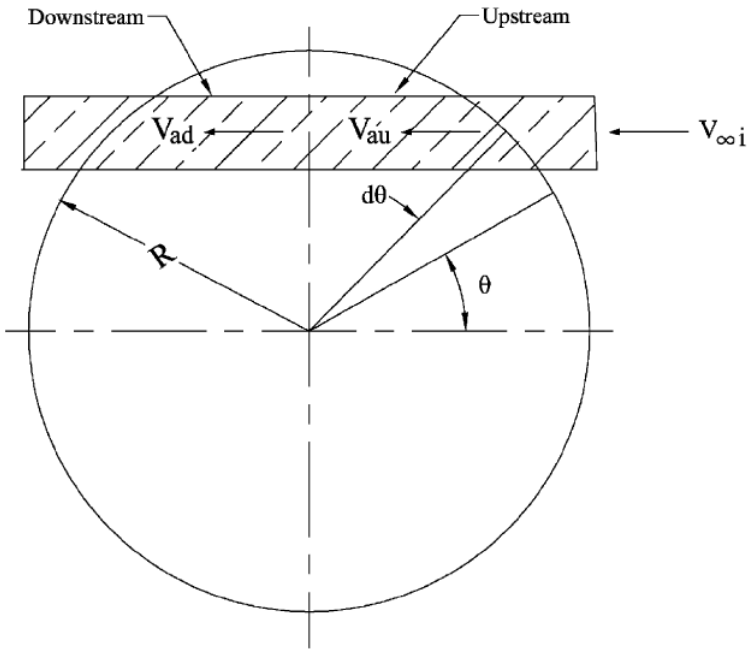

Figure 1.5: schematic overview double-multiple streamtube model [2]

Although this method models upwind and downwind regions separately, any induction effects from the downwind region to upwind region are still neglected. Paraschivoiu has made several based on the double-multiple streamtube model like the CARDAA, CARDAAV and CARDAAX codes. But in the research of Ferreira et al[31] the double-multiple streamtube model is proven to have fundamental flaws as it is not internally consistent with other models they are compared to. It is advised by them[31] to correct the model by empirical means.

1.5.4. ACTUATOR CYLINDER MODEL

Developed by Madsen[32], the actuator cylinder model (ACM) is a modification of the regular actuator disk model. Instead of modelling the VAWT rotor as a disk, the whole swept surface is instead used as actuator surface [32]. This swept surface has the circular or cylinderical shape, hence the actuator cylinder. The model is quasi-steady Eulerian and its implementation by Madsen is in 2D only to limit complexity[32]. The velocity induced by the normal loading $Q_n(\theta)$ and tangential loading $Q_t(\theta)$ can be computed analytically with this method[22]. θ is the azimuthal angle of the blade relative to the tower. Figure 1.6a shows a representation of the AC model with figure 1.6b the blade element form used by Madsen.

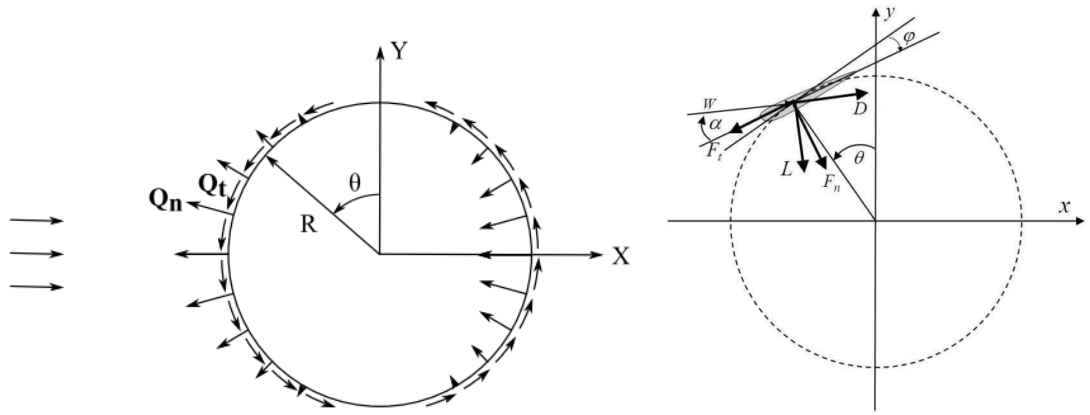

(a) 2D Actuator Cylinder Flow model[22]

(b) Blade element formulation of the AC method[32]

The loadings $Q_n(\theta)$ and $Q_t(\theta)$ can be given in the following equations 1.9 and 1.10 based on the derivations of Madsen[32]:

$$Q_t(\theta) = -B\frac{F_t(\theta)\cos\phi + F_n(\theta)\cos\phi}{2\pi R} \tag{1.9}$$

$$Q_n(\theta) = B\frac{F_n(\theta)\cos\phi - F_t(\phi)\sin\phi}{2\pi R} \tag{1.10}$$

With B the number of blades, R the turbine radius, ϕ the blade pitch angle, F_n and F_t are the blade forces per unit blade length in perpendicular direction respectively parallel direction of the swept surface. The mentioned parameters can be seen in figure 1.6b. To calculate the power generated by an ideal rotor, the ideal power generation P_i is given in equation 1.11 [32].

$$P_i = \int_0^{2\pi} v_n(\theta)Q_n(\theta)Rd\theta \tag{1.11}$$

With $v_n(\theta)$ the velocity component perpendicular to the swept surface. Then using the definition of the power coefficient:

$$C_{pi} = \frac{P_i}{\frac{1}{2}\rho V_\infty^3 2R} = \frac{\int_0^{2\pi} v_n(\theta)Q_n(\theta)Rd\theta}{\rho V_\infty^3} \tag{1.12}$$

The real power is then derived by Madsen[32] as

$$P = \frac{1}{2\pi}\int_0^{2\pi} B(F_t(\theta)\cos\phi + F_n(\theta)\sin\phi)R\Omega d\theta \tag{1.13}$$

With power coefficient C_p and thrust coefficient C_T

$$C_p = \frac{P}{\frac{1}{2}\rho V_\infty^3 2R} = \frac{\frac{1}{2\pi}\int_0^{2\pi} B(F_t(\theta)\cos\phi + F_n(\theta)\sin\phi)\Omega d\theta}{\rho V_\infty^3} \tag{1.14}$$

$$C_T = \frac{\int_0^{2\pi} (Q_n(\theta)\sin\theta + Q_t(\theta)\cos\theta)d\theta}{\rho V_\infty^2} \tag{1.15}$$

Madsen describes the flow around an actuator cylinder in 2D using Euler equations. The velocities can be described with equations 1.16a and 1.16b [32][22]. The equations have been non-dimensionalized with ρ, R and V_∞.

$$v_x = 1 + v_y \tag{1.16a}$$

$$v_y = w_y \tag{1.16b}$$

The continuity equation $\frac{\delta w_x}{\delta x} + \frac{\delta w_y}{\delta y} = 0$ and Euler equations

$$\frac{\delta w_x}{\delta x} + w_x\frac{\delta w_x}{\delta x} + w_y\frac{\delta w_x}{\delta y} = -\frac{\delta p}{\delta x} + f_x \tag{1.17a}$$

$$\frac{\delta w_y}{\delta x} + w_x\frac{\delta w_y}{\delta x} + w_y\frac{\delta w_y}{\delta y} = -\frac{\delta p}{\delta y} + f_y \tag{1.17b}$$

Madsen [32] then defines that

$$g_x = -(w_x\frac{\delta w_x}{\delta x} + w_y\frac{\delta w_x}{\delta y}) \tag{1.18a}$$

$$g_y = -(w_x\frac{\delta w_y}{\delta x} + w_y\frac{\delta w_y}{\delta y}) \tag{1.18b}$$

With all the above derived or defined the equation for pressure is then given by [32] as

$$\frac{\delta^2 p}{\delta x^2} + \frac{\delta^2 p}{\delta y^2} = (\frac{\delta f_x}{\delta x} + \frac{\delta f_y}{\delta y}) + (\frac{\delta g_x}{\delta x} + \frac{\delta g_y}{\delta y}) \tag{1.19}$$

When the pressure field is found equations 1.17a and 1.17b can be used to determine the velocity field. The solution then consist of a linear part and a non-linear part $w_x = w_x(f) + w_x(g)$ which can be summed[32]. Madsen found a solution for the linear part which is given in the equations below.

$$\begin{aligned} w_x(f) = &-\frac{1}{2\pi}\int_0^{2\pi} Q_n(\theta)\frac{-(x+\sin\theta)\sin\theta + (y-\cos\theta)\cos\theta}{(x+\sin\theta)^2 + (y-\cos\theta)^2}d\theta \\ &-\frac{1}{2\pi}\int_0^{2\pi} Q_t(\theta)\frac{-(x+\sin\theta)\cos\theta + (y-\cos\theta)\sin\theta}{(x+\sin\theta)^2 + (y-\cos\theta)^2}d\theta \\ &-(Q_n(\arccos y))^* + (Q_n(-\arccos y))^{**} \\ &-(Q_t(\arccos y)\frac{y}{\sqrt{1-y^2}})^* - (Q_t(-\arccos y)\frac{y}{\sqrt{1-y^2}})^{**} \end{aligned} \tag{1.20}$$

$$\begin{aligned} w_y(f) = &-\frac{1}{2\pi}\int_0^{2\pi} Q_n(\theta)\frac{-(x+\sin\theta)\cos\theta - (y-\cos\theta)\sin\theta}{(x+\sin\theta)^2 + (y-\cos\theta)^2}d\theta \\ &-\frac{1}{2\pi}\int_0^{2\pi} Q_t(\theta)\frac{-(x+\sin\theta)\sin\theta + (y-\cos\theta)\cos\theta}{(x+\sin\theta)^2 + (y-\cos\theta)^2}d\theta \end{aligned} \tag{1.21}$$

In the above equations 1.20 and 1.21, some terms are starred * or **. The terms marked as * shall be added inside the cylinder and the terms marked with * and ** shall be added behind the cylinder.

1.6. CASCADE MODEL

A different method for the analysis of VAWTs is the application of the cascade model first proposed by Hirsch and Mandal[33][2]. It is based on a analysis method used for turbomachinery which consists of stages of rotating blades and static vanes. In this method the blade sections of each blade are placed in a plane called the cascade. The blades are spaced evenly according to its circumferential spacing. A schematic overview of the cascade method can be found in figure 1.7. The flow conditions at each blade varies continuously as they rotate and differ from each other. The loadings can be calculated for each blade separately and the computations continue until a revolution has been made. Then the revolution averaged power can be determined[33].

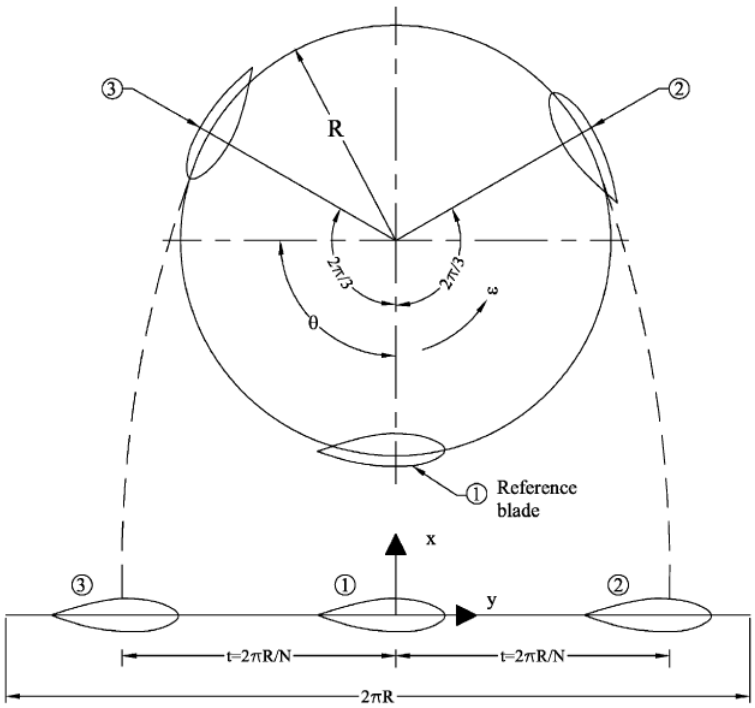

Figure 1.7: schematic overview of the cascade method [2]

The wake velocity and incoming freestream velocity in the cascade method is determined using Bernoulli's equation while the induced velocity is related to the wake velocity through a semi-empirical relations [2]. These relations for both the upwind and downwind part are given in the article of Islam et al as equations 1.22 and 1.23.

$$\frac{V_{au}}{V_\infty} = \left(\frac{V_e}{V_\infty}\right)^{k_i} \tag{1.22}$$

$$\frac{V_{ad}}{V_e} = \left(\frac{V_w}{V_e}\right)^{k_i} \tag{1.23}$$

or

$$\frac{V_{ad}}{V_\infty} = \frac{V_{ad}}{V_e}\frac{V_e}{V_\infty} = \frac{V_e}{V_\infty}\left(\frac{V_w}{V_e}\right)^{k_i} \tag{1.24}$$

Similar to the double multiple streamtube model V_{au} and V_{ad} are the induced velocities and V_e and V_w are the induced equilibrium velocity respectively wake velocity downwind. The factor k_i can be determined by experiments, and given in article [2] as $k_i = 0.425 + 0.332\sigma$ with σ the solidity. With the velocities known, the loadings of each blade can be determined with the blade element theory. Finally the torque and power coefficients can be calculated based on the loadings. The full derivation can be found in reference [33]. According to [33] and [2] the cascade model can predict the overall values of both low and high solidity turbines

quite well with reasonable computation time and accuracy. Furthermore it does not have convergence problems at high tip speed ratios and high solidities[33]. The instantaneous blade forces calculated by this model show improved correlation in comparison to those calculated by the conventional momentum models, but it is recommended by Hirsch to improve this model by adding a dynamic stall model.

1.7. VORTEX MODEL

The vortex model uses vortex singularities to solve the flows fields and is considered a medium fidelity compared to the momentum models. To understand how the vortex model works, a few fundamental theorems will be treated. This can be used for the application of the lifting line method. For the research in this report the lifting line solver CACTUS will be used.

1.7.1. KELVIN'S THEOREM

Kelvin's theorem describes that the circulation Γ_C around a closed curve C stays constant in time ($\frac{d\Gamma_C}{dt} = 0$). Consider figure 1.8 where an airfoil is positioned in a freestream U_∞ and this airfoil could be enclosed by a curve C (not shown in the drawing). To fulfill this theorem any change in bound vortex strength, indicated as $\Gamma_{airfoil}$ (also known as bound vortex Γ_b in figure 1.8, must be followed by a shed vortex with equal strength but opposite in sign at the trailing edge of an airfoil. Mathematically described as $\frac{D\Gamma}{Dt} = \frac{\Gamma_{airfoil}+\Gamma_{wake}}{\Delta t} = 0$[4]. This shed vortex by the airfoil is the so called starting vortex and forms the wake as can be seen in figure 1.8.

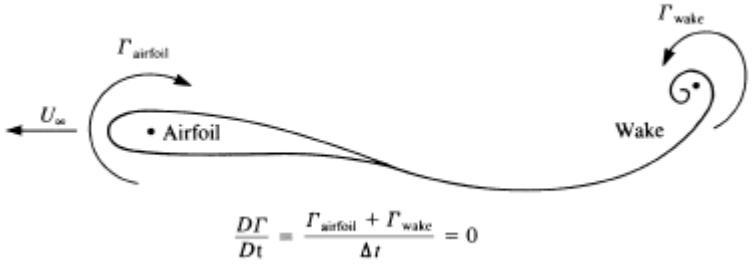

Figure 1.8: Wake vortex shed due to Kelvin's theorem [4]

1.7.2. KUTTA-JOUWKOWSKI THEOREM

In the section about Kelvin's theorem, the idea of constant circulation around a closed curve C was already discussed. This circulation Γ can also be related to lift on a lifting body via the Kutta-Jouwkowski theorem[34]. The theorem in equation 1.25 states that the lift per unit span L' is:

$$L' = \rho U_\infty \Gamma \tag{1.25}$$

Depending on how it is defined, sometimes there is a minus sign in equation 1.25. The direction of the vortex is just defined clockwise or counter clockwise. For numerical methods it is more interesting to compute the bound vortex strength (circulation) on an element. If the Kutta-Jouwkowski theorem is applied on a blade element with chord c and span b then equation 1.25 can be rewritten to $\Gamma = \frac{1}{2} C_L U c$.

1.7.3. HELMHOLTZ THEOREMS

The Helmholtz theorems state that a vortex filament in inviscid and incompressible flow contains the following characteristics[4][34]:

1. The vortex strength Γ is constant along the filament.
2. A vortex filament cannot end in a fluid, but must either form a closed loop, extend to the boundaries of the fluid or extend indefinitely.

The theorems lead to some implications when applying the Helmholtz theorem to a blade element. Suppose a bound vortex placed on the quarter chord line of a blade element in figure 1.10. Then the vortex filaments at the tips of the blade elements extend downstream, and continue as trailing vortices which might

be closed by a shed vortex from the blade element. This shed vortex is parallel to the bound vortex. It is also possible to form a so called horseshoe vortex at which the trailing vortices from the tips extend to infinity. Furthermore the strength of the full vortex filament is constant throughout its length. All the above mentioned theorems are applied in the lifting line method.

1.7.4. BIOT-SAVART LAW

The final important concept for the vortex model is the Biot-Savart law. Given a vortex filament with a certain strength Γ a velocity is induced at a certain point P in space. The Biot-Savart law relates that vortex strength to the induced velocity at the specific point using equation 1.26, see figure 1.9. This can be done for any arbitrary point in a space and thus a induced velocity field can be computed given a filament with known Γ.

$$\mathbf{U} = \frac{\Gamma}{4\pi} \frac{\mathbf{r}_1 \times \mathbf{r}_2}{|\mathbf{r}_1 \times \mathbf{r}_2|^2} \mathbf{r}_0 \cdot \left(\frac{\mathbf{r}_1}{\mathbf{r}_2} - \frac{\mathbf{r}_2}{\mathbf{r}_1} \right) \tag{1.26}$$

$\mathbf{r}_1$ and $\mathbf{r}_2$ are respectively the position vector from the start and end of the vortex filament to the arbitrary point P in the field. $\mathbf{r}_0$ is the vector from start of the filament to its end. Note that in this case it is assumed the vortex filament is straight, but it can be applied to filaments with arbitrary shapes. By assuming infinitesimal vortex filament lengths to describe any curve, the vortex strengths can be integrated along the whole filament. These vortex strengths together induce a velocity on any arbitrary point in the field. Therefore a relation is found between the induced velocity and the geometry of a lifting body.

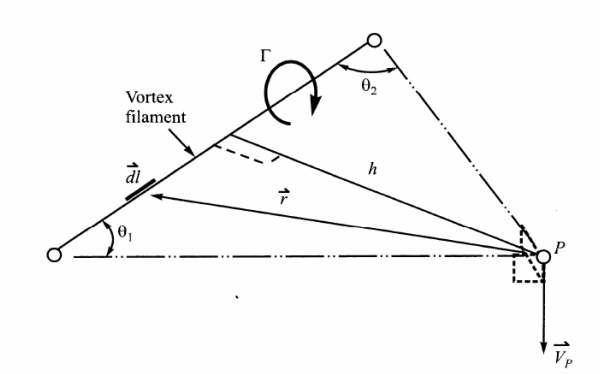

Figure 1.9: Induced velocity by the Biot-Savart law [5]

1.7.5. LIFTING LINE MODEL

Vortex models allow to solve the downwash velocity on a lifting body using the vortex distributions on the body. There are multiple ways to model the lifting body, for example the use of surfaces or lines. This section will focus only on the lifting line model (also called vortex line method or vortex lattice method) as this is of interest for the use of CACTUS. The other methods are out of scope for this thesis.

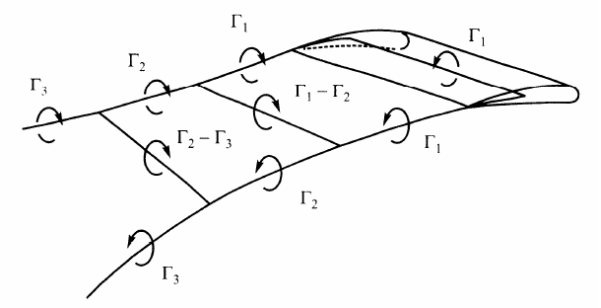

Figure 1.10: Schematic view of a vortex lattice element [5]

In the lifting line model the system of vortex singularities, common for more advanced methods, is replaced by a bound vortex line along the quarter chord line. The bound vortex strength for each element Γ_B

will be calculated using the Kutta-Jouwkowski theorem $\Gamma_B = \frac{1}{2} c C_L U_\infty$. For the use of this method, the lift and drag polars must be known in advance. In order to use the correct values from the lift and drag polars, the element's angle of attack α must be calculated using the downwash and freestream velocities. All loading coefficients on the element are then determined using α and the polars. The newly determined lift coefficient can be used again to determine the new bound vortex strength $\Gamma_{B,new}$. The newly computed and old $\Gamma_{B,old}$ are compared and possibly updated for further computations. Once convergence of the Γ_B value is reached, the process is completed. Sometimes filtering can be applied to ease the convergence in the next iteration. A filtering equation $\Gamma_{B,updated} = (1-D)\Gamma_{B,old} + D\Gamma_{B,new}$ can be applied to update the Γ_B for every blade element[35]. D is a damping factor which determines how smooth the update of the new Γ_B will be, but as consequence the computation time will increase. For the application of the lifting line method on a wing in steady state conditions this process would then be finished. The general flowchart of the non-linear lifting line method can be found in figure 1.11. All other coefficients like the blade tangential coefficient $C_T = C_L \sin\alpha - C_D \cos\alpha$ and normal coefficient $C_N = C_D \sin\alpha - C_L \cos\alpha$ can be derived from the basic lift and drag coefficients. The tangential coefficient can then be used to determine the torque coefficient C_Q and from there follows the power coefficient C_P of the rotor[6]. For a wind turbine the lifting line method is repeated for every timestep in a revolution until a certain amount of revolutions has been reached, or until the (revolution averaged) power coefficient C_P value is converged.
Based on the Helmholtz theorem discussed earlier, the bound vortex will convert into a trailing vortex at the tips of each element and the element also contains a shed vortex. The system of trailing and shed vortices will form the wake of the blade element. Figure 1.12 shows the lattices and points containing the bound vortex of several elements and its trailing and shed vortices in a numerical method developed by Strickland[6]. These vortex lattice points are the points connecting the vortex filaments and are convected in time. The trailing Γ_T and shed Γ_S vortex strength is related to the bound vortex strength Γ_B change. Numerically this can be given as equations 1.27a and 1.27b.

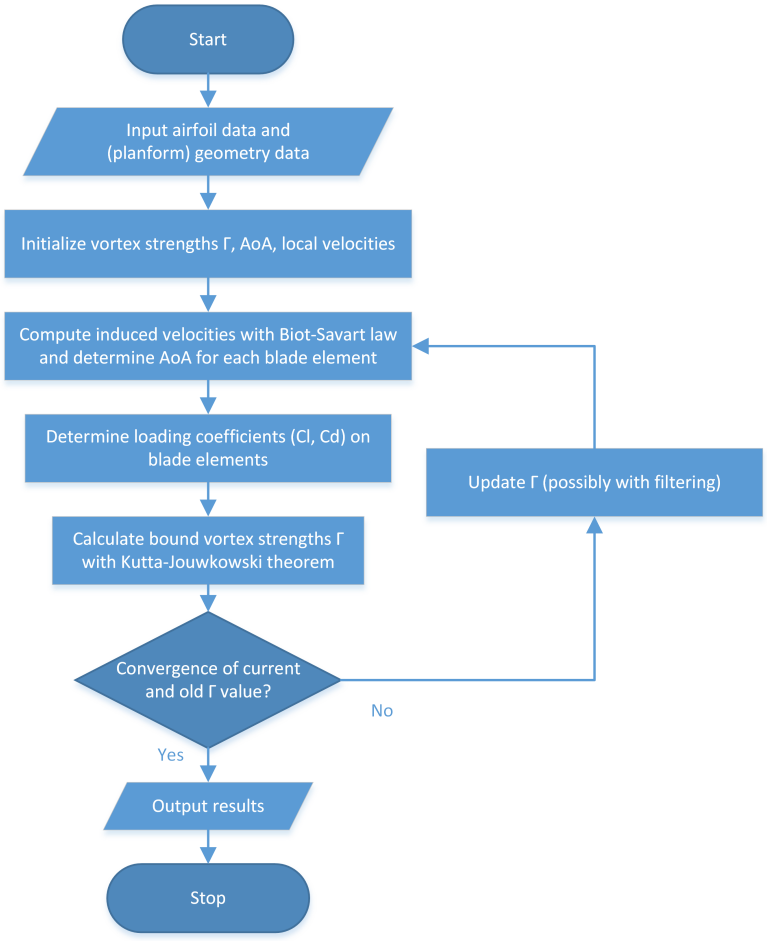

Figure 1.11: Flowchart for the (Weissinger) non-linear lifting line method

1.7.6. WAKE MODELS

In the last section the rotor wake which consists of the shed and trailing vortices were mentioned. Based on how these shed or trailing vortices are treated, the lifting line method either contains a free wake vortex model or a fixed wake vortex model[36]. In the fixed vortex wake, the advection of the lattice points of the trailing and shed vortex points are prescribed. Thus the influence by the induced velocities from other wake elements are ignored. As consequence the wake structure stays constant downstream. This method has lower fidelity as in reality there should be interference between the vortex elements in the wake. But it requires less intensive computational resources. In contrary to the fixed wake model, the free wake vortex model allows the mutual interference between wake vortex elements to advect its element downstream. Therefore the wake in a free vortex model can deform substantially over time[36]. While this is more realistic than and higher fidelity than the fixed vortex wake, this will also require more computational resources. The vortex lattice points of the wake will translate a certain distance per time interval. This distance $\Delta\mathbf{s}(i,j)$ in 3D space can numerically be described by $\Delta\mathbf{s}(i,j) = [\mathbf{U}(i,j) + U_\infty\mathbf{i}]\Delta t$. For more successive timesteps Strickland used an improved integration scheme $\Delta\mathbf{s}(i,j) = [\frac{3}{2}\mathbf{U}(i,j)_{t=NT} - \frac{1}{2}\mathbf{U}(i,j)_{t=NT-1} + U_\infty\mathbf{i}]\Delta t$ to determine the convected distance of the lattice points. With all the above mentioned techniques, the fundamentals for the application of the lifting line method for VAWTs is set here. Important note is that with the vortex method no pressure field is directly calculated, only the velocity field. Finally the regular vortex method is still a potential flow model and does not include thickness or displacement effects[37]. It also does not intrinsically model dynamic stall effects. Thus these effects must be determined via engineering models or taken into account via airfoil test data.

$$\Gamma_S(I,NT-1) = \Gamma_B(I,NT-1) - \Gamma_B(I,NT) \tag{1.27a}$$

$$\Gamma_T(I,NT-1) = \Gamma_B(I,NT) - \Gamma_B(I-1,NT) \tag{1.27b}$$

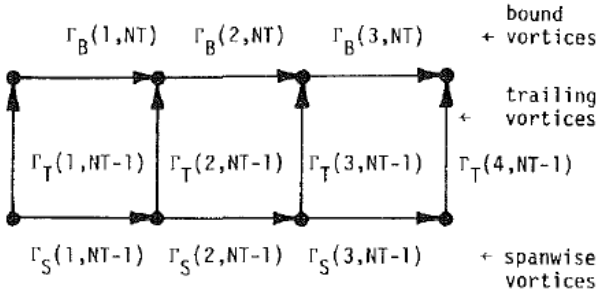

Figure 1.12: Numerical modelling of vortex lattices and nodes [6]

1.7.7. LIFTING LINE CODE: CACTUS

In this section CACTUS will be introduced, and its implementation and usage will be discussed. Code for Axial and Cross-flow TUrbine Simulation (CACTUS) is an open source 3D lifting line tool developed in Fortran by Sandia National Laboratories [17]. It is used to predict the aerodynamic performances of a HAWT, VAWT or a hydrokinetic turbine (an underwater VAWT). To model the wake, CACTUS uses the free wake vortex model and also contains many options for unsteady, viscous and compressible flow. CACTUS is originally based and extended on the VDART3 solver by Strickland et al[17][18]. It is one of the few tools available which can model struts in case of a VAWT, although it is limited to flat and fixed strut shape without the possibility to edit the strut parameters. It is considered a mid-fidelity method being more accurate than standard momentum models but computationally more efficient than CFD. It could be a very potential code for optimizing design of VAWT. As this is the program of interest for the thesis, we go more in depth in this part.

CACTUS uses blade elements and each of the sections can use specific aerodynamic characteristics[17]. Basic parametrization of these elements consists of the chords, position and orientation values. The aerodynamic loads of the blade element sections can be determined by known lift, drag and moment polar data of the airfoils representing the blade element sections[17]. CACTUS furthermore has the possibility to include strut elements which only accounts for drag and no lift.

CACTUS models the wake using freestream elements, trailing and spanwise wake vortices. The blade elements are modelled using a bound vortex attached at quarter chord position[17]. The bound vortex of each blade element Γ_i can be related to the lift coefficient via the Kutta-Jouwkowski theorem $\Gamma_i = \frac{1}{2}cUC_L$. Due to

Helmholtz theorem the trailing and spanwise wake vorticity can be equated to the change of bound vorticity. Furthermore the velocity field of the wake can be determined using the Biot-Savart law and the velocity field can be used again to determine the local inflow velocity for each blade element. All the blade elements together can then form a system of equations at every time step which can then be solved by CACTUS. The system of equations are represented by equations 1.28a and 1.28b solved implicitly via single fixed-point iteration[17]. Finally with the results of the iterations, the torque and power coefficients can be calculated. This process is repeated for all timesteps[17]. The amount of timesteps is user defined[18].

$$\alpha_{element}, V_{element} = f(\Gamma_{bound}, \Gamma_{trailing}, \Gamma_{spanwise}, freestream, geometry) \tag{1.28a}$$

$$\Gamma_B = f(C_{L,element}, V_{element}, geometry) \tag{1.28b}$$

For the advancement of the wake node positions CACTUS uses second order predictor explicit time advancement scheme. This is based on the midpoint rule where the wake node velocities at time $t + \frac{\Delta t}{2}$ are predicted using previous and current time steps[17]. For dynamic stall prediction, CACTUS is able to use, the Boeing-Vertol model, a modified version of the Gormont model. It can also use the more extensive Leishman-Beddoes model.

1.8. CFD

Although out of the scope of this thesis, a mention will be made for Computational Fluid Dynamics (CFD). CFD is the application of Navier-Stokes equations with possible additional models. The use of CFD consists of defining the VAWT geometry in 2D or 3D and the discretization of (fluid) volume of the simulation. Then the velocities, pressures and are directly solved. The application of CFD is a high-fidelity method but is also computationally expensive. Therefore it is not really used for practical engineering analysis[38]. Although the Navier-Stokes equations can be applied directly called Direct Numerical Simulation (DNS), it is impractical to do so due to the computational resources required for a simulation of this type. The reason is the turbulence phenomena for which the full range of length and time scales of the turbulence must be resolved. The resource requirements for this scales non-linearly with the Reynolds number of the flow. As such for high Reynold number flow these simulations are impractical to run.
As consequence several methods to model turbulence have been developed. One of the two main model is the Reynolds-Averaged Navier-Stokes (RANS) where the Navier-Stokes are time averaged [39] or the Large Eddy Simulation (LES). Many studies have been performed on VAWTs using CFD. Further readings about the applications of CFD in VAWT research can be found in [40], [41], [42], [39] and [13].

2

UNSTEADY AERODYNAMICS

This chapter discusses the topic of unsteady aerodynamics. The wake shed by the VAWT rotor consists of many unsteady flow phenomena as the blades and struts rotate perpendicular to the flow. Figure 2.1 shows some of these possible phenomena. These phenomena will have an impact on the performance of the turbine and on the near wake structure downstream.

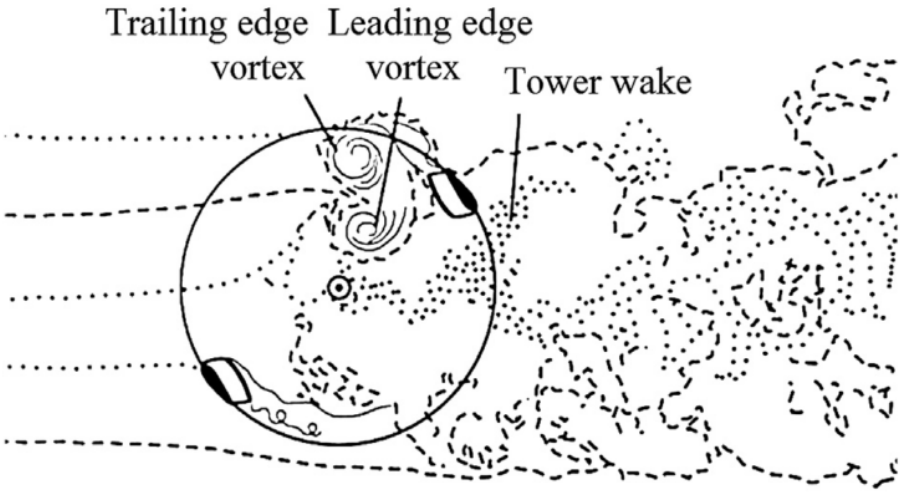

Figure 2.1: Unsteady effects encountered in the wake of a VAWT[7]

2.1. DYNAMIC STALL

Dynamic stall is an unsteady flow phenomenon that occurs when the blade's airfoil angle of attack α varies rapidly with time and also exceeds the normal static stall angle of attack. The blades and struts of a VAWT rotate in such a way that the α of the blades changes continuously along the azimuthal angle θ. Whether a dynamic stall process is initiated depends on several mechanisms like the breakdown of a (laminar) separation bubble or interaction between boundary layer and shock wave[8]. The phenomena is thus dependent on the Reynolds number and Mach number. The stall process then consists of several stages described in figure 2.2.

The first phase of the dynamic stall process is initiated when the angle of attack exceeds the static stall angle of the airfoil. This stall onset is indicated with number '2' in figure 2.2. Instead of the regular loss in lift due to static stall, the lift continues increasing with α. The next phase is characterized by the development of a dynamic stall vortex on the airfoil surface[8]. This vortex will advect downstream over the airfoil surface increasing the lift even more, but also leading to a pitching moment and increased drag of the airfoil as shown in phase '3' in figure 2.2. Finally the lift is fully lost when the dynamic stall vortex convects off the airfoil and the flow is fully separated and reattaches only below a certain α. They are given as phase '4' and '5' in figure

2.2. How the flow reattaches after separation and the α at which the flow reattaches again can be lower than the static stall angle. This effect is called hysteresis. Dynamic stall can lead to unsteady blade loads and thus blade fatigue[43][5].

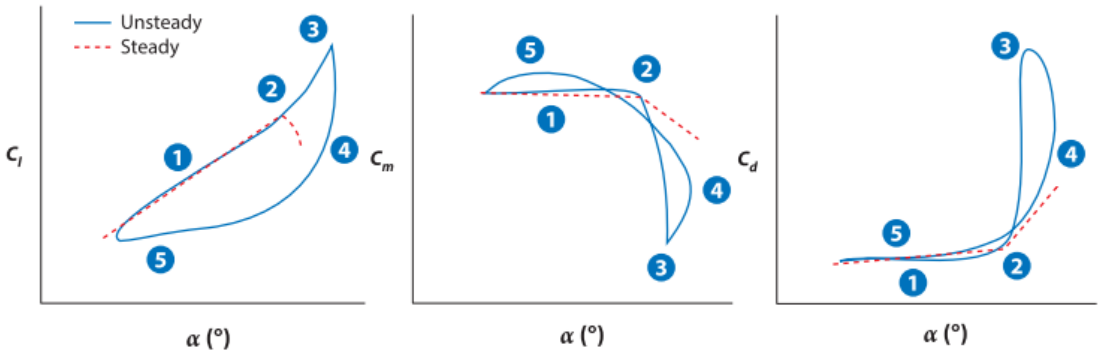

Figure 2.2: The typical airfoil C_l, C_d and C_m polars. Compared to the regular steady case, the hysteresis effect can be seen during dynamic stall[8].

2.2. DYNAMIC STALL MODELS

The dynamic stall process is complex as shown by [8], but nonetheless very important in VAWT analysis. To predict the dynamic stall phenomenon, different engineering models have been created. According to Borg[44] there are three main categories of dynamic stall models:

1. The modelling of the actual kinematics of dynamic stall known as indicial method[5]. It is a more fundamental approach where the vortex formation and shedding are modelled directly. The Leishman-Beddoes dynamic stall model[45] is an example of the indicial method.

2. Models that neglect the kinematics of the process and only model the characteristics of the aerodynamic loads. The ONERA model for dynamic stall[46] is a good example. The ONERA model does not try to directly model the effects of dynamic stall, but does directly simulate the aerodynamic responses in the time domain[46]. According to [46] this method give less accurate prediction of rotor blade loading compared to the other methods, but the main advantage of this model is that the governing system of equations can be linearized. As consequence the model is really suited for inclusion in analyses of rotor stability.

3. Models that use empirical equations to determine the effective angle of attack under dynamic conditions. This effective angle of attack is then used to determine a reference angle of attack for which the aerodynamic loading is determined[44][5]. A widely used model of this category[44] is the Gormont model[47]. There are also many derivatives based on the Gormont model like the Berg modification or Boeing-Vertol modification.

The indicial and Boeing-Vertol (Gormont) model will be discussed in the next sections as these are the two more known models and also used in the CACTUS software.

2.3. BOEING-VERTOL MODEL

The Boeing-Vertol model is a modification of the Gormont dynamic stall model[47] made by Strickland which is more suited for VAWTs[5]. The model is based on the observation that an airfoil appears to have stall onset at a higher α, when the stall condition is initiated at a significant angle of attack rate $\dot{\alpha}$[17]. In the Boeing-Vertol model the flow is assumed to be incompressible[5]. Another assumption is that the lift curve slope and zero lift angle of the airfoil does not change compared to the static stall situation. So the dynamic effects only change the stall angle of attack[5]. Finally the Boeing-Vertol model will be applied when α exceeds the static stall angle. The dynamic stall effect is modelled as modifications in lift, drag and moment on the airfoil using a modified reference angle of attack α_m. This lagged α_m can then be given as a function of the rate of angle of attack $\dot{\alpha}$ according to equation 2.1[17]. The lift, drag and moment coefficients are then given by 2.2a, 2.2b and 2.2c.

$$\alpha_m = \alpha - K_1\gamma\sqrt{\left(|\frac{c\dot{\alpha}}{2V}|\right)}S_{\dot{\alpha}} \tag{2.1}$$

$$C_L = \frac{\alpha}{\alpha_m - \alpha_0}C_L(\alpha_m) \tag{2.2a}$$

$$C_D = C_D(\alpha_m) \tag{2.2b}$$

$$C_M = C_m(\alpha_m) \tag{2.2c}$$

α is the blade's angle of attack, α_0 the blade's angle of attack at zero lift, $S_{\dot{\alpha}}$ the sign of $\dot{\alpha}$,K_1 and γ are empirical functions determined by experiments. γ is a function which depends on blade thickness and local Mach number[5]. Typical values of K_1 and γ are given in equations 2.3a, 2.3b, 2.3c and 2.3d.

$$\gamma_L = 1.4 - 6(0.06 - \frac{t}{c}) \tag{2.3a}$$

$$\gamma_D = 1 - 2.5(0.06 - \frac{t}{c}) \tag{2.3b}$$

$$\gamma_M = \gamma_D \tag{2.3c}$$

$$K_1 = 0.75 + 0.25S_{S\dot{\alpha}} \tag{2.3d}$$

The sign and magnitude of K_1 depends on $\dot{\alpha}$ via $S_{\dot{\alpha}}$. Note that the term $|\frac{c\dot{\alpha}}{2V_\infty}|$ in equation 2.1 looks very similar to the reduced frequency k often encountered in literature about unsteady flow behavior where $\dot{\alpha}$ relates to the angular frequency of the unsteady behavior.

2.4. INDICIAL MODEL

Another method for dynamic stall modelling is the indicial model which is more fundamental than the Boeing-Vertol model as it takes into account the kinematics of the whole process[44]. The effects are modelled separately and the indicial responses are then summed[5]. The indicial model uses a set of first order differential equations to model the dynamics and has three parts which are modelled[5][17]:

1. Unsteady attached flow.
2. Separated flow solution for nonlinear flow.
3. Deep stall for vortex induced loads.

2.4.1. ATTACHED FLOW

The attached flow part is first formulated with superposition of the indicial terms[45]. These terms consist of the circulatory and impulsive responses, which is represented by $C_N(t) = C_{N,circulatory}(t) + C_{N,impulsive}(t)$. C_N is the total normal force coefficient, $C_{N,circulatory}$ the circulatory part and $C_{N,impulsive}$ the impulsive part of the normal force coefficient. The circulatory part $C_{N,circulatory}(t) = C_{L_\alpha}\alpha_E\cos\alpha_E$ models the response due to the change in angle of attack α and includes a lagging behaviour[5]. α_E is the effective angle of attack. This effective angle of attack can then be modelled using indicial function $\phi_c(t)$, and angles of attack at a certain timestep n α_n and α_{n-1}. The indicial function contains a reduced time s which depends on the flow and thickness of the blade profile. Equations 2.4a-2.4d shows these relations.

$$\alpha_E = \alpha_{n-1} + \phi_c(t)\Delta\alpha \tag{2.4a}$$

$$\Delta\alpha = \alpha_n - \alpha_{n-1} \tag{2.4b}$$

$$\phi_c(t) = A_0 - A_1e^{-b_1s} - A_2e^{-b_2s} \tag{2.4c}$$

$$s = (1 - M^2)2V\frac{t}{c} \tag{2.4d}$$

$\phi_c(t)$ also contains the constants A_0, A_1, A_2, b_1, b_2 which must be determined using experiments[5]. The second part of the response is the non-circulatory part and is described in equations 2.5a and 2.5b. T_1 is characteristic time parameter.

$$C_{N,impulsive} = \frac{\phi_I(t)\Delta\alpha}{M} \tag{2.5a}$$

$$\phi_I(t) = e^{\frac{-t}{T_1}} \tag{2.5b}$$

Finally tangential force coefficient $C_{tangential} = C_{L_\alpha}\alpha_E \sin\alpha_E$ and the total drag can be approximated with $C_D(t) = C_N(t)\sin\alpha - C_{tangential}(t)\cos\alpha + C_{D0}$

2.4.2. NONLINEAR FLOW

The nonlinear flow solution for trailing edge separation is based on the theory of Kirchhoff[45][5]. To account for the nonlinear effect, an empirical function is used to describe the nonlinear part of the normal force $C_{N,nonlinear} = \frac{1}{4}C_{N,circulatory}(1+\sqrt{f})^2$, with f being the non-dimensional separation point[5]. This f is dependent on the angle of attack α and some empirical parameters.
To account for transient effects, which influences the separation point, the indicial method introduces two first order differential equations to model these effects. They can be found in equations 2.6a-2.6d. T_p and T_f are non-dimensional parameters depending on Mach number. C'_N models the pressure response while C'_{NF} models the boundary layer response[5].

$$C'_N = \phi_p(t)C_{N,nonlinear} \tag{2.6a}$$

$$\phi_p(t) = 1 - e^{\frac{-2Vt}{cTp}} \tag{2.6b}$$

$$C'_{NF} = \phi_F(t)C_N \tag{2.6c}$$

$$\phi_f(t) = 1 - e^{\frac{-2Vt}{cT_f}} \tag{2.6d}$$

2.4.3. DEEP STALL

The last part to model is when a vortex is generated at the leading edge of the blade profile which then convects downstream. This event leads to vortex lift, see figure 2.3 and is modelled as $C_{L,vortex} = C_{N,circulatory}(t)(1-K)$ with $K = \frac{1}{4}(1+\sqrt{f})^2$. According to Paraschivoiu the effect created by the vortex will lead to a delay in reattachment[5].

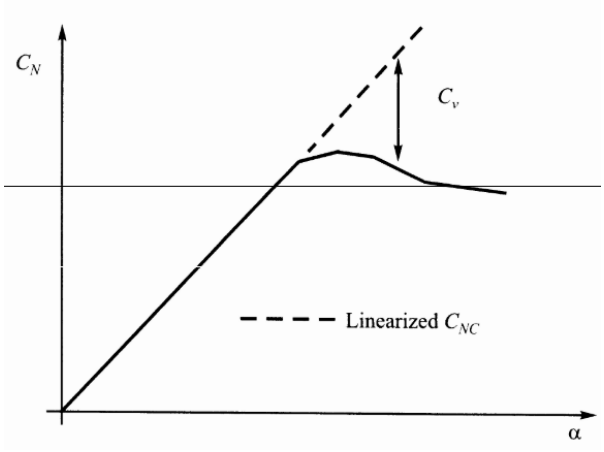

Figure 2.3: Vortex lift contribution due to deep stall [5]

2.4.4. LEISHMAN-BEDDOES MODEL

The Leishman-Beddoes model[45] is also an advanced model based on indicial formulation but is modified to give it more semi-empirical approach for representation of lift, drag and moment loadings under dynamic stall. This model is originally developed by Leishman and Beddoes for rotorcraft applications. This is done as a more accurate model was needed while keeping the computational costs practical[45]. According to [45] the model extends upon the indicial model and still uses the superposition of indicial responses for the attached flow behaviour. Furthermore it contains compressibility corrections to accurately model the unsteady aerodynamic response. Under attached flow conditions the Leishman-Beddoes model behaves like the indicial formulation[45]. Then the different phases of dynamic stall are represented in different ways. The onset of vortex shedding during dynamic stall will be represented according to Leishman using "a criterion for leading edge or shock induced separation based on the attainment of a critical leading edge pressure"[45]. The

induced vortex lift is modelled empirically and all other non-linearities regarding trailing edge separation will be modelled using the Kirchoff flow model. As can be read, this makes the Leishman-Beddoes model a very complex method. Nonetheless, they managed to implement this and validate their method.

2.5. MODEL COMPARISON

The performance between the Gormont and Leishman-Beddoes models were assessed by Dyachuk and Goude[25]. They implemented these models within a double multiple streamtube analysis of a 2D VAWT. The Leishman-Beddoes model showed better agreement with experimental data compared to the Gormont model in all conditions[25]. Another observation made by them was that the Leishman-Beddoes model is more stable. So with more accurate results and more stable simulation they concluded that the Leishman-Beddoes model outperforms the Gormont model[25]. This is also what the CACTUS manual suggests[18], but in addition it also mentions that the amount of time steps required to converge will increase when using the Leishman-Beddoes model[18]. Unfortunately the research of Dyachuk and Goude does not mention any simulation time of the assessed models.

2.6. TOWER SHADOW EFFECT

Borg et al[44] mention the effects of the support tower on the performance of the VAWT. The main cause is due to the blades crossing the low velocity wake created by the tower. This can contribute to periodic fluctuations in the power output of the VAWT[44]. Rezaeiha et al[48] studied these effects and concluded that based on the tower-to-rotor diameter ratio of 0.16, the reduction on C_p can be as high as 5.5%. With greater thickness the loss is larger due to the larger low velocity wake downstream of the tower[48]. Furthermore they concluded that for tower-to-rotor ratio bigger than 0.4 will cause blade-wake interactions between the vortices shed from the tower and the blades[48]. Finally the roughness effect of the tower was also studied. Roughness was added to the tower and this shifted the flow condition of the tower from subcritical to critical, resulting in a delay of flow separation. As result the tower wake width decreased and the blade was less affected by the wake. This led to an increase of VAWT performance[48].

2.7. BLADE-WAKE INTERACTIONS

Another unsteady phenomenon to consider for VAWTs are the non-linear interactions between the vortices in the wake and the blades. These vortices are for example generated by the blade tip in the upwind direction and are then convected downwind[40]. As consequence of these interactions there could be vibrations or unsteady loading on the blade[9]. Another issue could be aero-acoustic consequences due to vortex interacting, therefore generating unwanted sounds[9]. According to Ferrer and Willden blade-wake interactions are usually not modelled in lower fidelity models like the momentum models, but by understanding the blade-wake interactions these models can be improved to account for these effects[9].
Ferrer defined two physical processes causing blade-wake interactions. First this is the vortex shedding of the blade in the upwind side of the rotor and the convection of this vortex. Secondly is the rotation of the blades[9]. The type of interaction depends on the wake convection speed and the blade rotational speed. Ferrer and Willden expected three different types of blade-wake interaction with its limiting cases, and these limiting cases depend on the tip speed ratio λ and wake convection velocity U_i. The limiting cases for one blade are given in figure 2.4. The wake convection velocity is regarded as the induced velocity $U_i = a \cdot U_\infty$. So Ferrer and Willden derived that the time required for the wake to reach the downwind section can be approximated as $t_{wake} = \frac{D}{a \cdot U_\infty}$ and the time required for the blade to go from the most upwind position to the most downwind position (therefore turning 180°) is then given as $t_{blade} = \frac{\pi R}{R\omega}$ [9]. This leads the observation that when $t_{wake} < t_{blade}$ the wake will not interact with the blade, as the blade only passes the downwind section when the wake has already convected downwind (figure 2.4a). But when $t_{wake} \geq t_{blade}$ then the wake passes the downwind area while the blade also passes the downwind area, thus there could be blade-wake interaction[9]. Ferrer and Willden then makes the assumption for the limiting case $\frac{t_{wake}}{t_{blade}} = \frac{2R}{aU_\infty} / \frac{\pi R}{\omega R} \approx 1$. This equation can be rewritten and thus the first limiting tip speed ratio for blade-wake interaction is $\lambda \geq \frac{a\pi}{2}$ [9]. However according to the same authors there could still be blade-wake interactions for $\lambda \leq \frac{a\pi}{2}$, but they only occur at the lower rear quadrant due to the proximity of the blade to the shed wake in the lower circular half of the rotor (positions based on figure 2.4)[9]. Further derivations can be found in the paper[9]. The authors provided a summary for the limiting cases for 1-bladed VAWTs and 3-blade VAWTs, this can be found in table 2.1.

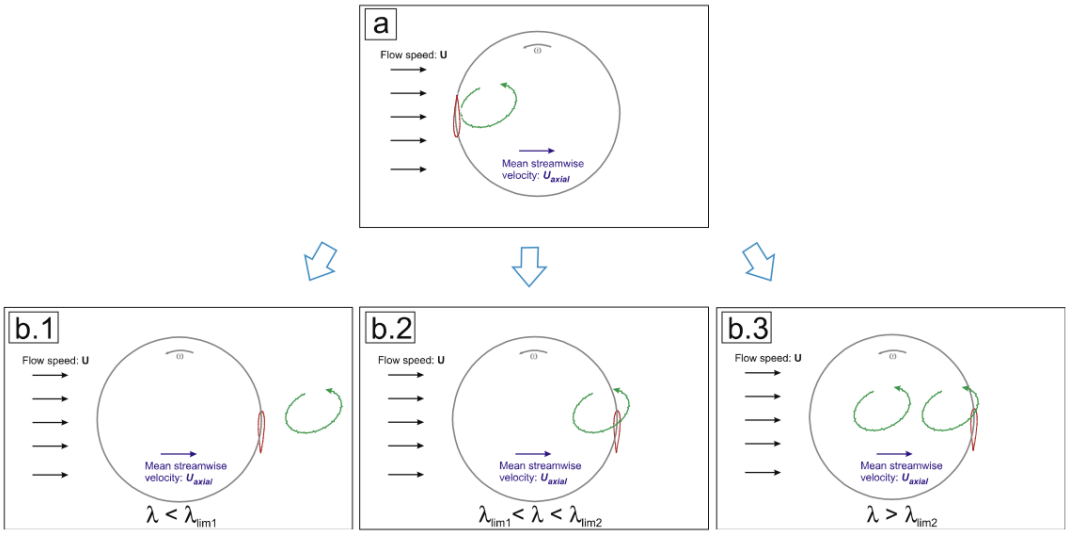

Figure 2.4: Schematic overview of the types of blade-wake interaction and its limiting condition by tip speed ratio λ. Situation a is the initial vortex shedding in the upwind region. λ in situation $b.1$ is sufficiently small and causes no blade-wake interaction. In the situations $b.2$ and $b.3$ the tip speed ratio is such that the wakes causes by the blade interacts with itself[9]

1-bladed				
Limits	$\lambda < a$	$a < \lambda < \frac{a\pi}{2}$	$\frac{a\pi}{2} < \lambda < \frac{3a\pi}{2}$	$\frac{3a\pi}{2} < \lambda$
Type of interaction	No interactions	Limited interaction	One wake	Two wakes or more
Force effect with azimuth θ	N/A	$180° < \theta < 270°$	$180° < \theta < 270°$	$180° < \theta < 360°$
3-bladed				
Limits	$\lambda < \frac{a\pi}{6}$	$\frac{a\pi}{6} < \lambda < \frac{a\pi}{2}$	$\frac{a\pi}{2} < \lambda < \frac{5a\pi}{2}$	$\frac{5a\pi}{2} < \lambda$
Type of interaction	Limited interaction	One wake	Two wakes	Three wakes or more
Force effect with azimuth	$180° < \theta < 270°$	$180° < \theta < 360°$	Everywhere	Everywhere

Table 2.1: Summary of the limiting cases for blade-wake interactions by Ferrer and Willden[9]

To validate their analysis of the bounds and the effects they employed Discontinuous Galerkin solver, a snapshot of the simulation can be found in figure 2.5. Figure 2.4 also shows where the blade and wake interact and at which tip speed ratio. Ferrer and Willden concluded that their analysis of the limits agrees well with the simulated results of the Discontinuous Galerkin (DG) solver. They also have checked the dependency on Reynolds number and came to the conclusion that the blade-wake interactions are similar on all Reynolds numbers[9].

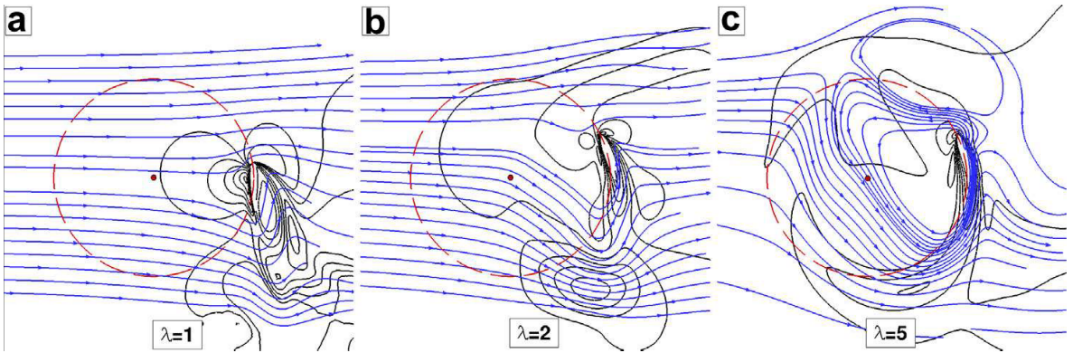

Figure 2.5: Result of DG simulation: Velocity magnitudes contours and streamlines for different λ. [9]

3

STRUT AERODYNAMIC MODELLING

The modelling of a strut in a VAWT is the point of interest for the thesis. This chapter will evaluate previous studies performed on this subject. The strut can under certain conditions produce lift, with aerodynamical mechanisms treated in the other chapter. Another interesting point of strut modelling is the drag caused by a strut. The strut drag consist of three main drag components: profile drag, friction drag and lift induced drag. An extra component can be added at the intersection between strut and blade, the interference drag.

3.1. STRUT-BLADE INTERFERENCE

The drag of intersecting bodies or with two bodies nearby each other is usually a bit higher than the combination of the drag components of the bodies isolated. This phenomena is called interference[10]. Interference drag is the extra drag component that occurs at intersections between two bodies [10]. The VAWT can contain struts which are connected to the blade, thus the interference drag at the joint between the strut and the blade should be taken into account.
This interference effect happens because the boundary layers of the bodies join together. The boundary layer is further retarded and in addition the pressure drag arises[10]. Interference drag is independent of the span but instead is only based on the dimensions of the blade section. In a study of Hoerner[10] it is mentioned that lift and inclination angle of the body will influence the amount of interference drag. In case of a lifting body, the increase of lift coefficient will lead to an increase in pressure gradient on the upper side of the lifting body near the intersection while decreasing the pressure gradient on the lower side of that intersection. Interference drag also increases approximately as square of the lift coefficient[10].
As specified earlier, inclined struts can lead to extra or less interference drag. There are two ways to incline a strut, longitudinally (sweep) and laterally (canting/inclination) relative to the freestream direction. For this research the interest is specifically in the laterally inclined strut. By laterally inclining the strut one of the corners become more narrow and thus increases separation which leads to increased interference drag[10]. Figure 3.1 shows the relation between the lateral inclination angle β and the increase in drag as consequence of the inclination. It can be seen in the figure that at higher inclination angles this drag increment becomes substantial.

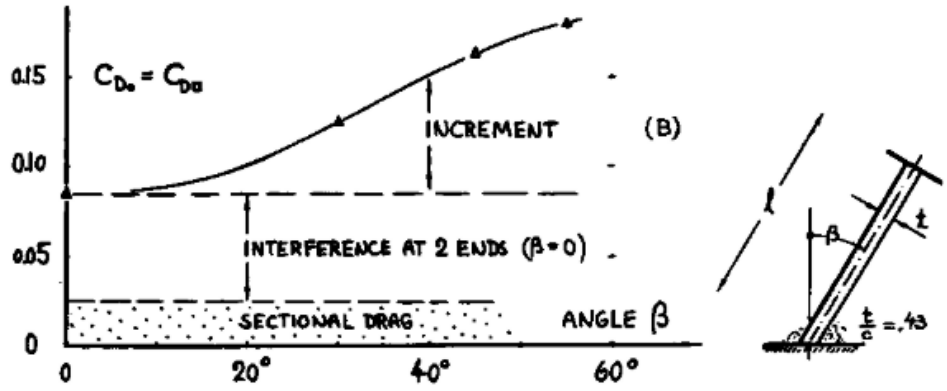

Figure 3.1: Increase in interference drag due to lateral inclination angle β [10]

Hoerner models these effects using data from experiments of the different possible situations[10]. For the case of a strut-blade T-shaped intersection without inclination this is approximated with equation 3.1 and figure 3.2. The interference drag in a T-shaped intersection is modelled as a function of only the thickness ratio of the strut. It can also be concluded from figure 3.2 that the application of fillets leads to a more linear relation between the strut's thickness ratio and interference drag. The filleting can thus lead to lower the interference drag, especially at higher thickness ratios.

$$C_{Dc} = \frac{\Delta D}{qc^2} = (17(\frac{t}{c})^2 - 0.05)(\frac{t}{c})^2 \tag{3.1}$$

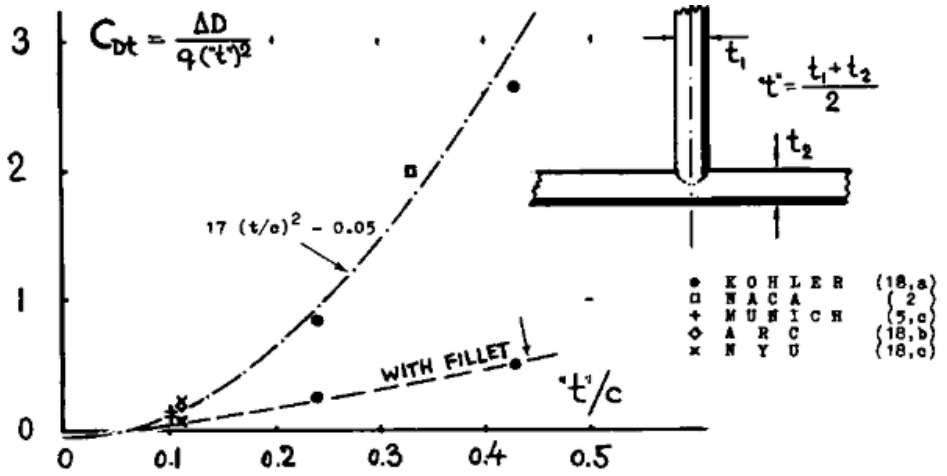

Figure 3.2: Interference drag coefficient of strut intersections against the thickness $\frac{t}{c}$ [10]

The tips of the blade and the intersection between blade and strut generate vortices. These shed vortices could lead to a reduction in lift and extra drag[44][10]. The extra drag component caused by lift is the so called lift-induced drag and is an important component of the drag caused by struts or blades.
One of the studies about struts as lifting bodies can be found in the research of Shires[11]. Shires developed the concept of a V-rotor VAWT, which functions similar to H-Darrieus with inclined struts. This NOVA V-VAWT can be seen in figure 3.3a. Shires attempts to predict the performance of the V-VAWT using modified version of Paraschivoiu's double-multiple streamtube method[11][5]. This modified model is able to evaluate lateral and vertical streamtubes through the rotor, and can predict the induced velocity field in 3D[11]. In addition the model also takes into account dynamic stall considerations, tower losses, tip losses and interference losses. To account for the aerodynamic losses due to vortex generation at the blade tips, a correction factor for induced lift is applied. This correction factor is based on the Prandtl lift correction factor used with blade element models for propellers and is given in equations 3.2a - 3.2c. The k value in equation 3.2c is the

loading efficiency factor.

$$C_{L,3D} = C_{L,2D}\frac{2}{\pi}\cos^{-1}(e^{-f}) \tag{3.2a}$$

$$f = \frac{N}{2}(\frac{1-\eta}{\eta \sin|\alpha_G|}) \tag{3.2b}$$

$$C_{D,induced} = \frac{C_{L,3D}^2}{e\pi AR} \tag{3.2c}$$

To model the horseshoe vortex at the intersection between the blade and strut, Shires uses the empirical relation given in equation 3.3 [11]. h is in this case the strut length and δ^* the end-wall boundary layer thickness. Finally the effect of the tower wake was also modelled with an extra correction factor $f_T = 1 - \frac{D_T}{D_R}$ applied to the induced velocity[11].
Shires compares the predictions from the model to measured data of different existing VAWTs and the measured data from the NOVA V-VAWT, and finds that the trends of the model and measurements agree well at higher wind speeds. But the model overpredicts the power generation at lower wind speeds[11]. Shires concludes that by adding some corrections to the double-multiple streamtubes method, it can lead to fairly acceptable performance predictions of a V-VAWT with struts.

$$C_{D,intersection} = \frac{1.9\delta^*}{h \cdot \frac{t}{c}} \tag{3.3}$$

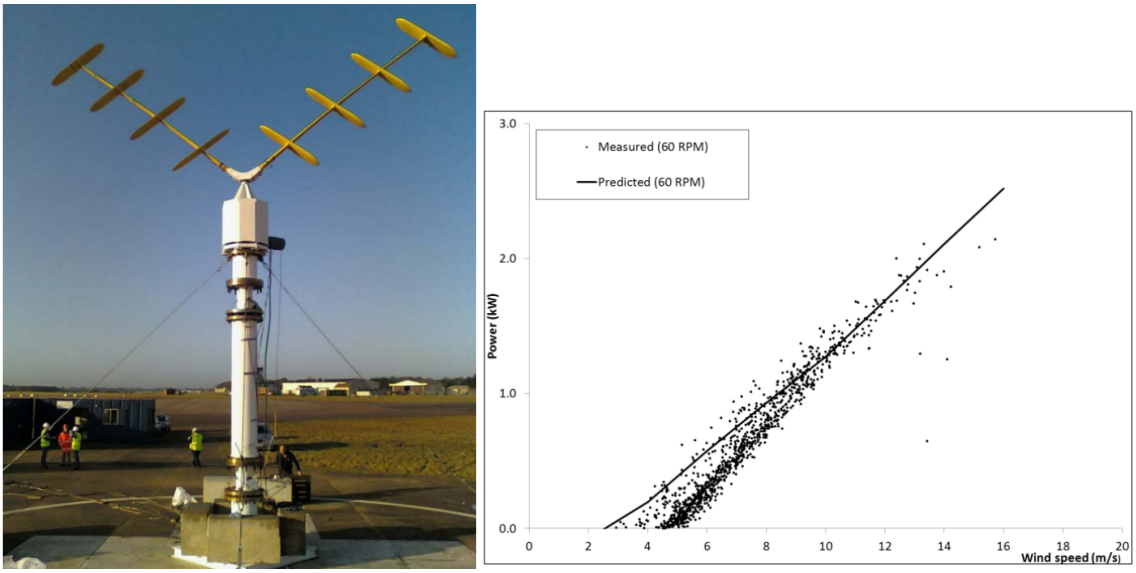

(a) The NOVA V-VAWT

(b) The measured and predicted power of the NOVA V-VAWT

Figure 3.3: Research of Shires on the NOVA V-VAWT[11]

3.2. PRESENCE OF STRUTS IN A VAWT

Siddiqui et al study the aerodynamic effects due to the presence of struts[12]. In this study a 3-bladed VAWT, including and excluding struts and tower, is modelled and the cases compared. The struts are placed and kept fully horizontal (thus zero inclination angle) thus it will not contribute to the production of lift. Their simulations are carried out for seven cycles and with seven different tip speed ratios λ for the case with only blades. This was once again repeated for the case with blades, struts and tower. The most important results can be found in figure 3.4c which shows the $\lambda - C_p$ curve with and without struts. It can be seen that the inclusion of struts elements decreases the C_p. The relative decrease of the C_p between the situations of excluding and including struts and hub increase at higher λ. According to Siddiqui et al this extra relative decrease of C_p is due to the decrease in torque produced by the VAWT when reaching higher tip speed ratios λ. Figures 3.4a and 3.4b shows the torque of the turbine during four revolutions for respectively $\lambda = 3.5$ and $\lambda = 4.5$. The difference between the two tip speed ratios is that the mean torque of the rotor drops at higher λ. It can also be concluded from the figure that the torque peak values in the plots decreases with the inclusion of strut and hub, therefore leading to the conclusion of torque decrease stated earlier[12].

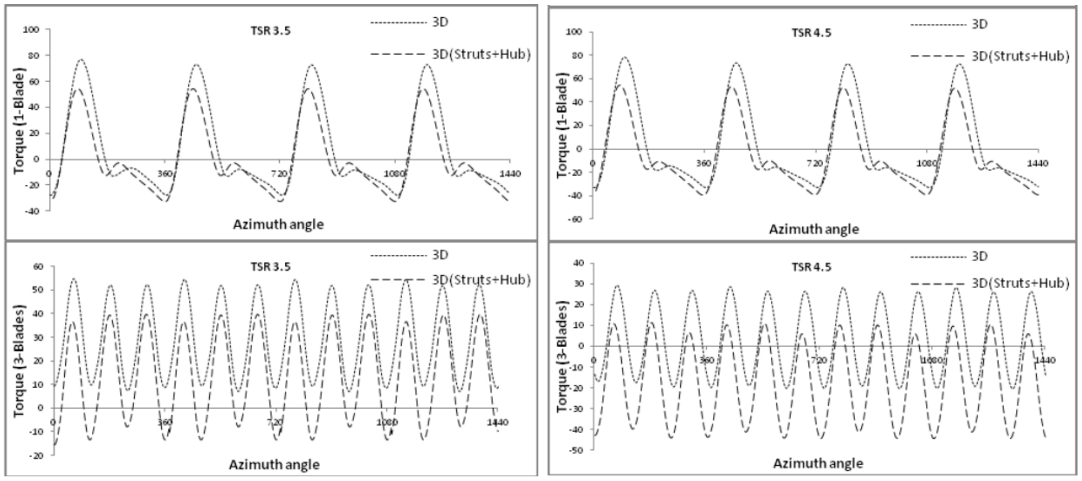

(a) Torque curve for four revolutions of the VAWT with and without struts and hub at $\lambda = 3.5$. The upper plot is for the case using one blade and the lower plot for the case using three blades.

(b) Torque curve four revolutions of the VAWT with and without struts and hub at $\lambda = 4.5$. The upper plot is for the case using one blade and the lower plot for the case using three blades.

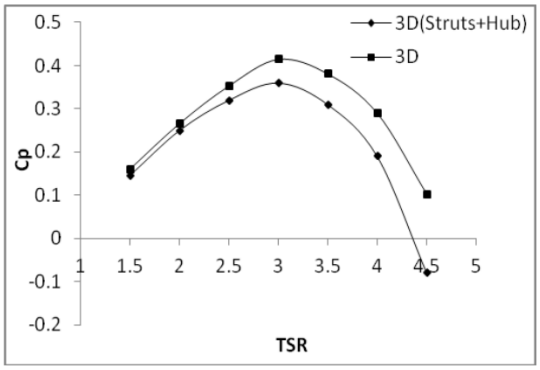

(c) The $\lambda - C_p$ curves for including and excluding struts and hub. The VAWT rotor contains three blades.

Figure 3.4: CFD simulation on a 3D VAWT with and without struts by Siddiqui et al[12]

Marsh et al.[13] delved deeper into the effects of struts on the vertical axis tidal turbine performances when applying different strut section geometries, different strut-blade joints and strut locations. The power curves and the torque fluctuation levels of three different strut configurations are determined. The configurations which are simulated can be found in figure 3.5a. They differ in strut section geometry by using either a NACA 0012 profile or a machined flat bar. Furthermore the locations of the strut can be positioned either at the end of the blade span or at quarter span position. Finally the connection type between the strut and blade is a faired joint or connection tab. All the simulation are performed using 3D CFD and validated with

experiments in a towing tank[13]. The turbulence model used for the simulation was the $\kappa - \omega$ SST due to the improved prediction of flow separation, adverse pressure gradient by including transport effects into the eddy-viscosity formulation[13]. Figure 3.5b shows the $C_P - \lambda$ curves based on the CFD simulations done by Marsh et al. The inflow velocity was $U_\infty = 1.5\frac{m}{s}$. The indications used for the configurations in figure 3.5a coincides with the indications for the curves in figure 3.5b. It can be seen that the strut location have an effect on the C_P curve and this effect can be seen in figure 3.5b when looking at the C_P curves for turbine A and turbine C. As turbine A and C are the same with the exception of strut placement, it can be said that the difference in C_P is caused by strut positions. It seems that the C_P decreases along the whole λ range when the struts are placed at quarter span of the blades. The decrements of C_P becomes larger at higher tip speed ratio as can be seen from figure 3.5b. The difference can become as high as 12.4% found by the simulation of Marsh et al[13]. According to [13] the increase in C_P when placing the struts at the end of the blade is due to the increase of effective blade length. The effect can be visualized and explained using figure 3.5c. There the differences in the vortex structures between turbine A and turbine C (same profiles) can clearly be seen. Turbine C generates vortices at the blade tip and the blade strut junction while turbine A generates vortices due blade tip and blade strut junction combined. The combined vortices at the blade tip minimizes flow disturbance over the blade and thus a higher C_P can be achieved[13].

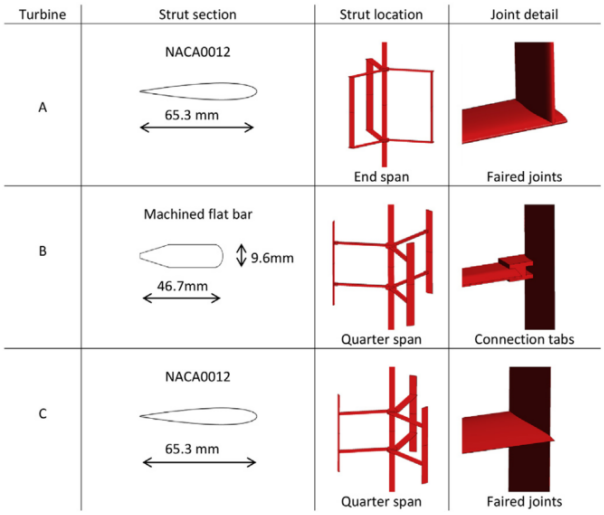

(a) The three different strut configurations which were simulated

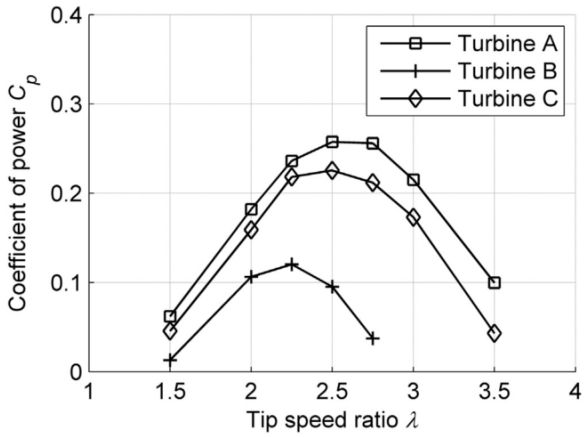

(b) $C_P - \lambda$ curves for the three configurations as described in figure 3.5a

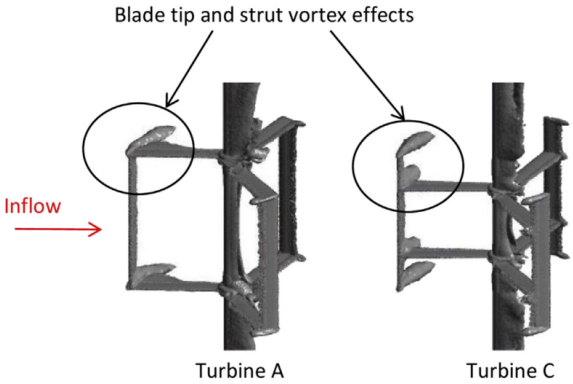

(c) Strut and tip vortex effects for different configurations

Figure 3.5: Research on strut configurations in a VAWT by Marsh et al [13]

Another study on VAWTs with (inclined) struts is performed by Mendoza and Goude[14]. The goal of this study is to improve the VAWT wind farm efficiency by deflecting the wake via pitched struts. By deflecting the wake in the upwind turbines, it is expected to improve the performance of the downwind turbines as the low velocity (low kinetic energy) wake from the upwind turbine would else cause lesser power generation on the downwind turbine[14][27]. Therefore in the study the actuator line model was used in combination with a dynamic stall model, similar to the actuator cylinder model of Madsen[32]. Figure 3.6a shows the proposed turbine by Mendoza[14]. These models were coupled with a CFD simulation.

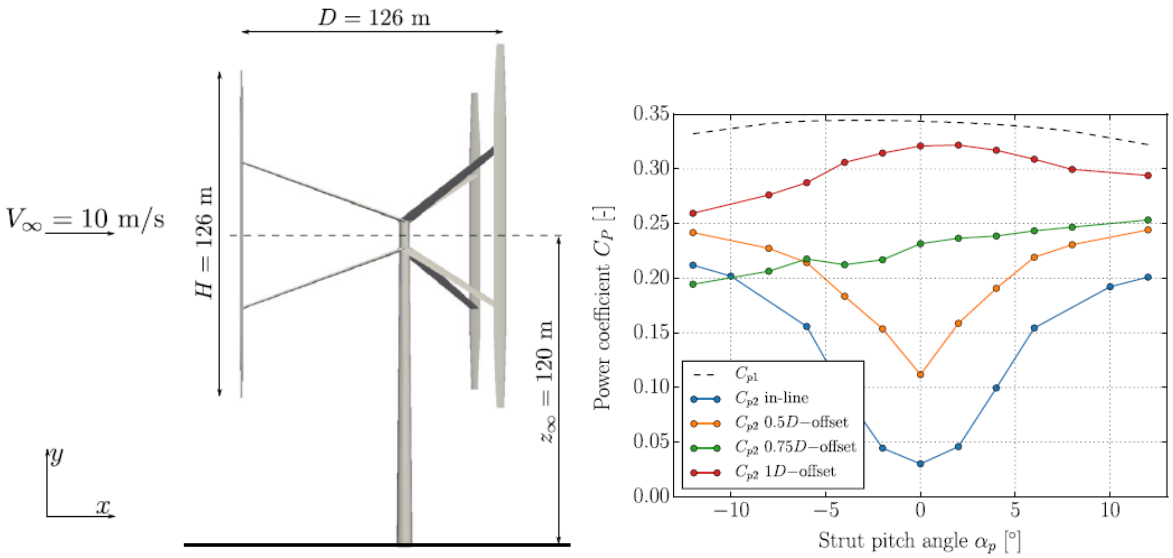

(a) The pictured VAWT using pitched/inclined struts in the study of Mendoza [14]

(b) Power coefficients of upwind turbine C_{p1} and downwind turbine C_{p2} for different offset in alignment of downwind turbine[14]

Figure 3.6: Simulation results and turbine of the research of Mendoza [14]

In his research he found that the introduction of a strut pitch angle in the upwind turbine will cause the wake to deflect. By doing so, the power coefficient of the upwind turbine drops by a few percent[14]. But for the downwind turbine the effects depends on how much the downwind turbine is aligned with the upwind turbine in freestream direction. Figure 3.6b shows the results on the power coefficients C_P of the up- and downwind turbine. When the downwind turbine is fully aligned with the upwind turbine, the result of wake deflection due to the pitched struts improves the power coefficient of the downwind turbine. This improvement relates to the strut pitch angle and thus the severity of the wake deflection as shown in figure 3.7. A positive pitch angle will deflect the wake vertically up and a negative angle will deflect the wake down. On the other hand the increased pitching angle can lead to minor reduced performance of the downwind turbine if the downwind turbine is at an certain offset relative to the upwind turbine. At an alignment offset of 1 rotor diameter of the downwind turbine, the strut pitch angle will have a negative impact on the C_P of the downwind turbine. In the study it is also shown that the wake from the upwind turbine behaves asymmetrical downstream due to the differences of velocity between the incoming flow and blade. The thrust loading vector is therefore not fully aligned in the downstream direction but is lightly skewed. This research shows that the struts of a VAWT can be used to control the wake to improve the performance of the downwind turbine with a minor loss of performance in the upwind turbine.

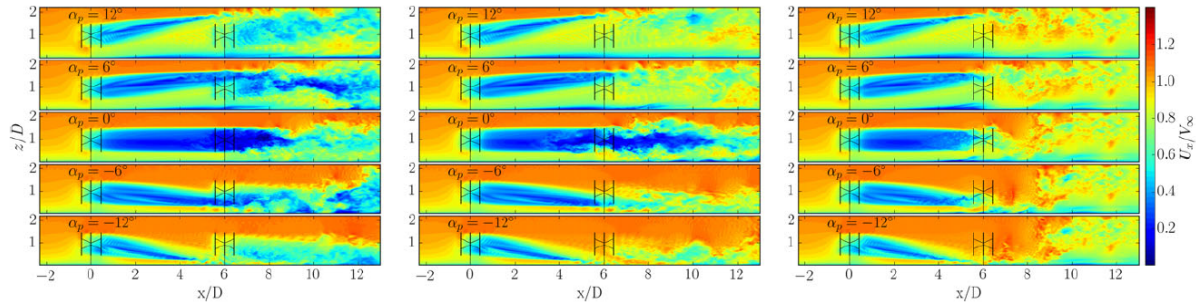

Figure 3.7: Normalized velocity field at the vertical middle plane for varying strut pitch angles. In the left figure the up- and downwind turbines are aligned, in the middle figure there is an offset of 0.5D and in the right figure there is an offset of 1D[14]

3.3. MODELS FOR INCLINED STRUT AND DOUBLE BLADED VAWTS

3.3.1. QUADRUPLE MULTIPLE STREAMTUBE METHOD

Hara et al.[15] studies the application of double bladed VAWT. The VAWT has two blades stacked next to each other to improve the self starting performance of the VAWT, as the double blades can produce a higher starting torque than the regular single blade VAWT[15][26]. This leads to the conclusion that double bladed VAWT has improved self starting performance at low tip speed ratio[15].

By inclining the struts against the horizontal plane, they can produce some lift[15]. This lift can then be used to increase the torque. The inclined strut can be related to research on double bladed VAWT, because looking at an inclined strut from a 2D top view perspective seems like a double bladed rotor. The research of Hara et al shows how to predict performances when taking into account the inclined struts as this can partially be considered a double bladed VAWT rotor[15][26]. The standard double blade VAWT and the inclined struts VAWT (butterfly VAWT) can be seen in figure 3.9.

To predict the performance of the double blade VAWT or the inclined struts of the butterfly VAWT, Hara et al used an extended method of the double multiple streamtube method called the quadruple multiple streamtube method (QMS)[15]. Instead of two rotor planes there would be four rotor planes, hence quadruple. Details about QMS itself can be found in their paper. The QMS model was validated using 2D CFD and it was found that their QMS model required some modifications. The effects of the inner rotor on the decrease of velocity upstream must be accounted for, and therefore they included a correction factor[15]. Although the results from QMS and CFD agree in general they noticed a discrepancy in the blade torque between QMS and CFD at the upwind side of the rotor. They could not find an explanation for the difference[15]. In general this QMS model have some potential for the performance prediction of double blade VAWT.

One of the point of interest is the research on inclined struts in VAWT. Hara et al have been doing research on butterfy wind turbines (BWT) which could already be seen in figure 3.9b [26]. In this kind of turbine the struts are inclined. Due to how the strut and blade are connected, the blades do not contain tips but instead the struts are seen as extensions[26].

Hara et al considered the effects of blade shapes, specifically the effects of symmetrical blades and cambered blades. The tests were done in the wind tunnel and CFD. It is concluded that cambered blade shapes are more suited at higher tip speed ratios while symmetrical blades provide better self starting performance of a VAWT. Their experimental results showed that using symmetrical blades at the inner rotor (struts) gives better torque improvement than cambered blade shape at low tip speed ratio[26].

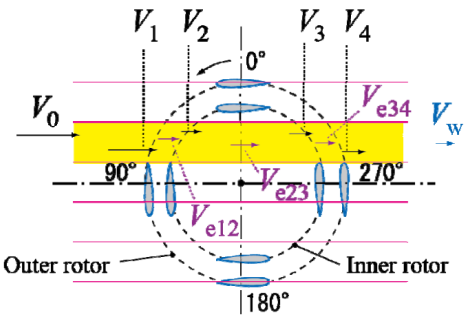

Figure 3.8: Quadruple multiple streamtube model by Hara et al[15]

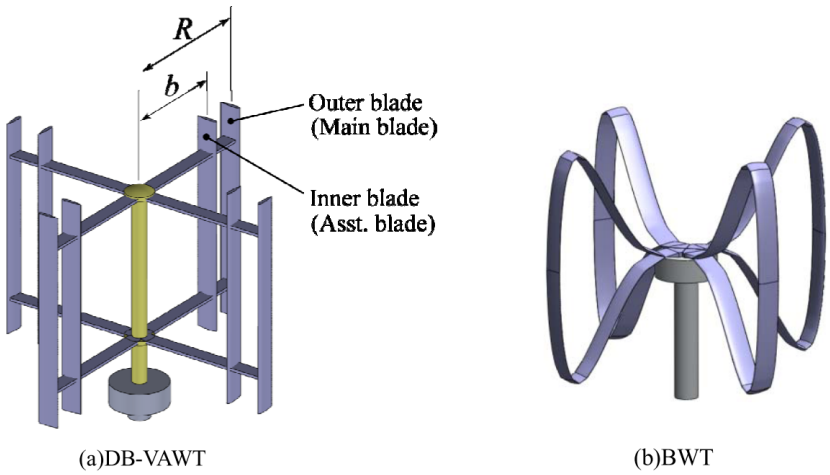

Figure 3.9: (a) the double blade VAWT (DB-VAWT) and (b) the butterfly VAWT (BWT)[15]

3.3.2. ACTUATOR CYLINDER SQUARED MODEL

De Tavernier[16] presents a paper where she extended the regular actuator cylinder model of Madsen[32]. Another actuator cylinder is introduced concentric within the main actuator cylinder. A turbine in another turbine in 2D as schematically shown in figure 3.10. The application of this model could be for example the earlier mentioned double blade VAWT or the butterfly VAWT in 2D of Hara et al. It could thus be used for struts which are inclined in a rotor. Compared to the original actuator cylinder model as explained in section 1.5.4, the induced velocity field in this case is the result of the influence by the inner and outer actuators[16]. This is possible because the solution model, Mod-lin, used is linear, while the non-linear parts are corrected for using a specific correction factor. But the induced velocity calculation does depend on the location, especially when these points are in or near the actuator cylinder. De Tavernier has modified the original code to include additional terms for these calculations when the locations are inside specific regions[16].

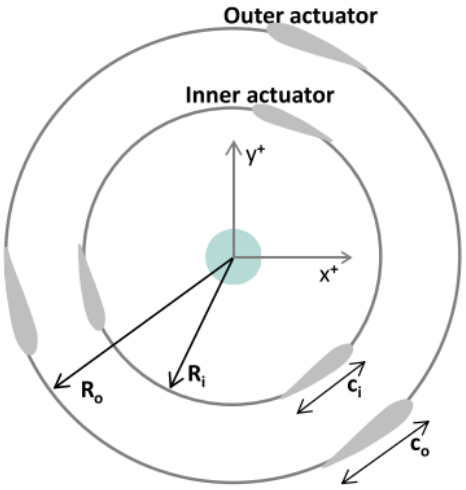

Figure 3.10: Schematic view of the proposed extension of the actuator model by De Tavernier[16]

In the study[16] the model is verified with a CFD simulation using OpenFOAM and compared with the original actuator cylinder model. The results were also compared to another 2D vortex model solver called U2DiVA. The wake trajectory by the inner and outer rotor and the velocity field of the simulation can be found in figure 3.11.

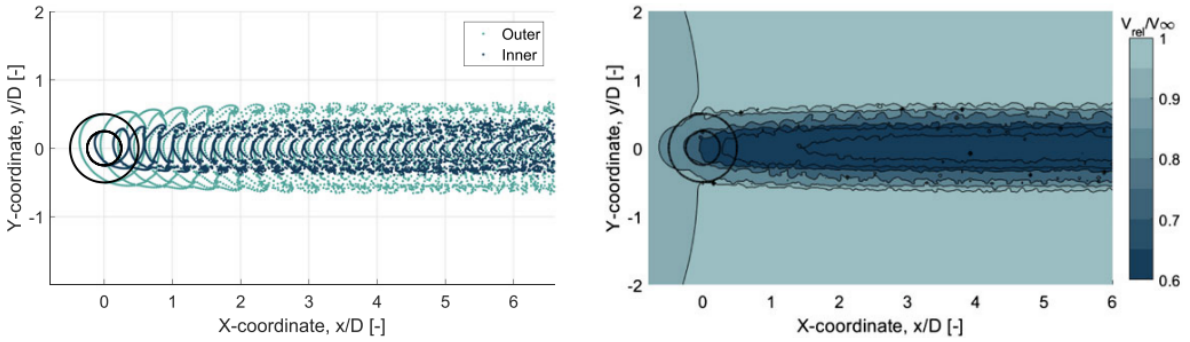

Figure 3.11: Simulation of the actuator model by De Tavernier[16]. On the left plot the wake of the inner and outer rotor is plotted. On the right side the velocity field is shown.

In her paper the results between the modified actuator-in-actuator cylinder and the regular actuator cylinder model are compared. This is shown in figure 3.12. The influence with a rotor in a rotor is that the tangential loadings of the modified actuator model is reduced in upwind but mainly in the downwind phase of the rotor. Thus the rotors will affect each other. In the comparison of U2DiVA with the model, it is shown in her paper that both models agree with each other at lower loaded case. At higher loaded cases the error between both models increase[16]. An explanation given by the author[16] is that wake expansions are not captured by the actuator cylinder model. As such their effects are not accounted for. Another observation made by the author is that the prediction of the model at the upwind part is more accurate than downwind due to the blade operating in the wake during the downwind phase[16]. But the extended actuator cylinder model is shown to have much potential by the author.

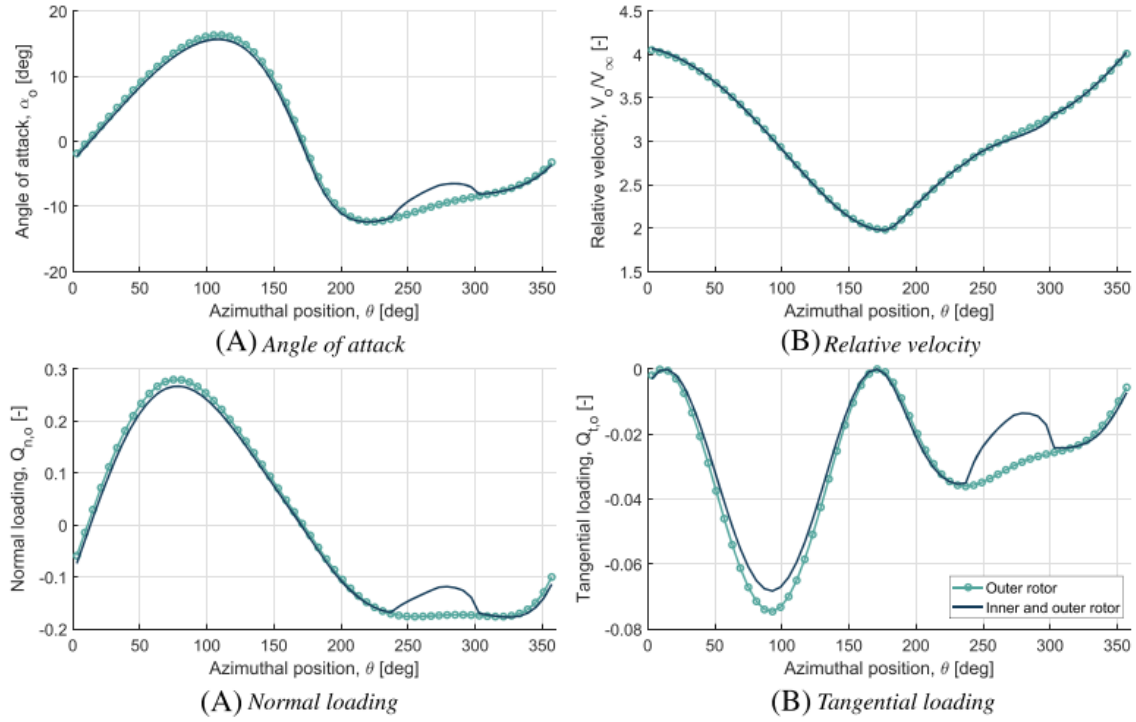

Figure 3.12: Comparison of the actuator model by De Tavernier[16] to the original (single) actuator version. Note the difference in the upstream part around $\theta = 90°$ and especially in the downstream part between $\theta = 200°$ and $\theta = 320°$ of the simulation.

4

CONCLUSION

The literature on the aerodynamics of VAWTs and the research performed by several researchers have been reviewed in this report. Most of the theory have been developed from blade element momentum theory and have been extended upon on, employing the use of multiple streamtubes and actuator disks. Some methods improve on this by taking the swept area of the VAWT as an actuator cylinder. This leads to low fidelity but fast and practical simulations. On the other hand there are the high fidelity simulations like CFD. But the downside is the high computational cost of these methods. Vortex methods are suitable in between mid-fidelity solutions. While these methods model more fundamental physics than regular momentum methods they are less computational intensive than CFD.
Due to the way the VAWTs operate, its blades intersect its own wake. The flow in which the blades operate contains many unsteady flow phenomena. As these phenomena will influence the performance of a rotor, researchers have tried to model and predict these phenomena. One of these of these effect commonly researched is dynamic stall. Multiple models based on different assumptions have been developed to predict dynamic stall. Gormont models are more based on empirical relations while the more complex Leishman-Beddoes models use a more fundamental approach.
Further research on VAWT have been performed by many scholars. A few of these studies which focused on struts were reviewed. Many researchers have developed or improved models to account for the struts. One of the most simple drag model is based on empirical means. Later on models are based on extension of momentum models. One example is the extension of the regular double-multiple streamtube method to quadruple-multiple streamtube model for the use on a VAWT with two rotors. Another model modified is the actuator cylinder model which is very suited for a VAWT. Limitation of these models is that they only work in the 2D case. For more advanced modelling studies, some of the researchers used CFD methods in combination with a momentum model. This way the wake effects can be studied. Based on these studies, it can be expected that the topology of the struts will cause different drag effects in the turbine. Most prominent are the strut-blade interference drag. Another effect related to blade-wake interactions are strut-wake interactions as the strut, like the blade, crosses its own wake. The phenomenon depends on the tip speed ratio of the rotor and the wake convection velocity. The consequences of these interactions can lead to unwanted aeroelastic and aero-acoustic behaviour. On the other hand, by introducing a pitching angle to the strut, it can also be used to beneficially deflect the wake to improve the behaviour of downwind turbines in windfarms. But whether the wake deflection by strut is beneficial or not depends on the wind farm setup.
In the second part of this report consists of the research on the effects of the presence of struts in a 3D VAWT with the lifting line solver CACTUS. The goal is to gain understanding of the influence struts will have on the rotor and the wake. Therefore the strut geometry must first be defined and modelled in CACTUS. Secondly, this study emphasizes on how struts affect VAWT performances with regard to loadings and power. The third point is the emphasis on the near and far wake generated by the rotor. The CACTUS software is first extended to allow the application of non-linear lifting line free vortex wake model on the struts. This extension makes it possible to model different geometries of the struts in a rotor and to model it in a more fundamental way than using empirical relations only. With the extended model, the struts are now able to produce lift and shed vortices which can interfere with the main rotor blades. This model was then used for a case study for varying parameters of a strut in the rotor. The variations in inclination angle, strut-blade attachment positions, tip speed ratio and the strut tip to blade gap are studied for their effects on the rotor performance and its wake.

With the tip of the struts closing in on the strut-blade interjunction point, the tip vortex of the strut functions as part of the strut-blade interference effects. This can cause a drop up to 15% of the C_P relative to a strutless turbine. With varying tip speed ratio λ it was shown that the optimal λ was relatively low at around $\lambda = 3.5$. At low tip speed ratios the C_Q contribution by the strut was negative but small. At higher λ this negative torque contribution by the strut could add up to a decent proportion of 25% the torque contribution by blade. Most of it caused by the downwind phase of the strut.
It was shown that the position of the strut blade interjunction has significant effect on the strut itself due to the downwash induced from the tip vortices of the main rotor blade. This downwash will cause a loading in Y direction (spanwise of rotor blades). As consequence a small induced angle can be detected on the struts. While in this case its effect on the loading generated by the strut is small, but it can be expected that this can have a more significant effect with inclined struts.
Finally the lifting line model on the struts was applied in combination with an inclined strut. This way the strut can produce actual torque and contribute to the power generation of the rotor. But doing so has an negative effect on the main rotor blade due to the shed vortices from the struts which interferes with the blades downwind. By inclining the struts, the torque is redistributed from the blades to the struts. However, there is still a net loss of power. This loss can be up to 5% depending on the inclination and approximately up to 7% relative to a strutless rotor. Furthermore the inclination of the struts deflects the wake and also causes it to become turbulent in after a few rotor radii as the wake from the struts and blades start to mix. The applied model for struts shows it is able to model the extra effects caused by the struts which would not have been possible in the original version of CACTUS.

4.1. RECOMMENDATIONS

The main goal to model the struts with a lifting line method and to perform a study with was achieved. However there were some issues which were not treated in this research. The modification of CACTUS to allow the struts to be modelled using the non-linear lifting line theory is a first step. But by doing so, the model of Hoerner[10] for strut-blade interference drag was not used any more as it was not compatible with the current implementation. Therefore the interconnection between strut and blade could not be modelled, but instead are just placed together with a zero gap between the strut's tip and the blade attachment point. While this does give some interactions between the strut and blade, some of the interference effects are not accounted for. Also the model of Hoerner was not completely implemented in the original CACTUS version, thus the original drag only strut bodies were always hardcoded to be uninclined. It is therefore advised to revise and reimplement this model again for future research.
While CACTUS itself has been validated with higher fidelity method[17], and shows good agreement with experiments. It is still advised to repeat this research with a higher fidelity method like CFD to verify the current results or compare it to results from other aerodynamic models. Finally the original plan was to include a three-bladed version of the rotor and asymmetrical positioned struts, but due to time constraints this could not be done any more. It is recommended to test for these cases as well to and compare it with the two bladed VAWT.

A

APPENDICES

A.1. HOW TO USE CACTUS

This section describes the use of CACTUS based on the manual of Murray and Barone[18]. CACTUS is based on VDART3 as mentioned earlier and has a Fortran codebase. The code will only run from the command line on Linux based system and will need some input files. These input files consist of the geometry file which describes the wind turbine's geometry in 3D according to a set of rules and the regular namelist input file which describes the general configuration and the case specifics. Furthermore a set of airfoil data is also required to supplement the geometry input file. CACTUS does not use a GUI for pre- or postprocessing, but for post processing external software like Paraview can be used for visualization. The general flow chart of CACTUS can be found in the next section.

GEOMETRY

CACTUS comes with a module to generate the turbine geometry file based on user input. This module is build in MATLAB/GNU Octave though, so this software is required to use the module. Alternatively it is possible to manually create the geometry file using only a notepad. But due to the expansive possibilities and complexity to model the geometry it is easier to use the module. Important to note is that the geometry module only contains possibility to generate standard HAWT or VAWT (H-Darrieus and normal Darrieus) constructions. For custom VAWT configurations either the MATLAB geometry module must be modified to suit this or the input file must be manually made.
CACTUS geometry only describes two different constructs: blades and struts. The blades are considered the lift generating body while the struts do only account for drag. In CACTUS this specifically means that only the blade can shed a free vortex wake while the strut constructs will only use empirical models. The blades and struts are decomposed into smaller elements. The amounts of elements can be defined by the user and will to a certain degree effect the accuracy of the simulation results, but also the calculation time. The positive flow direction is in the +x direction and the tower of the wind turbine point in the +y direction. Any ground planes or free surface will have their normal vectors pointing in +y direction [18].
The geometry file will consist of a header section with general information like turbine reference area, amount of blades and turbine rotation origin point. Furthermore each blade and strut construct will have to be described by its own section. Each section will contain the details of the element decomposition. Table A.1 consists of the file format for the CACTUS geometry file for a blade construct. For each blade header a list of numbers must be provided equal to the length of the amount of elements defined. In some cases the length of this list is equal to the amount of elements plus one. The required length is also indicated in table A.1 between the braces. For a strut construct it is in general similar except for few points. More details can be found in the CACTUS manual [18].

AIRFOIL DATA

When assigning blade constructs, airfoil data must be provided. Each element in a blade construct can be assigned to a specific airfoil. CACTUS imposes some requirements on the airfoil data. So first the foil coefficients specified are the lift, drag and pitching moment coefficients around the quarter chord point. The coefficients must be specified from an angle of attack of -180° to +180° for different Reynolds numbers. A

Header	Description
$NBlade$	Number of blades
$NStrut$	Number of struts
$RotN$	Turbine rotation axis normal vector (x y z)
$RotP$	Turbine rotation origin point (x y z)
$RefR$	Reference radius of the turbine in ft
$RefAR$	Ratio of turbine reference area and reference radius squared
Blade	
Blade i	Blade index (not used by CACTUS)
$NElem$	Number of elements for blade i
$FlipN$	Flips element's normal direction
QCx	x coordinates quarter chord line at element ends divided by reference radius. (NElem + 1)
QCy	y coordinates quarter chord line at element ends divided by reference radius. (NElem + 1)
QCz	z coordinates quarter chord line at element ends divided by reference radius. (NElem + 1)
tx	Blade unit tangent vector (rearward chord line direction) x component at element ends. (NElem + 1)
ty	Blade unit tangent vector (rearward chord line direction) y component at element ends. (NElem + 1)
tz	Blade unit tangent vector (rearward chord line direction) z component at element ends. (NElem + 1)
$CtoR$	Blade chord to turbine reference radius ratio at element ends. (NElem + 1)
PEx	Element center x coordinated divided by reference radius. (NElem)
PEy	Element center y coordinated divided by reference radius. (NElem)
PEz	Element center z coordinated divided by reference radius. (NElem)
nEx	Element unit normal vector x component. (NElem)
nEy	Element unit normal vector y component. (NElem)
nEz	Element unit normal vector z component. (NElem)
sEx	Element spanwise vector x component. (NElem)
sEy	Element spanwise vector y component. (NElem)
sEz	Element spanwise vector z component. (NElem)
$ECtoR$	Element chord to turbine reference ratio. (NElem)
$EAreaR$	Element area divided by turbine reference radius squared (NElem)
$iSect$	Index of the foil section data to be applied to each element. This index corresponds to the order in which the foil section data table files are supplied in the namelist input file. (NElem)

Table A.1: CACTUS input file format for blade construct as defined by [18]

maximum of 20 different Reynolds numbers is allowed for each airfoil with each case a maximum of 1000 entries for the angle of attacks. The sign convention in CACTUS is such that positive relative flow velocity in positive normal direction of the element will generate a positive angle of attack[18]. CACTUS software already contains some airfoil data files which can directly be used.

NAMELIST

The namelist input file consists of two parts, the configuration inputs and the case inputs. The configuration inputs specify solver settings like inclusion of compressibility effects or the model used for dynamic stall calculations. With case specific inputs operational parameters like freestream velocity, air density, rotor rotational speed, etc. It also directs which geometry to be used for the simulation. Therefore to run CACTUS, this file is the first input file accepted by CACTUS.

OUTPUTS

CACTUS returns several output files in CSV (comma separated values) format. Four different CSV files are generated containing the average performance data, temporal performance data, elements loading data and wall model data. Depending on the user inputs an extra file can be returned for the wake velocities deficits. These files can then be used for post processing.

A.1.1. VALIDATION OF CACTUS

CACTUS is validated in [17] and [31]. Ferreira et al compared multiple aerodynamic models with each other and concluded that models which explicitly models the wake showed good agreements between them[31]. Barone and Murray validated CACTUS using experimental data from the SANDIA 5m VAWT, SANDIA 34m VAWT and VAWT850. These data were compared against the results from simulations run in CACTUS. Only the results of the VAWT850 are shown here and can be found in figure A.1. To model the VAWT850 16 blade elements were used for each blade (two blades in total). 20 timesteps was used for each revolutions with in total 15 revolutions. Furthermore the Boeing-Vertol dynamic stall model was used in the simulation[17]. The Barone and Murray state that they carefully added excresence drag to the model to increase accuracy of the simulations. Excresence drag was chosen such that at high tip speed ratio the simulations and measurements would agree[17]. It can be seen in figure A.1b that the results of the measurements and simulations by CACTUS do agree very well except for higher wind speed were there is a significant difference between the simulation and measurement.

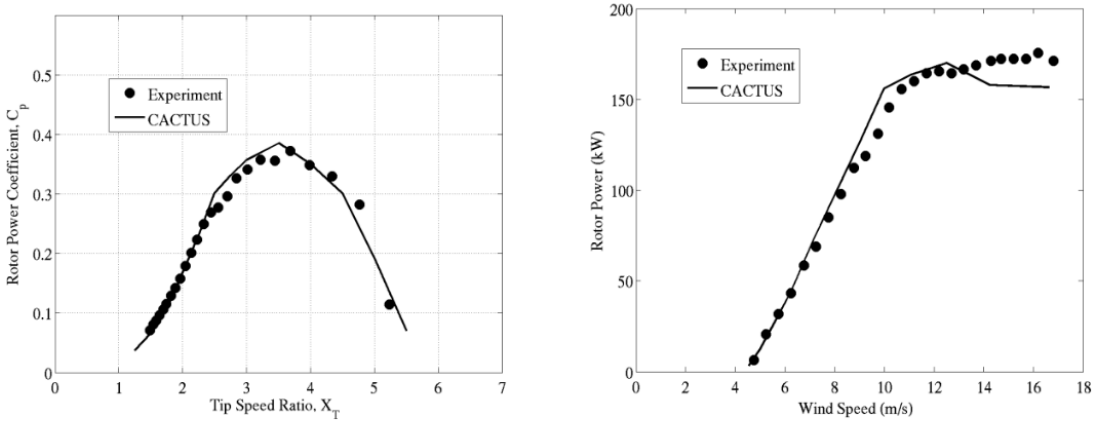

a) Power coefficient vs. tip speed ratio

b) Power vs. wind speed

Figure A.1: Comparison measurement VAWT850 turbine with CACTUS results at 13.62 RPM[17]

A.2. FLOW CHART OF CACTUS

The flowchart of CACTUS consists of two different sections. On the next page, first a general overview is given, but to keep clarity the lifting line computation mechanisms, in the general overview shown as the part within the dashed lines, are written in a simplified way. In the page thereafter a more detailed flowchart is given for the part within the dashed lines. This part is the core of the CACTUS software in which the vortex method is executed.

General flowchart CACTUS

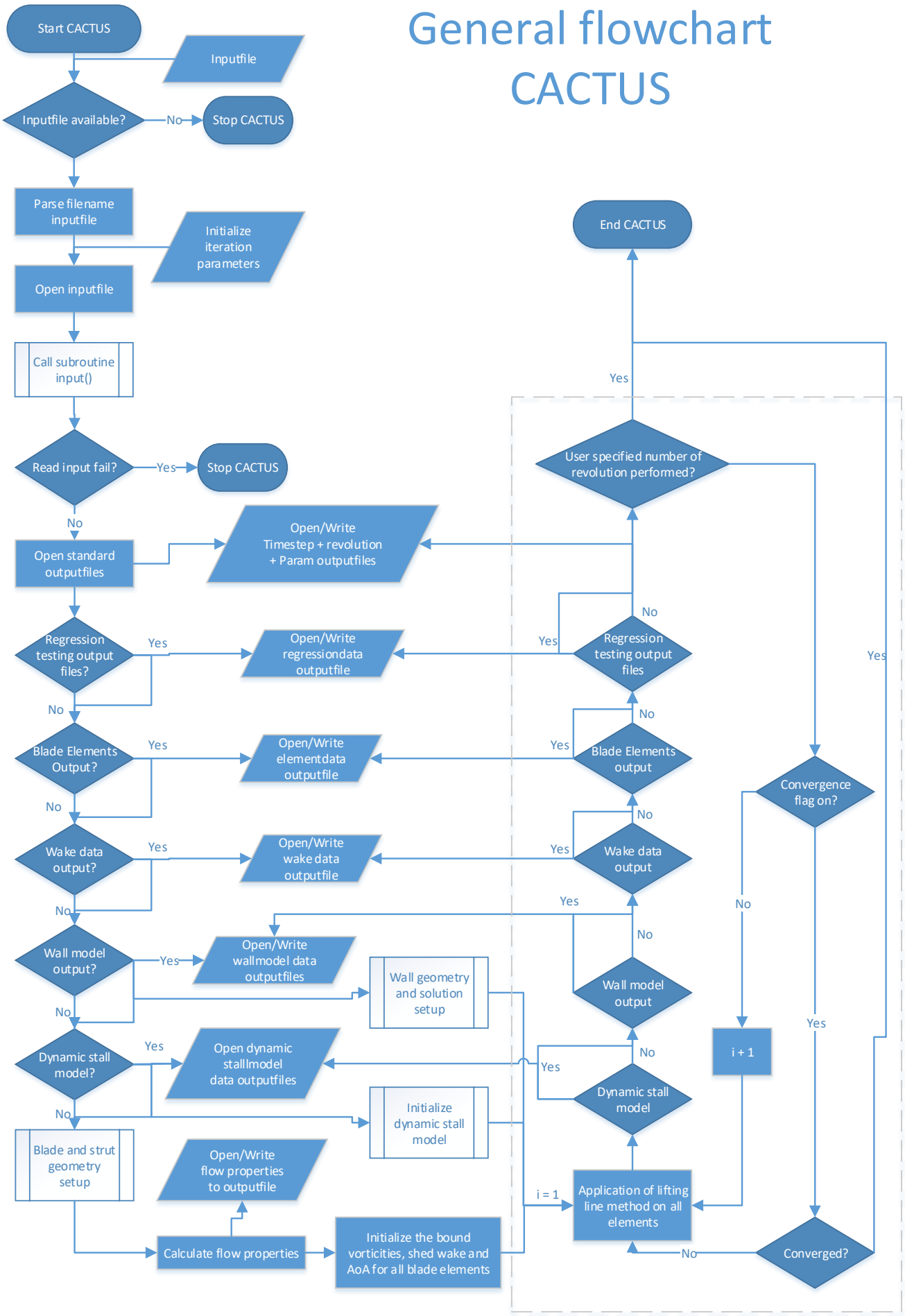

CACTUS Iteration detail part

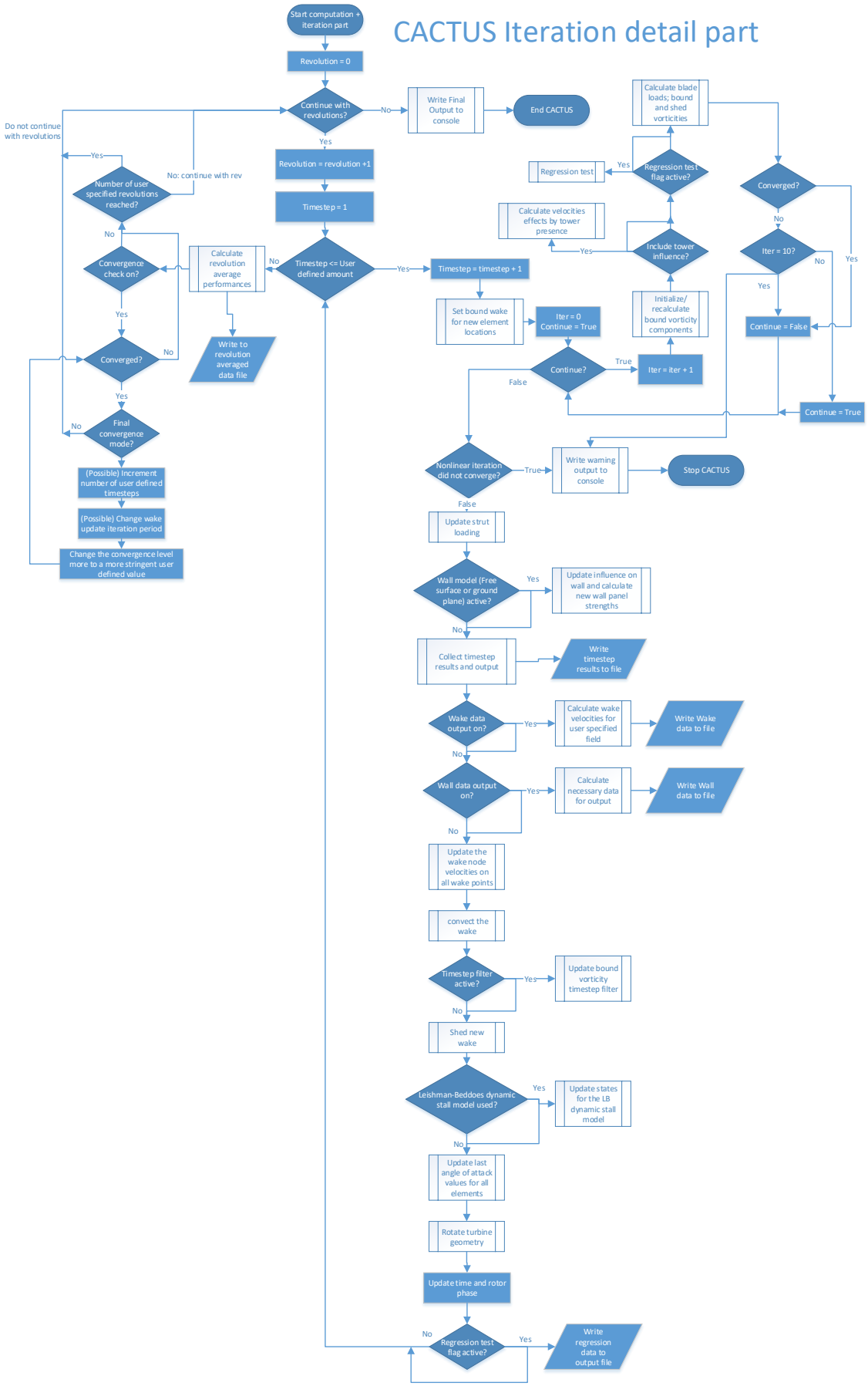

BIBLIOGRAPHY

[1] T. Burton, D. Sharpe, N. Jenkins, and E. Bossanyi, *WindEnergy Handbook* (John Wiley and sons, 2001) p. 642.

[2] M. Islam, D. S. Ting, and A. Fartaj, *Aerodynamic models for Darrieus-type straight-bladed vertical axis wind turbines,* Renewable and Sustainable Energy Reviews **12**, 1087 (2008).

[3] J. H. Strickland, *The Darrieus Turbine: A performance prediction model using multiple streamtubes*, Tech. Rep. (Sandia Laboratories, Albuquerque, 1975).

[4] J. Katz and A. Plotkin, *Low-Speed Aerodynamics , Second Edition*, 2nd ed. (Cambridge University Press, 32 Avenue of the Americas, New York, NY 10013-2473, USA, 2010) p. 629.

[5] I. Paraschivoiu, *Wind Turbine Design with Emphasis on Darrieus Concept,* (2002).

[6] J. H. Strickland, B. T. Webster, and T. Nguyen, *A Vortex Model of the Darrieus Turbine: An Analytical and Experimental Study,* Journal of Fluids Engineering **101**, 500 (1979).

[7] W. Tjiu, T. Marnoto, S. Mat, M. H. Ruslan, and K. Sopian, *Darrieus vertical axis wind turbine for power generation II: Challenges in HAWT and the opportunity of multi-megawatt Darrieus VAWT development,* Renewable Energy **75**, 560 (2015), arXiv:052011 .

[8] T. C. Corke and F. O. Thomas, *Dynamic Stall in Pitching Airfoils: Aerodynamic Damping and Compressibility Effects,* Annual Review of Fluid Mechanics **47**, 479 (2015).

[9] E. Ferrer and R. H. Willden, *Blade-wake interactions in cross-flow turbines,* (2015).

[10] S. F. Hoerner, *Fluid-Dynamic Drag Practical Information on Aerodynamic Drag and Hydrodynamic Resistance* (1965) pp. 3–9 – 3–28.

[11] A. Shires, *Development and evaluation of an aerodynamic model for a novel vertical axis wind turbine concept,* Energies **6**, 2501 (2013).

[12] M. S. Siddiqui, N. Durrani, and I. Akhtar, *Numerical Study to Quantify the Effects of Struts and Central Hub on the Performance of a Three Dimensional Vertical Axis Wind Turbine Using Sliding Mesh,* Volume 2: Reliability, Availability and Maintainability (RAM); Plant Systems, Structures, Components and Materials Issues; Simple and Combined Cycles; Advanced Energy Systems and Renewables (Wind, Solar and Geothermal); Energy Water Nexus; Thermal Hydraul , V002T09A020 (2013).

[13] P. Marsh, D. Ranmuthugala, I. Penesis, and G. Thomas, *Three-dimensional numerical simulations of straight-bladed vertical axis tidal turbines investigating power output, torque ripple and mounting forces,* Renewable Energy **83**, 67 (2015).

[14] V. Mendoza and A. Goude, *Improving farm efficiency of interacting vertical-axis wind turbines through wake deflection using pitched struts,* Wind Energy **22**, 538 (2019).

[15] Y. Hara, T. Kawamura, H. Akimoto, K. Tanaka, T. Nakamura, and K. Mizumukai, *Predicting double-blade vertical axis wind turbine performance by a quadruple-multiple streamtube model,* International Journal of Fluid Machinery and Systems **7**, 16 (2014).

[16] D. De Tavernier and C. Ferreira, *An extended actuator cylinder model: Actuator-in-actuator cylinder (AC-squared) model,* Wind Energy (2019), 10.1002/we.2340.

[17] J. Murray and M. Barone, *The Development of CACTUS, a Wind and Marine Turbine Performance Simulation Code,* 49th AIAA Aerospace Sciences Meeting including the New Horizons Forum and Aerospace Exposition , 1 (2011).

[18] J. C. Murray and M. Barone, *CACTUS User's Manual,* , 1 (2013).

[19] F. Gotzens, H. Heinrichs, J. F. Hake, and H. J. Allelein, *The influence of continued reductions in renewable energy cost on the European electricity system,* Energy Strategy Reviews **21**, 71 (2018).

[20] J. K. Kaldellis and D. Zafirakis, *The wind energy (r)evolution: A short review of a long history,* Renewable Energy **36**, 1887 (2011).

[21] H. J. Sutherland, D. E. Berg, and T. D. Ashwill, *A Retrospective of VAWT Technology,* Security , 1 (2012).

[22] Z. Cheng, H. A. Madsen, Z. Gao, and T. Moan, *Aerodynamic Modeling of Floating Vertical Axis Wind Turbines Using the Actuator Cylinder Flow Method,* Energy Procedia **94**, 531 (2016).

[23] B. Hand and A. Cashman, *Aerodynamic modeling methods for an offshore vertical axis wind turbine : a comparative study (Unpublished research),* Renewable Energy **129**, 12 (2017).

[24] C. S. Ferreira, *The near wake of the VAWT 2D and 3D views of the VAWT aerodynamics,* T.U.Delft Thesis , 304 (2009).

[25] E. Dyachuk and A. Goude, *Simulating dynamic stall effects for vertical axis wind turbines applying a double multiple streamtube model,* Energies **8**, 1353 (2015).

[26] Y. HARA, T. SUMI, T. EMI, M. YOKOYAMA, H. AKIMOTO, T. KAWAMURA, and T. NAKAMURA, *Effects of blade section on performance of butterfly wind turbines as double-blade VAWTs,* Journal of Fluid Science and Technology **10**, JFST0003 (2015).

[27] V. Mendoza, *Aerodynamic Studies of Vertical Axis Wind Turbines using the Actuator Line Model. Digital Comprehensive Summaries of Uppsala Dissertations from the Faculty of Science and Technology 1671*, Vol. 85 (2018).

[28] M. Yi and Q. Jianjun, *Numerical Study of Flow Field and Aerodynamic Performance of Straight Bladed VAWT at Variable Tip Speed Ratios,* The Open Mechanical Engineering Journal **1017 - 102**, 1017 (2015).

[29] Q. Li, T. Maeda, Y. Kamada, K. Shimizu, T. Ogasawara, A. Nakai, and T. Kasuya, *Effect of rotor aspect ratio and solidity on a straight-bladed vertical axis wind turbine in three-dimensional analysis by the panel method,* Energy **121**, 1 (2017).

[30] I. Paraschivoiu, *Double-Multiple Streamtube Model for Studying VAWT's,* Journal of Propulsion and Power **4**, 370 (1988).

[31] C. S. Ferreira, H. A. Madsen, M. Barone, B. Roscher, P. Deglaire, and I. Arduin, *Comparison of aerodynamic models for vertical axis wind turbines,* Journal of Physics: Conference Series **524** (2014), 10.1088/1742-6596/524/1/012125.

[32] H. A. Madsen, U. S. Paulsen, and L. Vitae, *Analysis of VAWT aerodynamics and design using the actuator cylinder flow model,* Journal of Physics: Conference Series **555** (2014), 10.1088/1742-6596/555/1/012065.

[33] M. A. Hirsch IH, *A cascade theory for the aerodynamic performance of Darrieus wind turbines,* Wind Engineering **11**, 164– (1987).

[34] J. Anderson, *Fundamentals of Aerodynamics* (McGraw-Hill Education, 2010).

[35] D. Owens, *Weissinger's model of the nonlinear lifting-line method for aircraft design,* (2013), 10.2514/6.1998-597.

[36] B. Xu, T. Wang, Y. Yuan, Z. Zhao, and H. Liu, *A simplified free vortexwake model of wind turbines for axial steady conditions,* Applied Sciences (Switzerland) **8** (2018), 10.3390/app8060866.

[37] S. Hauptmann, M. Bülk, L. Schön, S. Erbslöh, K. Boorsma, F. Grasso, M. Kühn, and P. W. Cheng, *Comparison of the lifting-line free vortex wake method and the blade-element-momentum theory regarding the simulated loads of multi-MW wind turbines,* Journal of Physics: Conference Series **555** (2014), 10.1088/1742-6596/555/1/012050.

[38] P. Tchakoua, R. Wamkeue, M. Ouhrouche, T. A. Tameghe, and G. Ekemb, *A new approach for modeling darrieus-type vertical axis wind turbine rotors using electrical equivalent circuit analogy: Basis of theoretical formulations and model development,* Energies **8**, 10684 (2015).

[39] A. Rezaeiha, H. Montazeri, and B. Blocken, *On the accuracy of turbulence models for CFD simulations of vertical axis wind turbines,* Energy **180**, 838 (2019).

[40] F. Balduzzi, J. Drofelnik, A. Bianchini, G. Ferrara, L. Ferrari, and M. S. Campobasso, *Darrieus wind turbine blade unsteady aerodynamics: a three-dimensional Navier-Stokes CFD assessment,* Energy **128**, 550 (2017).

[41] A. Rezaeiha, I. Kalkman, and B. Blocken, *CFD simulation of a vertical axis wind turbine operating at a moderate tip speed ratio: Guidelines for minimum domain size and azimuthal increment,* Renewable Energy **107**, 373 (2017).

[42] A. Rezaeiha, H. Montazeri, and B. Blocken, *Characterization of aerodynamic performance of vertical axis wind turbines: Impact of operational parameters,* Energy Conversion and Management **169**, 45 (2018).

[43] M. T. Brahimi and A. Allet, *Aerodynamic analysis models for vertical-axis wind turbines,* International Journal of Rotating Machinery **2**, 15 (1995).

[44] M. Borg, A. Shires, and M. Collu, *Offshore floating vertical axis wind turbines, dynamics modelling state of the art. part I: Aerodynamics,* Renewable and Sustainable Energy Reviews **39**, 1214 (2014).

[45] J. G. Leishman and T. S. Beddoes, *A Semi-Empirical Model for Dynamic Stall,* Journal of the American Helicopter Society **34**, 3 (1989).

[46] K. McAlister, O. Lambert, and D. Petot, *Application of the ONERA model of dynamic stall,* (1984).

[47] R. Gormont, *A Mathematical model of unsteady aerodynamics and radial flow for application to helicopter rotors,* , 1 (1973).

[48] A. Rezaeiha, I. Kalkman, H. Montazeri, and B. Blocken, *Effect of the shaft on the aerodynamic performance of urban vertical axis wind turbines,* Energy Conversion and Management **149**, 616 (2017).